REVERSE MICELLE SIZE AND STABILITY DURING ELECTROLYTE ENCAPSULATION AND IMPLICATIONS FOR THE SYNTHESIS OF NANOMATERIALS

BY

HOORSHAD FATHI-KELLY

A THESIS

SUBMITTED TO THE FACULTY OF

ALFRED UNIVERSITY

IN PARTIAL FULFILLMENT OF THE REQUIREMENTS
FOR THE DEGREE OF

DOCTOR OF PHILOSOPHY

IN

MATERIALS SCIENCE AND ENGINEERING

ALFRED, NEW YORK

APRIL, 2014

REVERSE MICELLE SIZE AND STABILITY DURING ELECTROLYTE ENCAPSULATION AND IMPLICATIONS FOR THE SYNTHESIS OF NANOMATERIALS

BY

HOORSHAD FATHI-KELLY

B.S. IRAN UNIVERSITY OF SCIENCE AND TECHNOLOGY (2008)

SIGNATURE OF AUTHOR_____

APPROVED BY _____
OLIVIA A. GRAEVE, ADVISOR

_____
WILLIAM M. CARTY, ADVISORY COMMITTEE

_____
ALASTAIR N. CORMACK, ADVISORY COMMITTEE

_____
VICTOR R. VASQUEZ, ADVISORY COMMITTEE

_____
YIQUAN WU, ADVISORY COMMITTEE

_____
CHAIR, ORAL THESIS DEFENSE

ACCEPTED BY _____
DOREEN D. EDWARDS, DEAN
KAZUO INAMORI SCHOOL OF ENGINEERING

ACCEPTED BY _____
NANCY J. EVANGELISTA, ASSOCIATE PROVOST
FOR GRADUATE AND PROFESSIONAL PROGRAMS
ALFRED UNIVERSITY

ACKNOWLEDGMENTS

Completing my PhD has been my most challenging accomplishment to date. I finished this journey with the help of many people that I would like to thank.

First and foremost I want to thank my parents, who are there for me no matter what and no matter how far apart we are. I remember when I was four years old and my Dad told me (translated), "Dokhmali, I do not want you to just be a doctor. I want you to be a scientist. Always pursue knowledge and make a good change in the world. Remember that knowledge is the biggest treasure a person can have." I did not really understand what he meant at the time, but I carried his message until it had meaning and it continues to inspire me. Thank you for teaching me not to be satisfied so easily and to learn as much as I can in all aspects of my life. My mother further nurtured this advice. She went above and beyond in preparing me along the way and encouraging me to be an educated and independent lady. Thank you for teaching and helping me to dream big and to pursue those dreams. My words cannot fully express my gratitude.

I was so far away from home during my PhD program. Furthermore, I could not go home. This was very difficult for me. Fortuneately, I have close family members and friends who helped comfort me during this challenging time, including my aunt Farideh, cousins Leila, Amirhossein, and Mehrdad, my brother Houd and his wife Carina, and my very good friends Laura and Shiva. Thank you all for being there for me. I am so blessed to have you all.

I also want to thank the love of my life, my husband, who was my mentor during the whole of my PhD education. I am so grateful for all the suggestions, motivation, and teaching me how to see the big picture of my project when I got stuck in the details. I learned a lot about organizing and interpreting data from him. He also encouraged me to be an independent researcher. Most of all, I thank him for the distractions from my education and thesis.

Some people really change your life. Dr. Graeve changed mine. She was in the first list of professors I emailed for applying to graduate school and she was the first who answered me. I appreciate all her help, guidance, and opportunity that she has provided not only in research, but also in life.

I want to thank all of my committee members. I am honored to have the name of all these smart people on my PhD dissertation. I have never had a chance to have a class with Dr. Carty, but from every committee meeting I have learned a lot form him and I enjoyed our discussions. Dr. Cormack, Dr. Vasquez, and Dr. Wu all provided valuable insights that improved the quality of my work.

Lastly, I want to thank Katie Decker. She really went above and beyond to help me finish my degree from across the country. I really could not have managed without her. She has such a kind soul.

TABLE OF CONTENTS

LIST OF TABLES

Page

LIST OF FIGURES

Page

ABSTRACT

A model for reverse micelle size with additions of salts, based on the formation of a pair of overlapping electrical double layers, has been developed. Specific ion effects demonstrate that reverse micelle size is proportional to ion hydration complex size and the electrical double layer thickness. Limited salt solubility has been observed due to one of two destabilization mechanisms: (1) one based on too small of an average reverse micelle size and (2) one based on too large of a hydrated ion size. Precursor limits for obtaining stable solutions once a precipitation reaction is initiated by mixing two reverse micellar solutions does not necessarily correlate to the salt solubility limits.

Analytical solutions of the model provide several parameters that are either not reported by other researchers at all or are not experimentally assessed by the methods presented within: (1) the critical potential, or potential minimum between the two overlapping electrical double layers, (2) the local ion concentration generating the critical potential, (3) the extent of Stern layer occupation in reverse micelles, and (4) an estimate of dielectric constant of the reverse micelle interior phase.

Changing the water to surfactant ratio, partial substitution of polar solvents for water, and partial substitution of cationic or nonionic surfactant for the anionic surfactant were investigated. None of these changes affect the critical potential, but do affect the local ion concentration at the critical potential. The estimated dielectric constant can also vary. Reduced water to surfactant ratio had the biggest effect on increasing local ion concentration, increasing dielectric constant for counterions of high valence, and is the only modification that increased reactant limits for obtaining stable precipitate solutions.

CHAPTER 1: INTRODUCTION

A. Foreword

Reverse micelle synthesis is a technique capable of producing novel designer nanoparticles. A relatively simple example is the formation of core-shell composite particles formed by subsequent precipitation reactions. However, the stability of the reverse micellar structures needs to be maintained during the precipitation reactions. Thus, there is a need to understand the limitations when adding precursors or when performing a precipitation reaction within reverse micelles and this is the primary focus of this thesis.

Chapter 1 of the thesis consists of a general introduction to reverse micelles, relevant applications of reverse micelles (including specific advantages of using reverse micelles), and the effect that salts have on reverse micelle size and stability. The introduction to reverse micelles includes basic concepts such as the reverse micelle structure and the concept of content exchange that is a central concept to reverse micelle synthesis of nanoparticles. All chapters after the introduction correspond to the effects that salts have on reverse micelle size and stability and the implications for reverse micelle synthesis. Basic theory that is relevant to this thesis is also provided, including the Gouy-Chapman theory and Stern model, which apply to an electrolyte solution adjacent to a charged surface.

Chapter 2 is the foundation for many of the remaining chapters. A qualitative model of reverse micelle size and stability when a salt is added to the reverse micelle system is presented in Chapter 2. The model is conceptually based on the Gouy-

Chapman theory. The model can explain the decrease in average reverse micelle size with increasing salt concentration and provides a mechanism for destabilization. Furthermore, the analysis of the model results in the development of a critical potential, the first known experimental extrapolation of such a parameter for reverse micelles. The critical potential is independent of the electrolytes that are added and therefore is a parameter that is defined by the system. All subsequent chapters focus on either continuing to develop the model described in Chapter 2 and/or on the stability of reverse micellar solutions once a precipitation reaction is initiated.

The focus of Chapter 3 is an evaluation of the qualitative model given in Chapter 2. Four scenarios are evaluated: (i) the qualitative model described in Chapter 2 with Na^+ counterions excluded from the electrical double layer, (ii) the qualitative model described in Chapter 2 modified by including Na^+ counterions in the electrical double layer, (iii) a modified model (Stern model) with Na^+ cations excluded from the electrical double layer, and (iv) the Stern model with Na^+ cations included in the electrical double layer. The computational exercise proves feasibility of the model and encourages further developing the model.

Experiments were performed to investigate specific ion effects and a summary is provided in Chapter 4. Specific ions have been introduced by encapsulating eleven different salts. Two forms of destabilization were observed, one based on a size limit for the reverse micelles and the other based on a size limit of the ions introduced into the reverse micelles. Reverse micelle size changes remain proportional to the electrical double layer thickness when any of the salts are added and results in a linear trend. A slope change at low concentrations occurs and has been used to determine that the

occupancy of the Stern layer is low (i.e. surfactant headgroups are highly dissociated). The slope of the linear fit can be correlated to the electrolyte cation valence and the line intercept can be correlated to the average hydrated ion size for the ions introduced by the specific salt. The slope of the fit as a function of the ion valence provides a method to estimate the dielectric constant of the reverse micelle interior and is a new method for experimentally determining such a value. When $HAuCl_4$ was encapsulated in reverse micelles, an increase in the average size is observed, which does not fit within the qualitative model developed in Chapter 2. Three possible explanations are given, one of which is used to develop a model that incorporates the effect that water can have on the reverse micelle size and stability and is a concept explored further in Chapter 5.

Chapter 5 is an exploration of reverse micelle stability when a precipitation reaction is initiated by mixing two reverse micellar solutions encapsulating different precursors. It was determined that the stability when initiating precipitation reactions is lower than the limitations imposed by the precursors and a stability diagram for precipitation is presented. The precursor solutions from randomly selected studies are also evaluated and the results demonstrate that the precipitation reactions were done with unstable precursor solutions. Reverse micelle growth occurs with salt additions when a cationic surfactant is used and supports an adjustment to the qualitative model that is presented in Chapter 4, in which the hydrogen bond network of the polar phase is an important consideration.

The work in Chapter 6 was performed with the intention of purposefully modifying the hydrogen bond network, either by increasing the interaction between water and surfactant molecules by decreasing the water to surfactant ratio or by partial

substitution of the water phase with another polar solvent. Changing the water to surfactant ratio affects the reverse micellar size and can be correlated to the electrical double layer thickness of the surfactant counterions. Substitution of the polar phase results in no reverse micelle size changes until relatively large amounts are substituted. The critical potential is unaffected by most of these changes, except for when $ZrOCl_2$ was added to a methanol-substituted system, but all changes cause differences in local ion concentrations at the critical potential. The system modifications generally improved the solubility of precursors in the reverse micelles. However, only decreasing the water to surfactant ratio results in a significant change to the estimate of the dielectric constant of the reverse micelle interior and improves the reverse micelle stability for precipitation reactions. Turbidity measurements were also evaluated for distinguishing points of instability and are found to be supplemental at best.

Chapter 7 contains the results from an investigation of the effects that cosurfactant substitutions for AOT have on reverse micelle size, how salts affect these modified systems, and whether or not reverse micelle stability can be improved when initiating a precipitation reaction. Cosurfactant substitutions cause a decrease in average reverse micelle size. Salts cause further size reduction in these systems and the size changes remain proportional to the electrical double layer thickness. The critical potential does not change by the modifications. Thus, the critical potential is identical for all conditions that were studied, except for when $ZrOCl_2$ is added to the system with methanol substituted for water in Chapter 6. The points of instability are either unaffected or reduced when using a cosurfactant and there is not a significant improvement in reverse

micelle stability when initiating a precipitation reaction for the types and concentrations of cosurfactants that are used. Chapter 8 includes a summary of all results.

B. Reverse Micelles

The first description of a reverse micelle structure was given by Hoar and Schulman, in 1943.[1] The basic structure Hoar and Schulman proposed is demonstrated in Figure 1-1. A small water droplet is stabilized in a bulk oil phase in the presence of a soap and cosurfactant in sufficient amount to cover the interface. The soap contains a hydrophobic tail and hydrophilic headgroup that extend into the oil and water phases, respectively. A cosurfactant (nonionic or counterionic compared to the soap) is often necessary to form reverse micellar structures. This simple model is still used today for the conceptualization of reverse micelles. However, one could argue that the exact structure of reverse micelles is still a mystery. For example, the structure of the water confined in the nanodomain of the reverse micelle differs from that of bulk water and has been actively researched.[2-9] The hydrogen bond network of the water inside the reverse micelle is pseudo-ordered due to the interactions both with other water molecules and the surfactant molecules at the reverse micelle surface and is further complicated by collective dynamics. The fluctuating structure of reverse micelles complicates analysis and separation of the independent and collective motions and interactions of the pseudo-crystalline molecular arrangements.[10,11]

The dynamic character of reverse micelles, making them difficult to characterize, is also responsible for providing the unique engineering opportunities that the scientific and engineering communities have been taking advantage of. The small sizes of reverse micelles (a few to a hundred nanometers) subject them to Brownian motion. Brownian

motion is the randomized motion of particles in a liquid (such as reverse micelles in an oil phase) as a result of the molecular-kinetic theory of heat. Brownian motion was named after botanist Robert Brown who observed the random motion of pollen particles in water.[12] The physics of Brownian motion was fully explained by Albert Einstein and then confirmed experimentally by Jean Baptiste Perrin.[13,14] Reverse micelles inevitably collide occasionally, as a result of Brownian motion, and two reverse micelles can fuse together temporarily before separating back into two distinct reverse micelles. The formation of the dimer structure by the fusion process allows for content exchange between the two reverse micelles, as illustrated in Figure 1-2. The concepts demonstrated in Figure 1-1 and Figure 1-2 are intensively studied, greatly expanded on, and utilized in novel ways with demonstrated advantages.

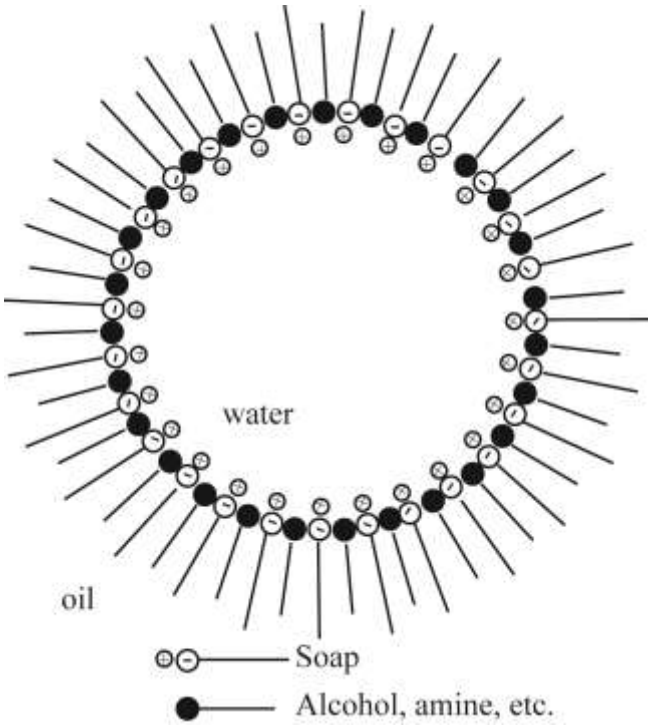

Figure 1 - 1. Schematic of the original reverse micelle structure concept, where a spherical water nanodomain is stabilized by surfactant at the interface of a bulk oil phase.

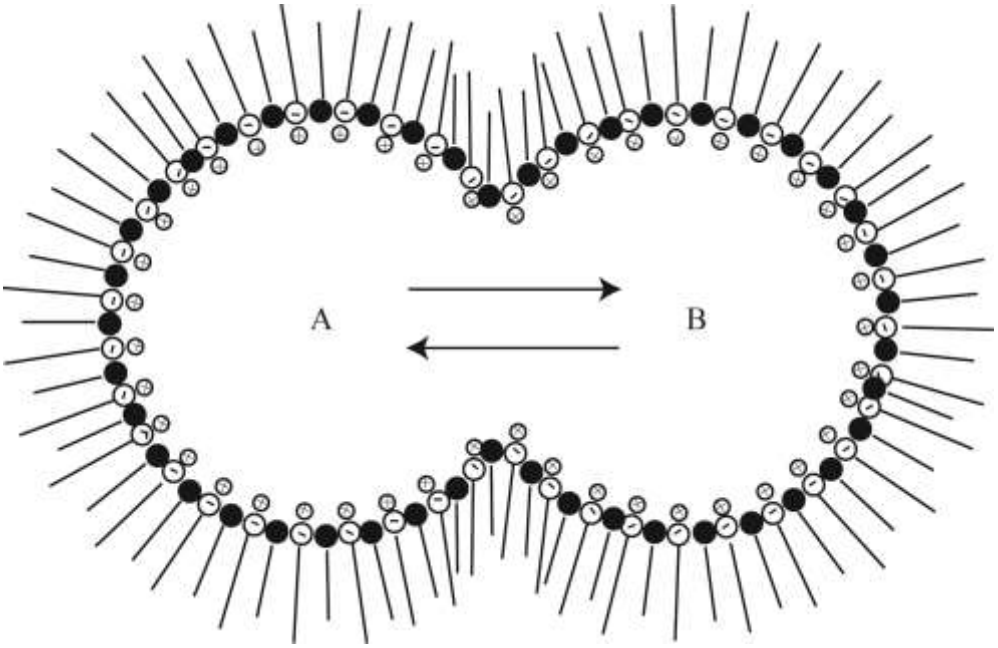

Figure 1 - 2. Schematic of content exchange between two reverse micelles, A and B, during a fusion-fission process.

1. Applications and Demonstrated Advantages

Scientists and engineers have been studying the use of reverse micelles for many applications. Table 1-I contains a list of common applications for which reverse micelles are directly applied, fundamentally explored, or already in use. The first example of inorganic nanoparticle synthesis by the reverse micelle technique was given by Boutonnet *et al*. and demonstrates that highly monodisperse metal catalyst particles of Pt, Pd, Rh, and Ir can be made.[108] Since the introduction of the reverse micelle synthesis technique, it is known as a technique capable of producing nanoparticles with a small and narrow size distribution. While this is a commonly cited advantage, controlled particle size and particle size distribution is well-established for other synthesis techniques as well. However, there are demonstrated advantages of reverse micelle synthesis that have become obvious from the intensive research efforts to obtain nanoparticles by this

technique. For example, room temperature synthesis of ceramic materials usually produces amorphous powders that require calcining to crystallize the material, but reverse micelle synthesis can be used to directly produce crystalline materials in some cases (see Table 1 - I).

Table 1 – I. Examples of Direct, Indirect, and Potential Applications of Reverse Micelles

Application	**References**
Biomedical characterization, diagnostics, and treatments	15-39
Biomimetic chemistry	40-63
Separation and extraction	41,46,64-70
Catalysis	40,42,71-85
Electronic, optic, and magnetic devices/sensors	79,86-107
Controlled nanoparticle synthesis	40,108-119
Polymerization	112,121-124
Microporous and mesoporous materials	125-130
Crystalline material synthesis near room temperature	110,127,128,131-138
Self-assembly	51,91,139-147

Petit and Pileni performed synthesis of CdS nanoparticles in reverse micelles and in hydrocarbon gels and studied them as catalysts for the photoreduction of methyl viologen (1,1′-dimethyl-4,4′-dipyridinium dichloride).[148] The yield of reduced viologen was five times higher for CdS in sodium docusate (AOT) reverse micelles when

compared to particles formed within AOT hydrocarbon gels and fifteen times higher in AOT reverse micelles when compared to CdS in bulk aqueous solution. The favorable reduction of the methyl violegen in AOT reverse micelles encapsulating CdS was attributed to interactions between cadmium ions and either AOT or hexametaphosphate molecules at the CdS particle surface, favoring sulfur vacancies, and the fact that local concentrations of methyl violegen are higher because of the small volumes of water in a reverse micelle solution compared to the bulk water solution. This suggests that accelerated catalytic reactions can be obtained within reverse micelles when the substrate is soluble in the reverse micelle water domains, but not the bulk organic phase because the partitioning to the low-volume water phase concentrates the substrate locally, as long as the catalyst surface-surfactant interactions do not deactivate or deteriorate the catalyst too significantly. Sun *et al.* prepared WO_3/ZrO_2 nanoparticles by the reverse micelle synthesis, incipient wet impregnation, and sol-gel methods.[149] The resulting powders were subjected to the same thermal treatments and placed in a fixed-bed reactor to test the catalytic activity of the nanoparticles for alkylation. The nanoparticles synthesized by the reverse micelle method had better performance than the nanoparticles produced by the other two methods and demonstrates that removal of the catalyst particles from the reverse micelle solution also can provide enhanced catalytic activity. Eriksson *et al.* have written a review article summarizing the synthesis and application of catalyst using the reverse micelle synthesis technique.[150]

The kinetics of the exchange process outlined in Figure 1-2 and consequences have been studied or discussed by many researchers.[46,87,112,116,151-157] Droplet exchange was found to occur a few orders of magnitude more slowly than the expected reverse

micelle collision rates, indicating that not all reverse micelle collisions result in fusion. This could be because collisions are prevented by electrostatic interactions between the reverse micelles.[158] Relevant time scales for reverse micelle dynamics and exchange have been discussed by Uskokovic and Drofenik.[118] Factors affecting the exchange rate include type of organic phase, type of surfactant, cosurfactants, water-to-surfactant ratio, temperature, pressure, salt concentration of polar phase, and reverse micelle size. The concept of interface rigidity/flexibility has been used to explain these effects. Variables that increase the interface rigidity, like strong interaction between a solubilized component and the surfactant at the interface for example, will cause a decrease in the exchange rate and vice versa. As little as 0.01-1% of collisions expected from Brownian motion might result in reverse micelle droplet exchange for a rigid surfactant film, whereas 10% might be expected for more flexible films. As a result, reaction rates and particle growth rates can be altered by several orders of magnitude when compared with the corresponding rates in bulk solution. Controlled particle growth rates provide opportunity to design particle size, particle size distribution, crystallinity, morphology, and crystal surface topography.[128,133,137,159-162]

Reddy *et al.* studied the ability of nanocrystalline nickel ferrite that was produced by either the reverse micelle synthesis method or hydrothermal synthesis to detect petroleum gas.[163] Both techniques presented advantages that would make them useful, depending on the particular application. The nickel ferrite prepared by hydrothermal synthesis had better gas sensitivity at low operating temperatures and was attributed to the presence of more oxygen vacancies. Overall, the nickel ferrite produced by the reverse micelle synthesis technique had a higher operating temperature, which results in

approximately six times faster response time than the material prepared by the hydrothermal method.

Shultz *et al.* demonstrated that ferrite nanoparticles produced by the reverse micelle synthesis method have enhanced behavior as magnetic resonance imaging (MRI) contrast agents when compared to a commercial MRI contrast agent.[102] The contrast agents were actually composite particles consisting of an iron core passivated by a ferrite shell that protected the interior from further oxidation. Similarly, many other researchers synthesized core-shell nanoparticles in reverse micelles to obtain multifunctional nanoparticles or for purposes of passivating the core.[16,24,29,164-190] Gold and silica shells are most common and can be functionalized for purposes of the self-assembling behaviors, bioinertness (silica), or attaching organic molecules such as enzymes or DNA, for example. Yang *et al.* demonstrated that photoluminescent CdTe quantum dots encapsulated in silica are highly efficient and the initial photoluminescent efficiency was stable because of the silica shell.[182] Lee *et al.* also demonstrated enhanced photostability of a fluorpolymer encapsulated in a silica shell having excellent potential for biosensing and biomedical engineering.[191]

Reverse micelles are also excellent candidates for biomolecular analysis.[192] The organic phase of reverse micelles is nearly transparent to terahertz electric waves. Furthermore, at low water to surfactant ratios, where the water is highly confined and not solvent-like, there is high probability of obtaining signals corresponding to an encapsulated biomolecule in the absence of noisy signal from a bulk solvent. Biomolecular NMR by encapsulating molecules into the interior of reverse micelles is also possible.[19,22,23,33] Alternatively, reverse micelles or nanoparticles synthesized by

reverse micelle synthesis can be functionalized to produce probes for biomolecular sensing and analysis.[24,193,194] Since reverse micelles create a biomimetic environment, it may also be possible to characterize bioreactions and bioprocesses within a reverse micelle containing solution.[53,195]

2. Effect of Dissolving Salts in the Reverse Micellar Polar Phase

The organic phase, surfactant, cosurfactant, polar phase, and relative quantities of each are all important parameters that affect reverse micelle size and stability. Either none or only one of the aforementioned variables will be intentionally altered per chapter of this thesis. Thus, any introduction related to these variables will be ignored here and introduced in the relevant chapter. Every chapter is based on the effect of salts dissolved into the polar phase on reverse micelle size and stability for the systems that are studied. Thus, a brief introduction on the effects that salts have on reverse micelle size and stability will be discussed in this section.

Maclay studied the effect of salts on the cloud point of nonionic surfactant emulsifiers, or point at which the microemulsion is destabilized and appears turbid.[196] The cloud point, or alternatively the solubilization capacity, was determined by titrating varying quantities of an electrolyte of constant concentration until a transition from transparent to a turbid solution is obtained. This became known as the titration method and has been the method of choice for many researchers studying the effect of electrolyte solutions on reverse micelle solutions. Maclay found that the cloud point decreases linearly with respect to the electrolyte concentration. The effect of alkali metal and multivalent cations was found to be roughly in the order of decreasing ion hydration. Aebi and Weibush also studied the effects that electrolyte solutions have on reverse

micelle solutions.[197] Their conclusion was that some of the water is bound to the surfactant so that it is no longer available to dissolve salts, resulting in lower solubility than expected. If the water-to-surfactant ratio was held constant, then the sodium chloride solubility limit remains at a constant concentration regardless of the concentration of reverse micelles in the bulk organic phase and is the premise for their conclusion.

Kitahara and Kon-no studied a few different electrolyte systems as well as acids and bases on the salting out effect with the intention of clarifying the mechanism of solubilization of water in the organic phase. [198] Furthermore, the solubilization behavior by nonionic surfactants and ionic surfactants were compared. Solubilization decreased when using ionic surfactant by the minor presence of every kind of salt and to a greater extent as concentration was increased. The solubilization in nonionic surfactants was not affected as much and depended on the type of electrolyte. Solubilization in the presence of salts and bases were similar when using nonionic surfactant and lower than the solubilization of acids. Solubilization was also improved by lowering the water-to-surfactant ratio and so decreased solubilization cannot be caused by the unavailability of water as Aebi and Weibush suggest because more water would be bound to the surfactant with decreasing water-to-surfactant ratio and would have caused a decrease in solubilization.[197]

Bedwell and Gulari studied electrolyte interactions in reverse micellar solutions and found that the electrolyte solution decreases the attractive interactions between reverse micelles and proposed hard-sphere like behavior when salts were added.[199] Reverse micelles of low water content behaved more like hard spheres than at high water

content. A hard-sphere model has been used by other researchers and can qualitatively fit small angle X-ray scattering patterns, but a quantitative scale indicates that the hard-sphere model is incorrect.[200,201] Furthermore, Bedwell and Gulari observed that the polydispersity of reverse micelle sizes decreases with added electrolyte. Thus, salt additions results in a more uniform reverse micellar solution and the reverse micelle have more rigid interfaces than the parent system without salt added. Increased interface rigidity is also observed by increasing the valence of the salt cation.[152]

Titration has been used by other researchers to study the effects of electrolyte solutions.[201-207] Instead of visual observation of the cloud point, electrical conductivity measurements have been made when high concentration of reverse micelles in the organic phase destabilize and form a bicontinuous structure, indicated by a sudden rise in conductivity of the solution.[78] These studies typically generate phase diagrams and sometimes indicate that the single-phase reverse micelle domain shrinks in area with salts added to the polar domain with respect to lower or no salt addition to the polar domain and suggests that salts decrease stability of the reverse micelles with respect to composition of the other components.

A geometric interpretation is often applied to average reverse micelle size and stability.[111,113,118,201,203,208-210] The geometric model considers that the curvature of the interface, and therefore size of the reverse micelle, is determined by the efficient packing of the surfactant around a curved interface according to its geometry. According to the geometric arguments, salts reduce the effective headgroup area of the surfactant by screening electrostatic interactions with adjacent surfactant molecules and explain reduction in reverse micelle size in the presence of an electrolyte solution. While

geometric arguments are made frequently, it is recognized that the relationship to reverse micelle stability is more complex.[201] Furthermore, electrostatic screening allows the headgroups to move into closer proximity to each other, but a decreasing reverse micelle size would generate a larger number of reverse micelles to preserve volume and increase the interfacial area so that the headgroups would move further apart on average. Thus, without significant compression of the polar phase, the geometric arguments cannot account for the decrease in reverse micelle size with increasing salt concentration that is commonly reported.

Practically every application for reverse micelles is influenced by dissolved salts. Salts have been found to influence the catalytic activity of enzymes entrapped in reverse micelles in different ways, sometimes enhancing or inhibiting activity.[52] Salts can also affect the configuration, and therefore stability, of biomolecules.[61] In another example, reverse micelle lithography was strongly influenced by electrolyte concentration and can be used to control the separation distance between the assembled reverse micelles.[104] When using reverse micelles for forward and backward extractions, salts can have beneficial and detrimental effects.[69] Salts must influence reverse micelle behavior to significantly influence each application. Determining the mechanisms by which salts affect reverse micelle behavior may explain the influence of reverse micelles on these various applications.

Reverse micellar solutions containing salts are the precursors to precipitating nanoparticles within the polar domain. It has been suggested that the precursor is very suitable if the solubility of the salt is not limited by specific interaction with either the surfactant or the solvent.[211] This is most likely for systems with nonionic surfactants, but

avoiding specific interactions is unlikely for many potential precursors for systems with ionic surfactants.[212] Thus, it is of paramount importance to understand the precursor limits within reverse micelles and is a primary motivation for studying the fundamental effects of salt concentration on reverse micelle size and stability. The titration method is not suitable because the salt concentration is a controlled variable (i.e. fixed). Calandra *et al.* demonstrated that the salt-to-surfactant corresponding to maximum solubilization of nickel chloride electrolyte solution varies with changing water-to-surfactant ratio in the water/AOT/isooctane system.[213] The specific mechanism by which the electrolyte solution affects reverse micelle stability was still not fully explained, but the concept of systematically changing the salt concentration while controlling other variables is more suitable for determining the specific effects that electrolyte solutions have on reverse micelle size and stability.

It is generally accepted that electrostatic forces between ions and the surfactant film influence the size and stability of reverse micelles.[113,118,156,214-216] However, a description of the electrostatic interactions using established theory and comparison to experiment is lacking, most likely because the assumptions used to develop the theory and intended use vary from the conditions within a reverse micelle. Comparing reverse micelle size and stability with systematic additions of salt to the Gouy-Chapman theory and Stern model is an important first step to determine the feasibility of using established theory to explain reverse micelle size and stability. It is worth mentioning that the interaction forces for curved surfaces (like the surfactant film of a reverse micelle for example) can be represented from the interaction energy of parallel plates so that reverse micelle behavior is likely comparable to the Gouy-Chapman theory.[217]

C. Surface Chemistry

The basic theory used throughout this thesis has been provided in an interfacial engineering textbook and the most important concepts are summarized here.[217] The purpose of the Gouy-Chapman theory is to understand the interaction of ions in an electrolyte solution with a charged surface. Analyzing the charge distribution surrounding a charged surface immersed in an electrolyte is the approach of the Gouy-Chapman theory. In the situation where an electrolyte solution is in contact with a charged surface, the ions are free to move through the volume of the solution in response to electrical fields, and the ions are also under the influence of thermal motion, an expression that incorporates two fundamental equations (the Poisson equation and the Boltzmann equation) to describe the interaction can be used.

The Poisson equation provides the relationship between the electrical potential Φ and charge density in vacuum and is given by:

$$\nabla^2\Phi = -\frac{\rho}{\varepsilon_o} \qquad (1)$$

The Boltzmann distribution expresses the compromise between molecular order and disorder. For the ions in solution, $z_i e\Phi$ represents the electrostatic energy of an ion of valence z_i at a point where the potential is Φ and e is the elementary charge constant. Then, the Boltzmann equation is:

$$c_i = c_{io}\exp\left(-\frac{z_i e\Phi}{kT}\right) \qquad (2)$$

where c_{io} is concentration of ions where $\Phi = 0$, which is usually taken as the bulk concentration. Near positively charged surface Φ is positive, and is negative when the charged surface is negative. Combining equation 1 and equation 2 gives the Poisson-

Boltzmann equation. The interest of this work is to focus on the variation of $\Phi(z)$ in the direction z away from a charged surface and the Poisson-Boltzman equation becomes:

$$\varepsilon_r \varepsilon_o \frac{d^2\Phi}{dz^2} = -\sum_i z_i e c_{io} \exp\left(-\frac{z_i e \Phi}{kT}\right) \qquad (3)$$

Situations in which $ze\Phi << kT$ are considered for an approximate solution to equation 3. The sum of positive and negative ion charge is zero because of the electroneutrality condition. Also, it is convenient to consider the following equation:

$$\kappa^2 = \sum_i \frac{(z_i e)^2 c_{io}}{\varepsilon_r \varepsilon_o kT} \qquad (4)$$

Using boundary conditions $\Phi \rightarrow \Phi_o$ as $z \rightarrow 0$ and $\Phi \rightarrow 0$ as z $\rightarrow \infty$ gives:

$$\Phi(z) = \Phi_o \exp(-\kappa z) \qquad (5)$$

which demonstrates that the electrostatic potential reduces exponentially with distance from a charged surface in an electrolyte at a rate determined by κ.

The quantity $1/\kappa$ has the dimension of length and is defined as the Debye screening length, or electrical double layer thickness, and is given by:

$$\frac{1}{k} = \left(\frac{e_r e_o kT}{1000 e^2 N_{AV} \sum_i z_i^2 c_{io}}\right)^{1/2} \qquad (6)$$

The Gouy-Chapman equation (equation 5) shows a reduction in the potential in the electrical double layer as a function of distance from a charged surface. Furthermore, based on equation 6, the higher the salt concentration and the higher the valence of the salt ions, the greater the electrical potential reduces a given distance away from the charged surface.

The Poisson-Boltzmann equation also leads to the relationship between surface charge density and potential at the charged surface and is given by:

$$\sigma_o = \varepsilon_r \varepsilon_o \kappa \Psi_o \qquad (7).$$

Overlap of two electrical double layers between a pair of charged surfaces separated by the distance on the order of $1/\kappa$ causes repulsion between them and the sum of these two overlapping electric potentials form a minimum between the two charged surfaces. The minimum will increase by increasing the salt concentration or ion valence if the distance between the two charged surfaces is held constant. Alternatively, if the overlapping potential remains constant, then the charged surfaces will move into closer proximity with increasing electrolyte concentration or higher valence because of compression of the two electrical double layers.

The Stern model provides one way to incorporate both finite ion size effects and ion-surface interactions into the electrical double layer model. This model divides the double layer into two segments via a hypothetical boundary located at a distance one ionic layer thick from the surface. This layer that is immediately in contact with the charged surface is known as the Stern layer and is treated as a capacitor. The thickness of the Stern layer is usually considered to be half of the distance between the charged surface and the surface of shear. The diffuse layer of the Gouy-Chapman theory extends from the shear plane, typically taken as twice the length of the Stern layer.

D. References

1. T.P. Hoar and J.H. Schulman, "Transparent Water-in-oil Dispersions: the Oleopathic Hydro-micelle," *Nature*, **152** [3847] 102-3 (1943).

2. R. Biswas, J. Furtado, and B. Bagchi, "Layerwise Decomposition of Water Dynamics in Reverse Micelles: A Simulation Study of Two-dimensional Infrared Spectrum," *J. Chem. Phys.*, **139** [14] 144906 11pp. (2013).

3. H. Murakami, T. Sada, M. Yamada, and M. Harada, "Nanometer-scale Water Droplet Free from the Constraint of Reverse Micelles at Low Temperatures," *Phys. Rev. B*, **88** [5] 052304 8pp. (2013).

4. T.H. van der Loop, M.R. Panman, S. Lotze, J. Zhang, T. Vad, H.J. Bakker, W.F.C. Sager, and S. Woutersen, "Structure and Dynamics of Water in Non-ionic Reverse Micelles: A Combined Time-resolved Infrared and Small Angle X-ray Scattering Study," *J. Chem. Phys.*, **137** [4] 044503 9pp. (2012).

5. R. Biswas, T. Chakraborti, B. Bagchi, and K.G. Ayappa, "Non-monotonic, Distance-dependent Relaxation of Water in Reverse Micelles: Propagation of Surface Induced Frustration along Hydrogen Bond Networks," *J. Chem. Phys.*, **137** [1] 014515 9pp. (2012).

6. T.Yu. Podlipskaya, A.I. Bulavcchenko, and L.A. Sheludyakova, "Properties of Water in Triton N-42 Reverse Micelles during the Solubilization of HCl Solutions According to FT-IR and Photon Correlation Spectroscopy," *J. Struct. Chem.*, **52** [5] 970-9 (2011).

7. I. Waluyo, D. Nordlund, U. Bergmann, L.G.M. Pettersson, and A. Nilsson, "Increased Fraction of Weakened Hydrogen Bonds of Water in Aerosol OT Reverse Micelles," *J. Chem. Phys.*, **131** [3] 031103 3pp. (2009).

8. D.E. Moilanen, E.E. Fenn, D. Wong, and M.D. Fayer, "Water Dynamics in Large and Small Reverse Micelles: from Two Ensembles to Collective Behavior," *J. Chem. Phys.*, **131** [1] 014704 9pp. (2009).

9. N.E. Levinger, and L.A. Swafford, "Ultrafast Dynamics in Reverse Micelles," *Annu. Rev. Phys. Chem.*, **60**, 385-406 (2009).

10. E.E. Fenn, D.B. Wong, and M.D. Fayer, "Water Dynamics in Small Reverse Micelles in Two Solvents: Two-dimensional Infrared Vibrational Echoes with Two-dimensional Background Subtraction," *J. Chem. Phys.*, **134** [5] 054512 11pp. (2011).

11. V.R. Vasquez, B.C. Williams, and O.A. Graeve, "Stability and Comparative Analysis of AOT/Water/Isooctane Revesre Micelle System Using Dynamic Light Scattering and Molecular Dynamics," *J. Phys. Chem. B*, **115** [12] 2979-87 (2011).

12. R. Brown, "Microscopical Observations of Active Molecules," *Edinburgh New Philos. J.*, **Jul-Sept.**, 358-71, (1828).

13. A. Einstein, "Über Die Von Der Molekularkinetischen Theorie der Wärme Geforderte Bewegung Von in Ruhenden Flüssigkeiten Suspendierten Teilchen," *Ann. Phys.,* **322** [8] 549-560 (1905).

14. J. Perrin, "Mouvement Brownien et Réalité Moléculaire," *Ann. Chim. Phys.*, **8** [18] 5-104 (1909).

15. E.M. Egorova and A.A. Revina, "Synthesis of Metallic Nanoparticles in Reverse Micelles in the Presence of Quercetin," *Colloids Surf., A*, **168** [1] 87-96 (2000).

16. S. Santra, R. Tapec, N. Theodoropoulou, J. Dobson, A. Hebard, and W. Tan, "Synthesis and Characterization of Silica-coated Iron Oxide Nanoparticles in Microemulsion: the Effect of Nonionic Surfactants," *Langmuir*, **17** [10] 2900-6 (2001).

17. C. Liu, B. Zou, A.J. Rondinone, and Z.J. Zhang, "Reverse Micelle Synthesis and Characterization of Superparamagnetic $MnFe_2O_4$ Spinel Ferrite Nanocrystallites," *J. Phys. Chem. B*, **104** [6] 1141-5 (2000).

18. Z. Ye, M. Tan, G. Wang, and J. Yuan, "Preparation, Characterization, and Time-resolved Fluorometric Application of Silica-coated Terbium(III) Fluorescent Nanoparticles," *Anal. Chem.*, **76** [3] 513-8 (2004).

19. M. Meier, A. Fink, and E. Brunner, "Reverse Micelles Dissolved in Supercritical Xenon: An NMR Spectroscopic Study," *J. Phys. Chem. B*, **109** [8] 3494-8 (2005).

20. Z. Ye, M. Tan, G. Wang, and J. Yuan, "Novel Fluorescent Europium Chelate-doped Silica Nanoparticles: Preparation, Characterization and Time-resolved Fluorometric Application," *J. Mater. Chem.*, **14** [5] 851-6 (2004).

21. X. Ren, X. Meng, and F. Tang, "Preparation of Ag-Au Nanoparticle and Its Application to Glucose Biosensor," *Sens. Actuators, B*, **110** [2] 358-63 (2005).

22. Z. Shi, R.W. Peterson, and A.J. Wand, "New Reverse Micelle Surfactant Systems Optimized for High-resolution NMR Spectroscopy of Encapsulated Proteins," *Langmuir*, **21** [23] 10632-7 (2005).

23. S. Doussin, N. Birlirakis, D. Georgin, F. Taran, and P. Berthault, "Novel Zwitterionic Reverse Micelles for Encapsulation of Proteins in Low-viscosity Media," *Chem. Eur. J.*, **12** [15] 4170-5 (2006).

24. J. L. Gong, J. H. Jiang, Y. Liang, G. L. Shen, and R. Q. Yu, "Synthesis and Characterization of Surface-enhanced Raman Scattering Tags with Ag/SiO_2 Core-shell Nanostructures Using Reverse Micelle Technology," *J. Colloid Interface Sci.*, **298** [2] 752-6 (2006).

25. Y. Kong, J. Peng, Z. Xin, B. Xue, B. Dong, F. Shen, and L. Li, "Selective Synthesis and Novel Properties of Single Crystalline α-$CoMoO_4$ Nanorods/Nanowhiskers," *Mater. Lett.,* **61** [10] 2109-12 (2007).

26. R. Venkatasubramanian, R.S. Srivastava, and R.D.K. Misra, "Comparative Study of Antimicrobial and Photocatalytic Activity in Titania Encapsulated Composite Nanoparticles with Different Dopants," *Mater. Sci. Technol.,* **24** [5] 589-95 (2008).

27. S.K. Basiruddin, A. Saha, N. Pradhan, and N.R. Jana, "Functionalized Gold Nanorod Solution via Reverse Micelle Based Polyacrylate Coating," *Langmuir,* **26** [10] 7475-81 (2010).

28. Y. Xiang, Y. Zhang, Y. Chang, Y. Chai, J. Wang, and R. Yuan, "Reverse-micelle Synthesis of Electrochemically Encoded Quantum Dot Barcodes: Application to Electronic Coding of a Cancer Marker," *Anal. Chem.,* **82** [3] 1138-41 (2010).

29. T. Jafari, A. Simchi, and N. Khakpash, "Synthesis and Cytotoxicity Assessment of Superparamagnetic Iron-gold Core-shell Nanoparticles Coated with Polyglycerol," *J. Colloid Interface Sci.,* **345** [1] 64-71 (2010).

30. F.N. Radwan, K.J. Carroll, and E.E. Carpenter, "Dual Mode Nanoparticles: CdS Coated Iron Nanoparticles," *J. Appl. Phys.,* **107** [9] 09B515 3pp. (2010).

31. G. Bhakta, R.K. Sharma, N. Gupta, S. Cool, V. Nurcombe, and A. Maitra, "Multifunctional Silica Nanoparticles with Potentials of Imaging and Gene Delivery," *Nanomed. Nanotechnology,* **7** [4] 472-9 (2011).

32. W. Gao, B. Sha, W. Zou, X. Liang, X. Meng, H. Xu, J. Tang, D. Wu, L. Xu, and H. Zhang, "Cationic Amylose-encapsulated Bovine Hemoglobin as a Nanosized Oxygen Carrier," *Biomaterials,* **32** [35] 9425-33 (2011).

33. R.W. Peterson, N.V. Nucci, and A.J. Wand, "Modification of Encapsulation Pressure of Reverse Micelles in Liquid Ethane," *J. Magn. Reson.,* **212** [1] 229-33 (2011).

34. Z. Song, R. Yuan, Y. Chai, W. Jiang, H. Su, X. Che, and X. Ran, "Simultaneous Immobilization of Glucose Oxidase on the Surface and Cavity of Hollow Gold Nanospheres as Labels for Highly Sensitive Electrochemical Immunoassay of Tumor Marker," *Biosens. Bioelectron.,* **26** [5] 2776-80 (2011).

35. S. Vrignaud, J.-P. Benoit, and P. Saulinier, "Strategies for the Nanoencapsulation of Hdrophilic Molecules in Polymer-based Nanoparticles," *Biomaterials,* **32** [33] 8593-604 (2011).

36. C. Ghatak, V.G. Rao, S. Mandal, R. Pramanik, S. Sarkar, P.K. Verma, and N. Sarkar, "Förster Resonance Energy Transfer among a Structural Isomer of Adenine and Various Coumarins inside a Nanosized Reverse Micelle," *Spectrochim. Acta, Part A*, **89**, 67-73 (2012).

37. C.-S. Lee, H.H. Chang, J. Jung, N.A. Lee, N.W. Song, and B.H. Chung, "A Novel Fluorescent Nanoparticle Composed of Fluorene Copolymer Core and Silica Shell with Enhanced Photostability," *Colloids Surf., B*, **91**, 219-25 (2012).

38. H. Murakami, Y. Toyota, T. Nishi, and S. Nashima, "Terhertz Absorption Spectrocopy of Protein-containing Reverse Micellar Solution," *Chem. Phys. Lett.*, **519-20**, 105-9 (2012).

39. L. Xue, F. Zou, Y. Zhao, X. Huang, and Y. Qu, "Nitrile Group as Infrared Probe for the Characterization of the Conformation of Bovine Serum Albumin Solubilized in Reverse Micelles," *Spectrochim. Acta, Part A*, **97**, 858-63 (2012).

40. J.H. Fendler, "Atomic and Molecular Clusters in Membrane Mimetic Chemistry," *Chem. Rev.*, **87** [5] 877-99 (1987).

41. E. Sheu, K.E. Goklen, T.A. Hatton, and S. H. Chen, "Small-angle Neutron Scattering Studies of Protein-reversed Micelle Complexes," *Biotechnol. Prog.*, **2** [4] 175-86 (1986).

42. C.P. Singh, D.O. Shah, and K. Holmberg, "Synthesis of Mono- and Diglycerides in Water-in-oil Microemulsions," *J. Am. Oil Chem. Soc.*, **71** [6] 583-7 (1994).

43. V. Papadimitriou, C. Petit, G. Cassin, A. Xenakis, and M.P. Pileni, "Lipase Catalyzed Esterification in AOT Reverse Micelles: A Structural Study," *Adv. Colloid Interface Sci.*, **54**, 1-16 (1995).

44. M.P. Pileni, J. Tanori, A. Filankembo, "Biomimetic Strategies for the Control of Size, Shape, and Self-organization of Nanoparticles," *Colloids Surf., A*, **123-124**, 561-73 (1997).

45. Y.-X. Chen, X.-Z. Zhang, K. Zheng, S.-M. Chen, Q.-C. Wang, and X.-X. Wu, "Protease-catalyzed Synthesis of Precursor Dipeptides of RGD with Reverse Micelles," *Enzyme Microb. Technol.*, **23** [3-4] 243-8 (1998).

46. S.P. Moulik and B.K. Paul, "Structure, Dynamics and Transport Properties of Microemulsions," *Adv. Colloid Interface Sci.*, **78** [2] 99-195 (1998).

47. S. Sarda, M. Heughebaert, and A. Lebugle, "Influence of the Type of Surfactant on the Formation of Calcium Phosphate in Organized Molecular Systems," *Chem. Mater.*, **11** [10] 2722-7 (1999).

48. A.M. Gonçalves, A.P. Serro, M.r. Aires-Barros, and J.M.S. Cabral, "Effects of Ionic Surfactants Used in Reversed Micelles on Cutinase Activity and Stability," *Biochim. Biophys. Acta*, **1480** [1-2] 92-106 (2000).

49. M.L.M. Fernandes, N. Krieger, A.M. Baron, P.P. Zamora, L.P. Ramos, and D.A. Mitchell, "Hydolysis and Synthesis Reactions Catalysed by *Thermomyces lanuginose* Lipase in the AOT/Isooctane Reversed Micellar System," *J. Mol. Catal. B*: *Enzym.*, **30** [1] 43-9 (2004).

50. S. Abel, M. Waks, W. Urbach, and M. Marchi, "Structure, Stability, and Hydration of a Polypeptide in AOT Reverse Micelles," *J. Am. Chem. Soc.*, **128** [2] 382-3 (2006).

51. H. Chen, B.H. Clarkson, K. Sun, J.F. Mansfield, "Self-assembly of Synthetic Hydroxyapatite Nanorods into an Enamel Prism-like Structure," *J. Colloid Interface Sci.*, **288** [1] 97-103 (2005).

52. M.A. Biasutti, E.B. Abuin, J.J. Silber, N.M. Correa, and E.A. Lissa, "Kinetics of Reactions Catalyzed by Enzymes in Solutions of Surfactants," *Adv. Colloid Interface Sci.*, **136** [1-2] 1-24 (2008).

53. A.K. Ganguli, J. Ahmed, S. Vaidya, and T. Ahmad, "Mimicking the Biomineralization of Aragonite (Calcium Carbonate) Using Reverse-micelles under Ambient Conditions," *J. Nanosci. Nanotechnol.*, **7** [6] 1760-7 (2007).

54. Y.-C. Hsiao, Y.-W. Lin, C.-K. Su, and B.-H. Chiang, "High Degree Polymerized Chitooligosaccharides Synthesis by Chitosanase in the Bulk Aqueous System and Reversed Micellar Microreactors," *Process Biochem.*, **43** [1] 76-82 (2008).

55. V. Dandavate, H. Keharia, and D. Madamwar, "Ethyl Isovalerate Synthesis Using *Candida rugosa* Lipase Immobilized on Silica Nanoparticles Prepared in Nonionic Reverse Micelles," *Process Biochem.*, **44** [3] 349-52 (2009).

56. S. Dasgupta and S. Bose, "Reverse Micelle-mediated Synthesis and Characterization of Tricalcium Phosphate Nanopowder for Bone Graft Applications," *J. Am. Ceram. Soc.*, **92** [11] 2528-36 (2009).

57. S. Dasgupta, A. Bandyopadhyay, and S. Bose, "Reverse Micelle-mediated Synthesis of Calcium Phosphate Nanocarriers for Controlled Release of Bovine Serum Albumin," *Acta Biomater.*, **5** [8] 3112-21 (2009).

58. J.-B. Brubach, A. Mermet, A. Filabozzi, A. Gerschel, D. Lairez, M.P. Krafft, and P. Roy, "Dependence of Water Dynamics Upon Confinement Size," *J. Phys. Chem. B*, **105** [2] 430-5 (2001).

59. L. Gebicka and E. Banasiak, "Interactions of Anionic Surfactants with Methemoglobin," *Colloids Surf., B,* **83** [1] 116-21 (2011).

60. C.F. Sailer, R.B. Singh, J. Ammer, E. Riedle, and I. Pugliesi, "Encapsulation of Dipehnylmethyl Phosphonium Salts in Reverse Micelles: Enhanced Biomolecular Reaction of the Photofragments," *Chem. Phys. Lett.*, **512** [1-3] 60-5 (2011).

61. J. Tian and A.E. García, "Simulations of the Confinement of Ubiquitin in Self-assembled Reverse Micelles," *J. Chem. Phys.*, **134** [22] 225101 11pp. (2011).

62. X. Cao, J. Yu, Z. Zhang, and S. Liu, "Bioactivity of Horseradish Peroxidase Entrapped in Silica Nanospheres," *Biosens. Bioelectron.*, **35** [1] 101-7 (2012).

63. A. Tiwari and A. Pandey, "Cyanobacterial Hdrogen Production – A Step Towards Clean Environment," *Int. J. Hydrogen Energ*, **37** [1] 139-50 (2012).

64. M. Goto, M. Kuroki, T. Ono, and F. Nakashio, "Protein Extraction by New Reversed Micelles with Di(Tridecyl) Phosphoric Acid," *Sep. Sci. Technol.*, **30** [1] 89-99 (1995).

65. D.S. Mathew and R-S. Juang, "Role of Alcohols in the Formation of Inverse Microemulsions and Back Extraction of Proteins/Enzymes in a Reverse Micellar System," *Sep. Purif. Methods*, **53** [3] 199-215 (2007).

66. A.B. Hemavathi, H.U. Hebbar, and K.S.M.S. Raghavvarao, "Reverse Micellar Extraction of Bromalain from *Ananas cosmosus* L. Merryl," *J. Chem. Technol. Biotechnol.*, **82** [11] 985-92 (2007).

67. Y. Fang, A. Bennett, and J. Liu, "Selective Transport of Amino Acids into the Gas Phase: Driving Forces for Amino Acid Solubilization in Gas-phase Reverse Micelles," *Phys. Chem. Chem. Phys.*, **13** [4] 1466-78 (2011).

68. C. Bauer, P. Bauduin, J.F. Dufrêche, T. Zemb, and O. Diat, "Liquid/Liquid Metal Extraction: Phase Diagram Topology Resulting from Molecular Interactions between Extractant, Ion, Oil and Water," *Eur. Phys. J. Spec. Top.*, **213** [1] 225-41 (2012).

69. T. Kinugasa, H. Kashima, S. Kumeno, S. Tanaka, and Y. Nishii, "Forward and Backward Extraction of Methylene Blue by Using AOT-isooctane Reversed Micellar Solution," *Sep. Sci. Technol.*, **47** [13] 19557-62 (2012).

70. S.H. Mohd-Setapar, S.N. Mohamad-Aziz, N.H. Harun, and S.H. Hussin, "Reverse Micelle Liquid-liquid Extraction of a Pharmaceutical Product," *Adv. Mater. Res.*, **545**, 240-4 (2012).

71. B.H. Robinson, "Colloid Chemistry: Applications of Microemulsions," *Nature*, **320** [6060] 309 (1986).

72. D.W. Matson, J.C. Linehan, J.G. Darab, and M.F. Buehler, "Nanophase Iron-based Liquefaction Catalysts: Synthesis, Characterization, and Model Compound Reactivity," *Energy Fuels*, **8** [1] 10-18 (1994).

73. F. Michel and M.P. Pileni, "Synthesis of Hydrophobic Ribonuclease by Using Reverse Micelles. Structural Study of AOT Reverse Micelles Containing Ribonuclease Derivatives," *Langmuir*, **10** [2] 390-4 (1994).

74. A.J. Zarur and J.Y. Ying, "Reverse Microemulsion Synthesis of Nanostructured Complex Oxides for Catalytic Combustion," *Nature*, **403** [6765] 65-7 (2000).

75. S.-S. Hong, M.S. Lee, S.S. Park, and G.-D. Lee, "Synthesis of Nanosized TiO_2/SiO_2 Particles in the Microemulsion and Their Photocatalytic Activity on the Decomposition of p-Nitrophenol," *Catal. Today*, **87** [1-4] 99-105 (2003).

76. A. Martínez-Arias, M. Fernández-García, A.-B. Hungría, J.C. Conesa, and G. Munuera, "Spectroscopic Characterization of Heterogeneity and Redox Effects in Zirconium-cerium (1:1) Mixed Oxides Prepared by Microemulsion Methods," *J. Phys. Chem. B*, **107** [12] 2667-77 (2003).

77. S. Eriksson, U. Nylén, S. Rojas, and M. Boutonnet, "Preparation of Catalysts from Microemulsions and Their Applications in Heterogeneous Catalysis," *Appl. Catal., A*, **265** [2] 207-19 (2004).

78. A.E. Giannakas, A.K. Ladavos, and P.J. Pomonis, "Preparation, Characterization, and Investigation of Catalytic Activity for NO + CO Reaction of $LaMnO_3$ and $LaFeO_3$ Perovskites Prepared via Microemulsion Method," *Appl. Catal., B*, **49** [3] 147-58 (2004).

79. M. Yuasa, K. Shimanoe, Y. Teraoka, and N. Yamazoe, "Preparation of Carbon-supported Nano-sized $LaMnO_3$ Using Reverse Micelle Method for Energy-saving Oxygen Reduction Cathode," *Catal. Today*, **126** [3] 313-19 (2007).

80. M. Ghiaci, H. Aghaei, and A. Abbaspur, "Size-controlled Synthesis of ZrO_2-TiO_2 Nanoparticles Prepared via Reverse Micelle Method Investigation of Particle Size Effect on the Catalytic Performance in Vapor Phase Beckmann Rearrangement," *Mater. Res. Bull.*, **43** [5] 1255-62 (2008).

81. Y. Qian, W. Wen, P.A. Adcock, Z. Jiang, N. Hakim, M.S. Saha, and S. Mukerjee, "PtM/C Catalyst Prepared Using Reverse Micelle Method for Oxygen Reduction Reaction in PEM Fuel Cells," *J. Phys. Chem.*, **112** [4] 1146-57 (2008).

82. G. Prieto, A. Martínez, P. Concepción, and R. Moreno-Tost, "Cobalt Particle Size Effects in Fischer-Tropsch Synthesis: Structural and *In Situ* Spectroscopic Characterization on Reverse Micelle-synthesized Co/ITQ-2 Model Catalysts," *J. Catal.*, **266** [1] 129-44 (2009).

83. C. An, R. Wang, S. Wang, and X. Zhang, "Converting AgCl Nanocubes to Sunlight-driven Plasmonic AgCl:Ag Nanophotocatalyst with High Activity and Durability," *J. Mater. Chem.*, **21** [31] 11532-6 (2011).

84. Z.-H. Lu, H.-L. Jiang, M. Yadav, K. Aranishi, and Q. Xu, "Synergistic Catalysis of Au-Co@SiO_2 Nanospheres in Hydrolytic Dehydrogenation of Ammonia Borane for Chemical Hydrogen Storage," *J. Mater. Chem.*, **22** [11] 5065-71 (2012).

85. S.T. Hussain, Rashid, D. Anjum, A. Siddiqa, and A. Badshah, "Synthesis of Visible Light Driven Cobalt Tailored Ag_2O/TiON Nanophotocatalyst by Reverse Micelle Processing for Degradation of Eriochrome Black T," *Mater. Res. Bull.*, **48** [2] 705-14 (2013).

86. V. Chhabra, M. Lal, A.N. Maitra, and P. Ayyub, "Preparation of Ultrafine High Density Gamma Ferric Oxide Using Aerosol OT Microemulsion and Its Characterization," *Colloid Polym. Sci.*, **273** [10] 939-46 (1995).

87. V. Pillai, P. Kumar, M.J. Hou, P. Ayyub, and D.O. Shah, "Preparation of Nanoparticles of Silver Halides, Superconductors and Magnetic Materials Using Water-in-oil Microemulsions as Nano-reactors," *Adv. Colloid Interface Sci.*, **55** [1] 241-69 (1995).

88. J. Tanori, N. Duxin, C. Petit, I. Lisiecki, P. Veillet, and M.P. Pileni, "Synthesis of Nanosize Metallic and Alloyed Particles in Ordered Phases," *Colloid Polym. Sci.*, **273** [9] 886-92 (1995).

89. X.M. Lin, C.M. Sorensen, K.J. Klabunde, and G.C. Hajipanayis, "Control of Cobalt Nanoparticle Size by Germ-growth Method in Inverse Micelle System: Size-dependent Magnetic Properties," *J. Mater. Res.*, **14** [4] 1542-7 (1999).

90. F. Parapour, D.F. Kelley, and R.S. Williams, "Spectrocopy of Eu^{3+}-doped PtS_2 Nanoclusters," *J. Phys. Chem.*, **102** [41] 7971-7 (1998).

91. M.P. Pileni, A. Taleb, and C. Petit, "Silver Metal Nanosized Particles: Control of Particle Size, Self Assemblies in 2D and 3D Superlattices and Optical Properties," *J. Dispersion Sci. Technol.*, **19** [2-3] 185-206 (1998).

92. M. Meyer, C. Wallberg, K. Kurihara, and J.H. Fendler, "Photosensitized Charge Separation and Hydrogen Production in Reversed Micelle Entrapped Platinized

Colloidal Cadmium Sulphide," *J. Chem. Soc., Chem. Commun.*, **1984** [2] 90-1 (1984).

93. E.E. Carpenter, C. Sangregorio, and C.J. O'Connor, "Synthesis of Antiferromagnetic Macromolecular Particles," *Mol. Cryst. Liq. Cryst.*, **334** [1] 641-9 (1999).

94. P.A. Dresco, V.S. Zaitsev, R.J. Gambino, and B. Chu, "Preparation and Properties of Magnetite and Polymer Magnetite Nanoparticles," *Langmuir*, **15** [6] 1945-51 (1999).

95. J.A. Johnson, M.-L. Saboungi, P. Thiyagarajan, R. Csencsits, and D. Meisel, "Selenium Nanoparticles: A Small-angle Neutron Scattering Study," *J. Phys. Chem. B*, **103** [1] 59-63 (1999).

96. S. Li, V.T. John, G.C. Irvin, S.H. Rachakonda, G.L. McPherson, and C.J. O'Connor, "Synthesis and Magnetic Properties of a Novel Ferrite Organogel," *J. Appl. Phys.*, **85** [8] 5965-7 (1999).

97. P.N. Prasad, G.S. He, M.P. Joshi, J. Swiatkiewicz, G. Manchala, M. Lal, A. Biswas, and K.-S. Kim, "Nanostructured Materials and Composites for Optical Power Limiting," *Nonlinear Opt.*, **21**, 39-47 (1999).

98. C.M. Bender, J.M. Burlitch, D. Barber, and C. Pollock, "Synthesis and Fluorescence of Neodymium-doped Barium Fluoride Nanoparticles," *Chem. Mater.*, **12** [7] 1969-76 (2000).

99. B.A. Smith, J.Z. Zhang, A. Joly, and J. Liu, "Luminescence Decay Kinetics of Mn^{2+}-doped ZnS Nanoclusters Grown in Reverse Micelles," *Phys. Rev. B*, **62** [3] 2021-8 (2000).

100. C.-H. Lu and S.K. Saha, "Synthesis of Spinel Lithium Manganate Powdesr Using an Inverse Emulsion Process," *J. Mater. Sci. Lett.*, **20** [20] 1841-3 (2001).

101. K. M. Reddy, L. Satyanarayana, S.V. Manorama, R.D.K. Misra, "A Comparative Study of the Gas Sensing Behavior of Nanostructured Nickel Ferrite Synthesized by Hydrothermal and Reverse Micelle Techniques," *Mater. Res. Bull.*, **39** [10] 1491-8 (2004).

102. M.D. Shultz, S. Calvin, P.P. Fatouros, S.A. Morrison, E.E. Carpenter, "Enhanced Ferrite Nanoparticles as MRI Contrast Agents," *J. Magn. Magn. Mater.*, **311** [1] 464-8 (2007).

103. S. Choi, S.-W. Tae, J.-H. Seo, and H.-K. Jung, "Preparation of Blue-emitting $CaMgSi_2O_6:Eu^{2+}$ Phosphors in Reverse Micellar System and Their Application to

Transparent Emissive Display Devices," *J. Solid State Chem.*, **184** [6] 1540-4 (2011).

104. V.V. Terkhin, O.V. Dement'eva, A.V. Zaitseva, and V.M. Rudoy, "Diblock Copolymer Micellar Lithography:1. Intermicellar Interactions and Pathways for Control of Monomicellar Film Structure," *Colloid J.*, **73** [5] 697-706 (2011).

105. J.-U. Kim, M.-H. Lee, and H. Yang, "Synthesis of $Zn_{1-x}Cd_xS$:Mn/ZnS Quantum Dots and Their Application to Light-emitting Diodes," *Nanotechnology*, **19** [46] 465605 5pp. (2008).

106. T. Forestier, A. Kaiba, S. Pechev, D. Denux, P. Guionneau, C. Etrillard, N. Daro, E. Freysz, and J.-F. Létard, "Nanoparticles of $[Fe(NH_2\text{-trz})_3]Br_2\text{-}3H_2O$ (NH_2-trz=2-amino-1,2,4-triazole) Prepared by the Reverse Micelle Technique: Influence of Particle and Coherent Domain Sizes on Spin-crossover Properties," *Chem. Eur. J.*, **15** [25] 6122-30 (2009).

107. B.-J. Hwang, K.-F. Hsu, S.-K. Hu, M.-Y. Cheng, T.-C. Chou, S.-Y. Tsay, R. Santhanam, "Template-free Reverse Micelle Process for the Synthesis of a Rod-like $LiFePO_4$/C Composite Cathode Material for Lithium Batteries," *J. Power Sources*, **194** [1] 515-9 (2009).

108. M. Boutonnet, J. Kizling, P. Stenius, and G. Maire, "The Preparation of Monodisperse Colloidal Metal Particles from Microemulsions," *Colloids. Surf.*, **5** [3] 209-25 (1982).

109. M.P. Pileni, I. Lisiecki, L. Motte, C. Petit, J. Cizeron, N. Moumen, and P. Lixon, "Synthesis "In Situ" of Nanoparticles in Reverse Micelles," *Prog. Colloid Polym. Sci.*, **93**, 1-9 (1993).

110. C.B. Murray, D.J. Norris, and M.G. Bawendi, "Synthesis and Characterization of Nearly Monodisperse CdE (E = S, Se, Te) Semiconductor Nanocrystallites," *J. Am. Chem. Soc.*, **115** [9] 8706-15 (1993).

111. M.P. Pileni, "Reverse Micelles as Microreactors," *J. Phys. Chem.*, **97** [27] 6961-73 (1993).

112. J. Eastoe and B. Warne, "Nanoparticle and Polymer Synthesis in Microemulsions," *Curr. Opin. Colloid Interface Sci.*, **1** [6] 800-5 (1996).

113. J.H. Adair, T. Li, T. Kido, K. Havey, J. Moon, J. Mecholsky, A. Morrone, D.R. Talham, M.H. Ludwig, and L. Wang, "Recent Developments in the Prepration and Properties of Nanometer-size Spherical and Platelet-shaped Particles and Composite Particles," *Mater. Sci. Eng., R* **23** [4-5] 139-242 (1998).

114. M.I. Freedhoff, A.P. Marchetti, and G.L. McLendon, "Optical Properties of Nanocyrstalline Silver Halides," *J. Lumin.,* **70** [1-6] 400-413 (1996).

115. L. Qi, J. Ma, H. Cheng, and Z. Zhao, "Synthesis and Characterization of Mixed CdS-ZnS Nanoparticles in Reverse Micelles," *Colloids Surf., A,* **111** [3] 195-202 (1996).

116. W.F.C. Sager, "Controlled Formation of Nanoparticles from Microemulsions," *Curr. Opin. Colloid Interface Sci.,* **3** [3] 276-83 (1998).

117. K. Holmberg, "Surfactant-templated Nanomaterials Synthesis, "Surfactant-templated Nanomaterials Synthesis," *J. Colloid Interface Sci.,* **274** [2] 355-64 (2004).

118. V. Uskoković and M. Drofenik, "Synthesis of Materials within Reverse Micelles," *Surf. Rev. Lett.,* **12** [2] 239-77 (2005).

119. J. Eastoe, M.J. Hollamby, and L. Hudson, "Recent Advances in Nanoparticle Synthesis with Reversed Micelles," *Adv. Colloid Interface Sci.,* **128-130**, 5-15 (2006).

120. A. Hammouda, Th. Gulik, and M.P. Pileni, "Synthesis of Nanosize Latexes by Reverse Micelle Polymerization," *Langmuir,* **11** [10] 3656-9 (1995).

121. A. Koné, M.M. Dieng, J.-J. Aaron, M. Lazerges, M. Jouini, S. Aeiyach, and P.C. Lacaze, "AOT Reverse Micelle, A New Organized Medium for the Electrosynthesis of Polyaromatic Hydrocarbons; Application to the Electropolymerization of Biphenyl," *Synth. Met.,* **150** [3] 227-39 (2005).

122. D. Han, Y. Chu, L. Yang, Y. Liu, and Z. Lv, "Reversed Micelle Polymerization: A New Route for the Synthesis of DBSA-polyaniline Nanoparticles," *Colloids Surf., A,* **259** [1-3] 179-87 (2005).

123. S. Jiao, J. Tu, C. Fan, J. Hou, and D.J. Fray, "Electrochemically Assembling of a Porous Nano-polyaniline Network in a Reverse Micelle and its Application in a Supercapacitor," *J. Mater. Chem.,* **21** [25] 9027-30 (2011).

124. L. Hu, J. Tu, S. Jiao, J. Hou, H. Zhu, and D.J. Fray, "*In Situ* Electrochemical Polymerization of a Nanorod-PANI-graphene Composite in a Reverse Micelle Electrolyte and its Application in a Supercapacitor," *Phys. Chem. Chem. Phys.,* **14** [45] 15652-6 (2012).

125. X.X. Zhu, K. Banana, and R. Yen, "Pore Size Control in Cross-linked Polymer Resins by Reverse Micellar Imprinting," *Macromolecules,* **30** [10] 3031-5 (1997).

126. T.V. Anuradha and S. Ranganathan, "Synthesis of Mesoporous Materials Based on Titanium(IV)Oxide and Titanium Nitride," *Nanostruct. Mater.*, **12** [5] 1063-9 (1999).

127. R. Singh and P.K. Dutta, "Cyrstal Growth of Faujasitic Microporous Zincophosphate Crystals Using Reverse Micelles as Reactants," *Langmuir,* **16** [9] 4148-53 (2000).

128. R. Singh, J. Doolitle, Jr., M.A. George, and P.K. Dutta, "Novel Surface Structure of Microporous Faujasitic-like Zincophosphate Crystals Grown in Reverse Micelles," *Langmuir,* **18** [21] 8193-7 (2002).

129. R. Palkovits and S. Kaskel, "Reverse Micelle-mediated Synthesis of Zirconia with Enhanced Surface Area Using Alcothermal Treatment," *J. Mater. Chem.*, **16** [4] 391-4 (2006).

130. F. Gu, Z. Wang, D. Han, C. Shi, and G. Guo, "Reverse Micelles Directed Synthesis of Mesoporous Ceria Nanostructures," *Mater. Sci. Eng., B,* **139** [1] 62-8 (2007).

131. K.S.N. Reddy, L.M. Salvati, P.K. Dutta, P.B. Abel, K.I. Suh, "Reverse Micelle Based Growth of Zincophosphate Sodalite: Examination of Crystal Growth," *J. Phys. Chem.*, **100** [23] 9870-80 (1996).

132. P.K. Dutta, M. Jakupca, K.S.N. Reddy, and L. Salvati, "Controlled Growth of Microporous Crystals Nucleated in Reverse Micelles," *Nature*, **374** [6517] 44-6 (1995).

133. L. Qi, J. Ma, H. Cheng, and Z. Zhao, "Reverse Micelle Formation of $BaCO_3$ Nanowires," *J. Phys. Chem. B,* **101** [18] 3460-3 (1997).

134. C.E. Bunker, B.A. Harruff, P. Pathak, A. Payzant, L.F. Allard, and Y.-P. Sun, "Formation of Cadmium Sulfide Nanoparticles in Reverse Micelles: Extreme Sensitivity to Preparation Procedure," *Langmuir*, **20** [13] 5642-44 (2004).

135. S.A. Morrison, C.L. Cahill, E.E. Carpenter, S. Calvin, R. Swaminathan, M.E. McHenry, and V.G. Harris, "Magnetic and Structural Properties of Nickel Zinc Ferrite Nanoparticles Synthesized at Room Temperature," *J. Appl. Phys.*, **95** [11] 6392-5 (2004).

136. Y. Lee, J. Lee, C.J. Be, J.-G. Park, H.-J. Noh, J.-H. Park, and T. Hyeon, "Large-scale Synthesis of Uniform and Crystalline Magnetite Nanoparticles Using Reverse Micelles as Nanoreactors under Reflux Conditions," *Adv. Funct. Mater.*, **15** [3] 503-9 (2005).

137. J.-L. Lemyre and A.M. Ritcey, "Synthesis of Lanthanide Fluoride Nanoparticles of Varying Shape and Size," *Chem. Mater.*, **17** [11] 3040-3 (2005).

138. N. Wang, X. Wang, L. Yang, and H. Chen, "Morphology and Size Control of Nanocalcium Carbonate Crstyallised in Reverse Micelle System with Cationic Surfactant Cetyltrimethylammonium Bromide," *Micro Nano Lett.*, **8** [2] 94-8 (2013).

139. L. Motte, F. Billoudet, E. Lacaze, and M.-P. Pileni, "Self-organization of Size-selected Nanoparticles into Three-dimensional Superlattices," *Adv. Mater.*, **8** [12] 10-18-20 (1996).

140. M.P. Pileni, "Nanosized Particles Made in Colloidal Assemblies," *Langmuir*, **13** [13] 3266-76 (1997).

141. A. Taleb, C. Petit, and M.P. Pileni, "Synthesis of Highly Monodisperse Silver Nanoparticles from AOT Reverse Micelles: A Way to 2D and 3D Self-organization," *Chem. Mater.*, **9** [4] 950-9 (1997).

142. C.T. Seip and C.J. O'Connor, "The Fabrication and Organization of Self-assembled Metallic Nanoparticles Formed in Reversed Micelles," *Nanostruct. Mater.*, **12** [1-4] 183-6 (1999).

143. C. Petit, A. Taleb, and M.P. Pileni, "Cobalt Nanosized Particles Organized in a 2D Superlattice: Synthesis, Characterization, and Magnetic Properties," *J. Phys. Chem.*, **103** [11] 1805-10 (1999).

144. M. Li, H. Schnablegger, and S. Mann, "Coupled Synthesis and Self-assembly of Nanoparticles to Give Structures with Controlled Organization," *Nature*, **402** [6760] 393-5 (1999).

145. C.L. Kitchens, M.C. McLeod, and C.B. Roberts, "Chloride Ion Effects on Synthesis and Directed Assembly of Copper Nanoparticles in Liquid and Compressed Alkane Microemulsions," *Langmuir*, **21** [11] 5166-73 (2005).

146. S. Krishnamoorthy, K.K. Manipaddy, and F.L. Yap, "Wafer-level Self-organized Copolymer Templates for Nanolithography with Sub-50 nm Feature and Spatial Resolutions," *Adv. Funct. Mater.*, **21** [6] 1102-12 (2011).

147. R.K. Gupta, S. Krishnamoorthy, D.Y. Kusuma, P.S. Lee, and M.P. Srinivasan, "Enhancing Charge-storage Capacity of Non-volatile Memory Devices Using Template-directed Assembly of Gold Nanoparticles," *Nanoscale*, **4** [7] 2296-300 (2012).

148. C. Petit and M.P Pileni, "Synthesis of Cadmium Sulfide in Situ in Reverse Micelles and in Hydrocarbon Gels," *J. Phys. Chem.*, **92** [8] 2282-6 (1988).

149. W. Sun, L. Xu, Y. Chu, and W. Shi, "Controllable Synthesis, Characterization, and Catalytic Properties of WO_3/ZrO_2 Mixed Oxides Nanoparticles," *J. Colloid Interface Sci.*, **266** [1] 99-106 (2003).

150. S. Eriksson, U. Nylên, S. Rojas, and M. Boutonnet, "Preparation of Catalysts from Microemulsions and Their Applications in heterogeneous Catalysis," *Appl. Catal., A,* **265** [2] 207-19 (2004).

151. P.D.I. Fletcher, A.M. Howe, and B.H. Robinson, "The Kinetics of Solubilisate Exchange between Water Droplets of a Water-in-oil Microemulsion," *J. Chem. Soc., Faraday Trans.*, **83** [4] 985-1006 (1987).

152. R.P. Bagwe and K.C.Khilar, "Effects of the Intermicellar Exchange Rate and Cations on the Size of Silver Chloride Nanoparticles Formed in Reverse Micelles of AOT," *Langmuir*, **13** [24] 6432-8 (1997).

153. R.P. Bagwe and K.C. Khilar, "Effects of Intermicellar Exchange Rate on the Formation of Silver Nanopartilces in Reverse Microemulsions of AOT," *Langmuir,* **16** [3] 905-10 (2000).

154. J.P. Cason, K. Khambaswadkar, and C.B. Roberts, "Supercritical Fluid and Compressed Solvent Effects on Metallic Nanoparticle Synthesis in Reverse Micelles," *Ind. Eng. Chem. Res.*, **39** [12] 4749-55 (2000).

155. M.L. Curri, A. Agostiano, L. Manna, M.D. Monica, M. Ctalanao, L. Chiavarone, V. Spagnolo, and M. Lugara, "Synthesis and Characterization of CdS Nanoclusters in a Quaternary Microemulsion: the Role of Cosurfactant," *J. Phys. Chem. B,* **104** [35] 8391-7 (2000).

156. B.L. Cushing, V.L. Kolesnichernko, and C.J. O'Connor, "Recent Advances in the Liquid-phase Syntheses of Inorganic Nanoparticles," *Chem. Rev.*, **104** [9] 3893-946 (2004).

157. M.G. Spirin, S.B. Brichkin, and V.F. Razumov, "Specific Features of the Preparation of AgI Nanocrystals in Reverse Micelles of Aerosol OT," *Colloid J.*, **66** [4] 477-81 (2004).

158. M.F. Hsu, E.R. Dufresne, and D.A. Weitz, "Charge Stabilization in Nonpolar Solvents," *Langmuir,* **21** [11] 4881-7 (2005).

159. U. Natarajan, K. Handique, A. Mehra, J.R. Bellare, and K.C. Khilar, "Ultrafine Metal Particle Formation in Reverse Micellar Systems: Effects of Intermicellar Exchange on the Formation of Particles," *Langmuir*, **12** [11] 2670-8 (1996).

160. C.-L. Chiang, M.-B. Hsu, and L.-B. Lai, "Control of Nucleation and Growth of Gold Nanoparticles in AOT/Span80/Isooctane Mixed Reverse Micelles," *J. Solid State Chem.*, **177** [11] 3891-5 (2004).

161. S. Sadasivan, D. Khushanlani, and S. Mann, "Synthesis of Calcium Phosphate Nanofilaments in Reverse Micelles," *Chem. Mater.*, **17** [10] 2765-70 (2005).

162. S. Vaidya, P. Rastogi, S. Agarwal, S.K. Gupta, T. Ahmad, A.M. Antonelli, Jr., K.V. Ramanujachary, S.E. Lofland, and A.K. Ganguli, "Nanospheres, Nanocubes, and Nanorods of Nickel Oxalate: Control of Shape and Size by Surfactant and Solvent," *J. Phys. Chem.*, **112** [33] 12610-15 (2008).

163. K.M. Reddy, L. Satyanarayana, S.V. Manorama, and R.D.K. Misra, "A Comparative Study of the Gas Sensing Behavior of Nanostructured Nickel Ferrite Synthesized by Hydrothermal and Reverse Micelle Techniques," *Mater. Res. Bull.*, **39** [10] 1491-8 (2004).

164. C.J. O'Connor, C. Seip, C. Sangregorio, E. Carpenter, S. Li, G. Irvin, and V.T. John, "Nanophase Magnetic Materials: Synthesis and Properties," *Mol. Cryst. Liq. Cryst.*, **335** [1] 423-42 (1999).

165. C.T. Seip and C.J. O'Connor, "The Fabrication and Organization of Self-assembled Metallic Nanoparticles Formed in Reverse Micelles," *Nanostruct. Mater.*, **12** [1-4] 183-6 (1999).

166. E.E. Carpenter, "Iron Nanoparticles as Potential Magnetic Carriers," *J. Magn. Magn. Mater.*, **225** [1-2] 17-20 (2001).

167. J. Lin, W. Zhou, A. Kumbhar, J. Wiemann, J. Fang, E.E. Carpenter, and C.J. O'Connor, "Gold-coated Iron (Fe@Au) Nanoparticles: Synthesis, Characterization, and Magnetic Field-induced Self-assembly," *J. Solid State Chem.*, **159** [1] 26-31 (2001).

168. C.J. O'Connor, V. Kolesnichenko, E. Carpenter, C. Sangreorio, W. Zhou, A. Kumbhar, J. Sims, and F. Agnoli, "Fabrication and Properties of Magnetic Particles with Nanometer Dimensions," *Synth. Met.*, **122** [3] 547-57 (2001).

169. W.L. Zhou, E.E. Carpenter, J. Lin, A. Kumbhar, J. Sims, and C.J. O'Connor, "Nanostructures of Gold Coated Iron Core-shell Nanoparticles and the Nanobands Assembled under Magnetic Field," *Eur. Phys. J. D*, **16** [1] 289-92 (2001).

170. T. Tago, Y. Shibata, T. Hatsuta, K. Miyajima, M. Kishida, S. Tashiro, and K. Wakabayashi, "Synthesis of Silica-coated Rhodium Nanoparticles in Reversed Micellar Solution," *J. Mater. Sci.*, **37** [5] 977-82 (2002).

171. M. Wu, Y.D. Zhang, S. Hui, T.D. Xiao, S. Ge, W.A. Hines, and J.I. Budnick, "Structure and Magnetic Properties of SiO_2-coated Co Nanoparticles," *J. Appl. Phys.*, **92** [1] 491-5 (2002).

172. E.E. Carpenter, S. Calvin, R.M. Stroud, and V.G. Harris, "Passivated Iron as Core-shell Nanoparticles," *Chem. Mater.*, **15** [17] 3245-6 (2003).

173. T. Kinoshita, S. Seino, K. Okitsu, T. Nakayama, T. Nakagawa, and T.A. Yamamoto, "Magnetic Evaluation of Nanostructure of Gold-iron Composite Particles Synthesized by a Reverse Micelle Method," *J. Alloys Compd.*, **359** [1-2] 46-50 (2003).

174. T. Tago, S. Tashiro, Y. Hashimoto, K. Wakabayashi, and M. Kishida, "Synthesis and Optical Properties of SiO_2-coated CeO_2 Particles," *J. Nanopart. Res.*, **5** [1-2] 55-60 (2003).

175. C.R. Vestal, and Z.J. Zhang, "Synthesis and Magnetic Characterization of Mn and Co Spinel Ferrite-silica Nanoparticles with Tunable Magnetic Core," *Nano Lett.*, **3** [12] 1739-43 (2003).

176. S.-J. Cho, S.M. Kauzlarich, J. Olamit, K. Liu, F. Grandjean, L. Rebbouh, and G.J. Long, "Characterization and Magnetic Properties of Core/Shell Structured Fe/Au Nanoparticles," *J. Appl. Phys.*, **95** [11] 6804-6 (2004).

177. Z. Ye, M. Tan, G. Wang, and J. Yuan, "Preparation, Characterization, and Time-resolved Fluorometric Application of Silica-coated Terbium(III) Fluorescent Nanoparticles," *Anal. Chem..*, **76** [3] 513-8 (2004).

178. S.-J. Cho, J.-C. Idrobo, J. Olamit, K. Liu, N.D. Browning, and S.M. Kauzlarich, "Growth Mechanism and Oxidation Resistance of Gold-coated Iron Nanoparticles," *Chem. Mater.*, **17** [12] 3181-6 (2005).

179. S.-J. Cho, A.M. Shahin, G.J. Long, J.E. Davies, K. Liu, F. Grandjean, and S.M. Kauzlarich, "Magnetic and Mössbauer Spectral Study of Core-shell Structured Fe/Au Nanoparticles," *Chem. Mater.*, **18** [4] 960-7 (2006).

180. J. Wang, W.B. White, and J.H. Adair, "Dispersion of SiO_2-based Nanocomposites with High Performance Liquid Chromatography," *J. Phys. Chem. B*, **110** [10] 4679-85 (2006).

181. Y.-J. Kim, J.-H. Yu, and J.-H. Ahn, "Preparation of Au and Au-coated Fe Nanopowder by Microemulsion," *J. Alloys Compd.*, **434-435**, 675-7 (2007).

182. P. Yang, M. Ando, and N. Murase, "Encapsulation of Emitting CdTe QDs within Silica Beads to Retain Initial Photoluminescence Efficiency," *J. Colloid Interface Sci.*, **316** [2] 420-7 (2007).

183. R. Koole, M.M. van Schooneveld, J. Hilhorst, C. de Mello Donegá, D.C. 't Hart, A. van Blaaderen, D. Vanmaekelbergh, and A. Meijerink, "On the Incorporation Mechanism of Hydrophobic Quantum Dots in silica Spheres by a Reverse Microemulsion Method," *Chem. Mater.*, **20** [7] 2503-12 (2008).

184. N. Hagura, W. Widiyastuti, F. Iskandar, K. Okuyama, "Characterization of Silica-coated Silver Nanoparticles Prepared by a Reverse Micelle and Hydrolysis-condensation Process," *Chem. Eng. J.*, **156** [1] 200-5 (2010).

185. H.T. Xue and P.Q. Zhao, "Synthesis and Magnetic Properties from Mn-doped CdS/SiO_2 Core-shell Nanocrystals," *J. Phys. D: Appl. Phys.*, **42** [1] 015402 5pp. (2009).

186. F.N. Radwan, K.J. Carrol, and E.E. Carpenter, "Dual Mode Nanoparticles: CdS Coated Iron Nanoparticles," *J. Appl. Phys.*, **107** [9] 09B515 3pp. (2010).

187. C. Li, Z. Li, X. Du, and H. Guo, "Synthesis and Magnetic Properties of FePt/Silica Core-shell Nanoparticles," *Adv. Mater. Res.*, **178**, 291-5 (2011).

188. S. Wang, C. Li, P. Yang, M. Ando, and N. Murase, "Silica Encapsulation of Highly Luminescent Hydrophobic Quantum Dots by Two-step Microemulsion Method," *Colloids Surf., A*, **395**, 24-31 (2012).

189. M. Yadav, A.K. Singh, N. Tsumori, and Q. Xu, "Palladium Silica Nanosphere-catalyzed Decomposition of Formic Acid for Chemical Hydrogen Storage," *J. Mater. Chem.*, **22** [36] 19146-50 (2012).

190. G. Bahmanrokh, M. Hashim, N. Soltani, I. Ismail, P. Vaziri, M. Navaseri, M. Erfani, and S. Kanagesan, "High Coercivity Sized Controlled Cobalt-gold Core-shell Nano-crystals Prepared by Reverse Microemulsion," *Mater. Res. Bull.*, **48** [10] 4039-47 (2013).

191. C.-S. Lee, H.H Chang, J. Jung, N.A. Lee, N.W. Song, and B.H. Chung, "A Novel Fluorescent Nanoparticle Composed of Fluorene Copolymer Core and Silica Shell with Enhanced Photostability," *Colloids Surf., B*, **91**, 219-25 (2012).

192. H. Murakami, Y. Toyota, T. Nishi, and S. Nashimi, "Terahertz Absorption Spectroscopy of Protein-containing Reverse Micellar Solution," *Chem. Phys. Lett.*, **519-520**, 105-9 (2012).

193. R. Adhikary, C.A. Barnes, and J.W. Petrich, "Solvation Dynamics of the Fluorescent Probe PRODAN in Heterogeneous Environments: Contributions from the Locally Excited and Charge-transferred States," *J. Phys. Chem. B*, **113** [35] 11999-12004 (2009).

194. J.A. Gutierrez, R.D. Falcone, J.J. Silber, and N.M. Correa, "C343 Behavior in Benzene/AOT Reverse Micelles. The Role of the Dye Solubilization in the Non-polar Organic Pseudophase," *Dyes Pigm.,* **95** [2] 290-5 (2012).

195. R. Zhu, R. Lu, and A. Yu, "Photophysics and Locations of IR125 and C152 in AOT Reverse Micelles," *Phys. Chem. Chem. Phys.,* **13** [46] 20844-54 (2011).

196. W.N. Maclay, "Factors Affecting the Solubility of Nonionic Emulsifiers," *J. Colloid Sci.,* **11** [3] 272-85 (1956).

197. C.M. Aebi and J.R. Wiebush, "Solubility of Sodium Chloride in Organic Solvents with Aerosol OT in the Presence of Moisture," *J. Colloid Sci.,* **14** [2] 161-7 (1959).

198. A. Kitahara and K. Kon-no, "Mechansism of Solubilization of Water in Nonpolar Solutions of Oil-soluble Surfactants: Effect of Electrolytes," *J. Phys. Chem.,* **70** [11] 3394-8 (1966).

199. B. Bedwell and E. Gulari, "Electrolyte-moderated Interactions in Water/Oil Microemulsions," *J. Colloid Interface Sci.,* **102** [1] 88-100 (1984).

200. S. Brunetti, D. Roux, A.M. Bellocq, G. Fourche, and P. Bothorel, "Micellar Interactions in Water-in-oil Microemulsions. 2. Light Scattering Determination of the Second Virial Coefficient," *J. Phys. Chem.,* **87** [6] 1028-34 (1983).

201. J.E. Puig and I. Rodríguez-Siordia, L.I. Rangel-Zamudio, J.F. Billman, and E.W. Kaler, "Properties and Structures of Three- and Four-component Microemulsions," *Langmuir,* **4** [4] 806-12 (1988).

202. G.D. Rees, R. Evans-Gowing, S.J. Hammond, and B.H. Robinson, "Formation and Morphology of Calcium Sulfate Nanoparticles and Nanowires in Water-in-oil Microemulsions," *Langmuir,* **15** [6] 1993-2002 (1999).

203. A. Filankembo, P. André, I. Lisiecki, C. Petit, T. Gulik-Krzywicki, B.W. Ninham, and M.P. Pileni, "Mesostructured Fluids: Supra Aggregates Made of Interdigitated Reverse Micelles," *Colloids Surf., A,* **174** [1-2] 221-32 (2000).

204. Y. Huang, T. Ma, J.-L. Yang, L.-M. Zhang, J.-T. He, and H.-F. Li, "Preparation of Spherical Ultrafine Zirconia Powder in Microemulsion System and Its Dispersibility," *Ceram. Int.,* **30** [5] 675-81 (2004).

205. D. Makovec, A. Košak, and M. Drofenik, "The Preparation of MnZn-ferrite Nanoparticles in Water-CTAB-hexanol Microemulsions," *Nanotechnology,* **15** [4] S160-6 (2004).

206. D. Liu, J. Ma, H. Cheng, and Z. Zhao, "Solubilization Behavior of Mixed Reverse Micelles: Effect of Surfactant Component, Electrolyte Concentration, and Solvent," *Colloids Surf., A*, **143** [1] 59-68 (1998).

207. A. Nanni and L. Dei, "$Ca(OH)_2$ Nanoparticles from W/O Microemulsions," *Langmuir*, **19** [3] 933-8 (2003).

208. I. Lisiecki, M. Björling, L. Motte, B. Ninham, and M.P. Pileni, "Synthesis of Copper Nanosize Particles in Anionic Reverse Micelles: Effect of the Addition of a Cationic Surfactant on the Size of the Crystallites," *Langmuir*, **11** [7] 2385-92 (1995).

209. V. Papadimitriou, C. Petit, G. Cassin, A. Xenakis, and M.P. Pileni, "Lipase Catalyzed Esterification in AOT Reverse Micelles: A Structural Study," *Adv. Colloid Interface Sci.*, **54**, 1-16 (1995).

210. C. Bauer, P. Bauduin, J.F. Dufrêche, T. Zemb, and O. Diat, "Liquid/Liquid Metal Extraction: Phase Diagram Topology Resulting from Molecular Interactions between Extractant, Ion, Oil and Water," *Eur. Phys. J. Spec. Top.*, **213** [1] 225-41 (2012).

211. N. Houyi, S. Taichene, and L. Ganzuo, "Preparation of Monodisperse Nickel (Cobalt) Boride Catalyst Using Reversed Micellar System," *J. Dispersion Sci. Technol.*, **13** [6] 647-56 (1992).

212. K. Shinoda and B. Lindman, "Organized Surfactant Systems: Microemulsions," *Langmuir*, **3** [2] 135-49 (1987).

213. P. Calandra, G. Di Marco, A. Ruggirello, and V.T. Liveri, "Physico-chemical Investigation of Nanostructures in Liquid Phases: Nickel Chloride Ionic Clusters Confined in Sodium Bis(2-ethylhexyl) Sulfosuccinate Reverse Micelles," *J. Colloid Interface Sci.*, **336** [1] 176-82 (2009).

214. G. Capuzzi, F. Pini, C.M.C. Gambi, M. Monduzzi, and P. Baglioni, "Small-angle Neutron Scattering of $Ca(AOT)_2/D_2O$/Decane Microemulsions," *Langmuir*, **13** [26] 6927-30 (1997).

215. C.F. Yang and J.Y. Chen, "Synthesis of Stabilizaed Zirconia Ultrafine Powders Using AOT-isooctane-water Reverse Micelles," *J. Mater. Sci. Lett.*, **16** [11] 936-8 (1997).

216. X. Li, C.-K. Loong, P. Thiyagarajan, G.A. Lager, and R. Miranda, "Small-angle Neutron Scattering Study of Nanophase Zirconia in a Reverse Micelle Synthesis," *J. Appl. Cryst.*, **33** [1] 628-31 (2000).

217. Stokes, R. J.; Fennell Evans, D. *Fundamentals of Interfacial Engineering*, pp.36-9. Wiley-VCH: New York, 1996.

CHAPTER 2: IONIC CONCENTRATION EFFECTS ON REVERSE MICELLE SIZE AND STABILITY IN THE WATER-AOT-ISOCTANE SYSTEM

A. Introduction

Reverse micelle synthesis, sometimes called microemulsion synthesis, is a bottom-up method of synthesizing nanopowders that can allow for precise control of the powder crystallite and/or precipitate size.[1-5] However, the effect that precursors have on reverse micelle size and stability is not clear. Recent work has begun to provide a systematic investigation of the effect that salt additions have on the structure and stability of reverse micelles through the use of molecular dynamics in conjunction with experimental observations using dynamic light scattering.[6,7] It has been demonstrated that reverse micelle size is a strong function of the molarity of salt additives, decreasing with additions of solute. It seems reasonable to assume that the size decrease cannot be sustained indefinitely with solute additions and that the system will eventually destabilize. In this contribution, a mechanism for system destabilization using the concept of an electrical double layer is proposed. This concept provides an explanation of the features of destabilization, including initial decrease in reverse micelle size, the destabilization concentration, and the effect of cation valence, allowing definite predictions to be made as to the specific concentration of solute that will result in system destabilization. A critical potential for system destabilization is also extracted.

It is well-known that stable reverse micellar solutions, which are homogeneous/isotropic systems and consist of only one phase, are in dynamic equilibrium and fluctuate (rupture and reform) on a short time scale. A nonstable reverse

micellar solution, on the other hand, is one in which a significant amount of system components are not forming these dynamic reverse micelles over a longer time scale but are forming a secondary phase in equilibrium with the primary reverse micellar phase. This would consist, for example, of a two-phase system that contains a reverse micellar solution as the primary phase and water as a secondary phase. The aim of this contribution is to define the conditions that control the formation of a two-phase system from a single-phase system as increasing amounts of solutes are added. These effects have important implications for the synthesis of nanoparticles. If the reverse micelles are not stable before the precipitates are formed, then the advantage of reverse micelle synthesis is lost. Essentially, a two-phase system may be hard to control, resulting in issues with reproducibility. In addition, the loss of the reverse micelles may create a wide size distribution when synthesizing nanoparticles, as larger particles can form in the coalesced water phase.

Many researchers have observed that the water-to-surfactant ratio (ω_o) is an important variable in reverse micelle synthesis, arguably the most important for determining the reverse micelle droplet size, where the droplet size is increased with increasing ω_o.[8-10] Additionally, a correlation between the precipitate size of the synthesized nanopowders, the reverse micelle droplet size, and the water-to-surfactant ratio is commonly provided in the literature,[11-14] although several authors report that ω_o is not the only variable affecting precipitate size.[15,16] Refined and complete metrics are necessary for efficient utilization of reverse micelle synthesis and control over precipitate size. A first step in this direction is the determination of the controlling parameters that define the size and stability of reverse micelles with the incorporation of salts, since salts

are an essential component for the reverse micelle synthesis of nanopowders. Some studies have demonstrated that salt additions cause a decrease in the size of reverse micelles,[9,17] while others have demonstrated that salt additions cause an increase.[18] There are also some reports that have demonstrated no changes.[10,19] These contradictory results demonstrate the need to clarify the conditions for which size changes are observed and the mechanisms involved in such changes. In fact, mechanisms of salt additions in regular micelle (oil-in-water microemulsion) behavior[20-25] have demonstrated that increasing salt concentrations cause swelling of micelles and then a spherical to ellipsoidal shape transition.[26-28] Specifically, Missel *et al*.[20,22] have demonstrated that the chemical potentials of the spherical and ellipsoidal shapes can be explained using the Guoy-Chapman and DLVO theories.[29] In this contribution, a detailed analysis of reverse micelle behavior with the addition of NH_4OH, $ZrOCl_2$, and $Al(NO_3)_3$ is presented. Several important effects have been discovered that are peculiar to these systems, including the importance of considering the local cation valence of a salt regardless of the actual form of the ion complex that forms, the solubility of NH_4OH in isooctane, and the effects of salt concentration and valence on the stability of reverse micelles. A critical potential between two overlapping electrical double layers is also presented, which defines the potential for instability of reverse micelles.

E. Experimental Methods

In order to prepare the reverse micelle solutions for this study, an initial solution consisting of 8.891 g of sodium bis(2-ethylhexyl) sulfosuccinate (98+% AOT, Sigma-Aldrich, St. Louis, MO) and 100 mL of isooctane (2,2,4-trimethylpentane, 99+%, Sigma-

Aldrich, St. Louis, MO) was prepared by stirring for 30 min. Separate solutions were prepared containing various molarities of $ZrOCl_2 \cdot 8H_2O$ (99.9985%, Alfa Aesar, Ward Hill, MA), NH_4OH (28-30% NH_3, Alfa Aesar, Ward Hill, MA), or $Al(NO_3)_3 \cdot 9H_2O$ by mixing with 3.6 mL of distilled water and stirring for 30 min. Solutions with molarities from 0 to 1 M (based on the amount of water volume) for the $ZrOCl_2$ and $Al(NO_3)$ were prepared in increments of 0.1 M. For $ZrOCl_2$, these molarities correspond to 0.0116, 0.232, 0.348, 0.464, 0.580, 0.696, 0.812, 0.928, 1.044, and 1.160 g of salt. For $Al(NO_3)_3$, these molarities correspond to 0.118, 0.236, 0.353, 0.471, 0.589, 0.707, 0.824, 0.942, 1.060, and 1.178 g of salt. The amount of water associated with the salts, (i.e., the waters of hydration) was considered negligible in comparison to the 3.6 mL of water solvent, and therefore corrections were not made. For the case of NH_4OH, solutions of molarities 0, 0.05, and 0.2-1.4 M (based on the amount of water and isooctane volume) were prepared. These molarities correspond to 0.306, 1.223, 2.445, 3.667, 4.890, 6.112, 7.335, and 8.557 g of NH_4OH. These amounts of ammonium hydroxide have significant amounts of water and must be corrected for. For increasing molarities, amounts of 3.48, 3.10, 2.61, 2.11, 1.61, 1.11, 0.62, and 0.12 g of water were added for preparation of the solutions instead of 3.6 g. Preparation of the reverse micelle solutions involves mixing each salt solution with AOT solution for 2 hours. The water-to-surfactant ratio (ω_o) for all compositions was fixed at ten.

The size of the reverse micelles was measured by dynamic light scattering (DLS) on a Nanotrac ULTRA instrument (Microtrac, Montgomeryville, PA). The average of five runs was considered one measurement, each performed for 15 s, according to manufacturer specifications and ASTM standard E2490-09. Five of these measurements

were made for each sample to determine error values. The isooctane fluid constants used for analysis were an index of refraction of 1.40 and a viscosity of 0.542 cP at 20°C. An index of 1.48 was utilized for the reverse micelles, although for small reverse micelle sizes having a unimodal distribution, the index of refraction is found to be negligible and does not affect the computation. ASTM standard E2490-09 warns that dynamic light scattering does not produce an absolute size value and that volume average distributions are only suitable for comparison purposes, such as for observing size changes. The interest of this work is to observe size changes resulting in observable trends. As such, and in addition to the relative ease of measuring and analyzing data, DLS is particularly suitable for experimentally observing the effects of salt additives on reverse micelle size.

F. Results and Discussion

1. Effect of Increasing Salt Additions on Reverse Micelle Sizes

The volume-average size distributions of the reverse micelles in the water-AOT-isooctane solutions containing NH_4OH are illustrated in Figure 2-1. The average reverse micelle size at the lowest molarity of 0.05 M is 9.2 nm (Figure 2-1a), slightly lower than the 10.4 nm average size of the reverse micelles without any salts. As the molarity is increased, the average reverse micelle size decreases and the distributions become narrower. The solutions transition from transparent to turbid at 0.6 M, indicating a breakdown of the microemulsion. Above 0.6 M (Figure 2-1b) the reverse micelle solutions no longer exhibit distributions exclusively at the lower sizes. Instead, structures around 1 μm are also evident, although their population frequency is significantly lower than the distribution for the reverse micelle size distributions at the lower end of the scale. For clarity, the y-axis in Figure 2-1b is truncated. The distributions at the lower

end of the scale for these higher molarities have an average size of around 7.8 nm, which does not change with molarity. These distributions are believed to be reverse micelles; however, it is possible for other structures or local phase separation to be present. Figure 2-2 illustrates this trend (squares), where the decrease in average size occurs up to 0.6 M, with little change for concentrations above 0.6 M. At the higher salt concentrations, phase separation is evident when mixing is stopped and water droplets coalesce. Thus, the higher molarities represent the onset of reverse micelle destabilization and the structures of larger sizes are, indeed, water droplets in what is now a two-phase system of reverse micelles in the oil phase and a second phase of coalesced water.

The NH_4OH molarity is based on the total volume of liquid (i.e., the water plus isooctane). If one assumes that the NH_4OH is not soluble in isooctane and the molarity is based on the salt contained only inside the water cores, one finds that the size of the reverse micelles does not change significantly with increasing molarity (diamonds in Figure 2-2). It is possible that a considerable amount of the ammonium hydroxide is dissolved in the isooctane; thus, the molarity inside the water domains after the formation of the reverse micellar solutions is lower than the molarity of the water/ammonium hydroxide solutions prepared initially, as justified below.

Ammonium hydroxide has been known to exist as a solution of NH_3 molecules that are hydrogen bonded with water molecules rather than separate NH_4^+ and OH^- ions in solution.[30] The dissociation constant for ammonium hydroxide in water is approximately 1.710×10^{-5} at room temperature.[31] Thus, for the concentrations used in

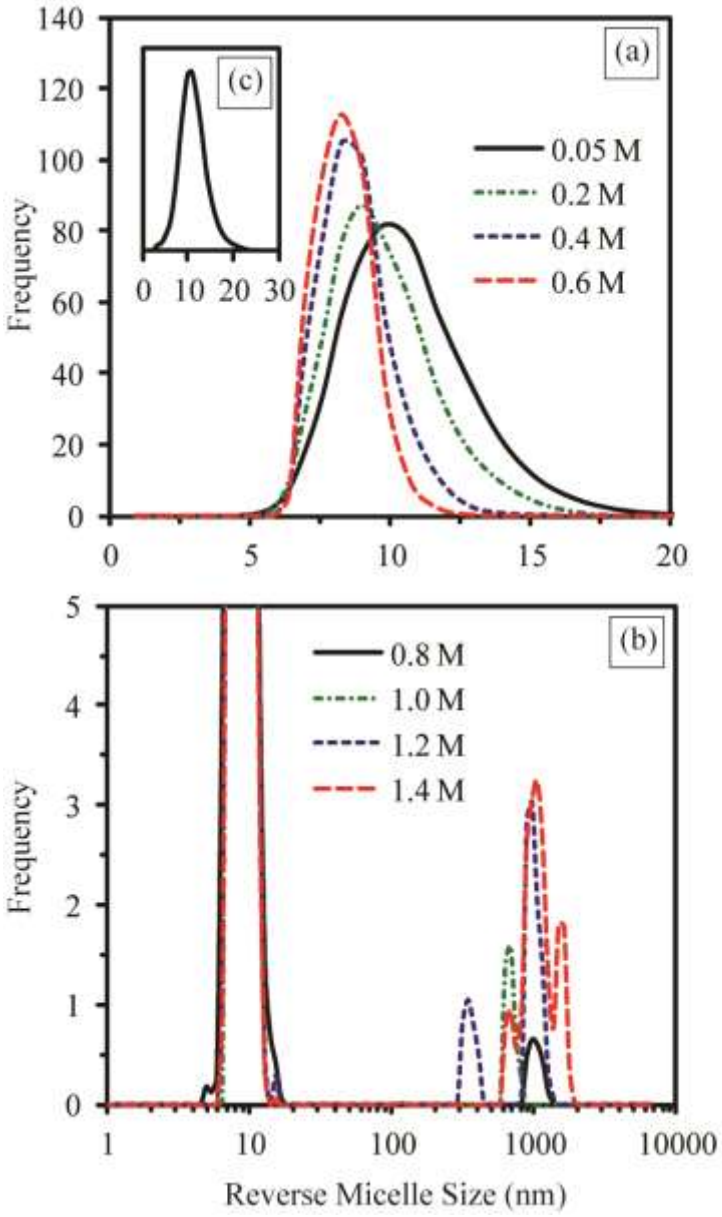

Figure 2 - 1. Reverse micelle size for water/AOT/isooctane solutions containing NH_4OH (a) before destabilization, and (b) after destabilization. (c) Reverse micelle size distribution for the AOT/water/isooctane system without any salt additions.

this study, no more than about 2% of NH_3 dipoles are expected to become protonated and form the NH_4^+ cation. The solubility of NH_3 in water is nearly 30 weight percent at room temperature, which corresponds to roughly two water molecules per ammonia molecule in a typical solution. Assuming one of these molecules associates with an NH_3 molecule

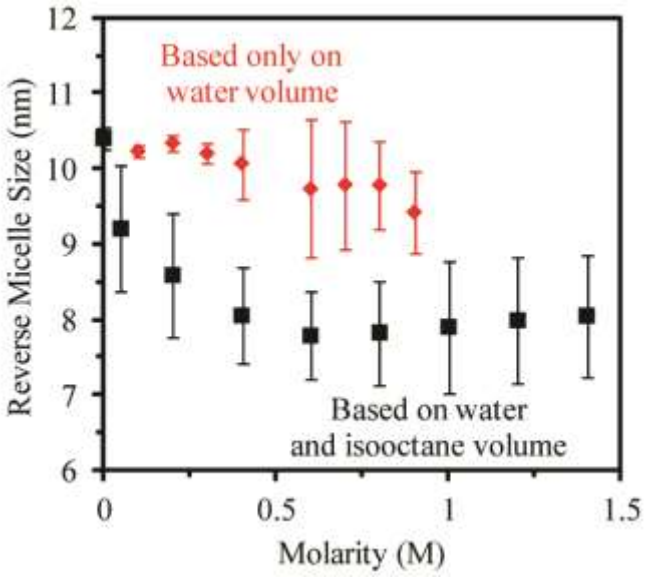

Figure 2 - 2. Change in average reverse micelle size with respect to solution molarity in the NH_4OH system based solely on the volume of water in the micelle solution (diamonds) and on the water plus isooctane volume in the micelle solution (squares).

to form NH_4OH, then the other water molecule in the solution can be considered free water, resulting in an effective solution that consists of NH_4OH and H_2O on a per mole basis. Therefore, attempting to add ammonium hydroxide solution directly into isooctane would result in coalescence of the free water. In the special case of reverse micelles, the free water in the ammonium hydroxide solution can stay inside the water cores, while the NH_4OH complex (i.e., $NH_3 + H_2O$) can travel into the isooctane as a pair with another NH_4OH complex, since by itself it is polar and not able to dissolve in a nonpolar solvent. Pairs of NH_4OH complexes become nonpolar if their net dipole moments arrange themselves opposite to each other, after which they can dissolve in a nonpolar solvent such as isooctane. Another possibility is that NH_3 partitions into the water and isooctane phases due to reasonable solubility of NH_3 in isooctane while leaving behind all water in the reverse micelle core. Analysis (to be discussed in section 2) better supports the

former explanation. Thus, the assumption that NH_4OH is only present inside the water domains in reverse micelle solutions is not accurate.

The decrease in reverse micelle size also takes place for solutions containing $Al(NO_3)_3$ and $ZrOCl_2$, as illustrated in Figure 2-3. Again, there is a significant decrease in reverse micelle size as molarity is increased. However, the point of destabilization occurs at a value around 0.4 M for the $Al(NO_3)_3$ system and 0.3 M for the $ZrOCl_2$ system, at a lower concentration than for the NH_4OH sytem. Beyond this point, the change in size is small. The additional size decrease at the higher molarities, beyond the concentration where the reverse micelles become destabilized, while minimal, may be related to the fact that $Al(NO_3)_3$ and $ZrOCl_2$ take waters of hydration with them in the newly formed water phase of the two-phase system. This would result in lowering of the ω_o value for the remaining reverse micelles, reducing the average micelle size further.

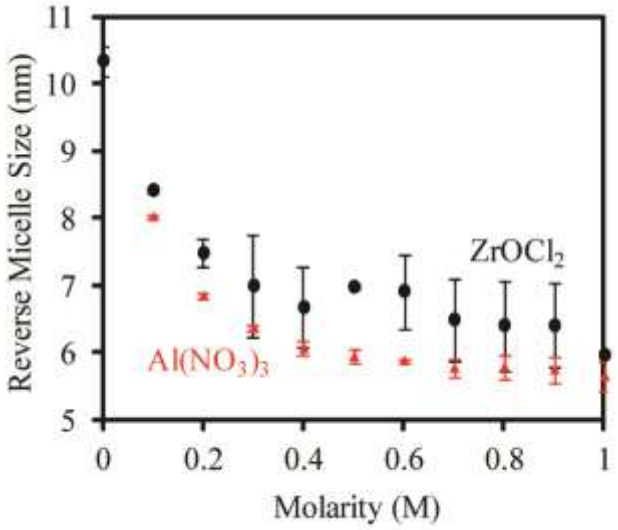

Figure 2 - 3. Change in average reverse micelle size with respect to molarity in the $ZrOCl_2$ and $Al(NO_3)_3$ systems.

A simplified illustration and proposed model of charge separation in reverse micelles are given in Figure 2-4a for the case of $Al(NO_3)_3$ reverse micelle solutions. Since the surfactant head groups are negatively charged, the positive Al^{3+} counterions are closer to the edges of the water cores while the $(NO_3)^-$ co-ions are forced to the center of the water core. This results in a core-shell structure, with the outermost layer consisting of a shell of negative charge due to the surfactant headgroups, a middle shell of positive charge due to the presence of the Al^{3+} counterions, and a core of negative charge due to the $(NO_3)^-$ co-ions. Thus, counterions concentrate at the surfactant surface layer, while co-ions are segregated to the core. The presence of salt counterions close to surfactant headgroups is experimentally confirmed using $[Ru(bpy)_3]^{2+}$ as a probe in the water/AOT/isooctane system.[32] The surfactant Na^+ counterions are also expected to segregate to the core of the reverse micelles, as the Al^{3+} ions with their higher oxidation states are able to displace the sodium ions from the immediate proximity of the negatively charged surfactant headgroups.[28]

The potentials in the reverse micelle cores can be described by adopting the Gouy-Chapman concept that describes how a charged surface and an adjacent electrolyte solution interact.[29] This theory describes the electrical potential as a decaying exponential with distance from a charged surface. The theory is developed for planar surfaces and, with modifications, can also be used for explaining interactions at a convex surface. It is unclear if the theory can be used for relatively low diameter concave systems like the interior of a reverse micelle. Despite this uncertainty, analysis using the basic concepts of the Gouy-Chapman theory is used as a first step, realizing that modifications may be necessary. If the theory fails to properly explain the reverse

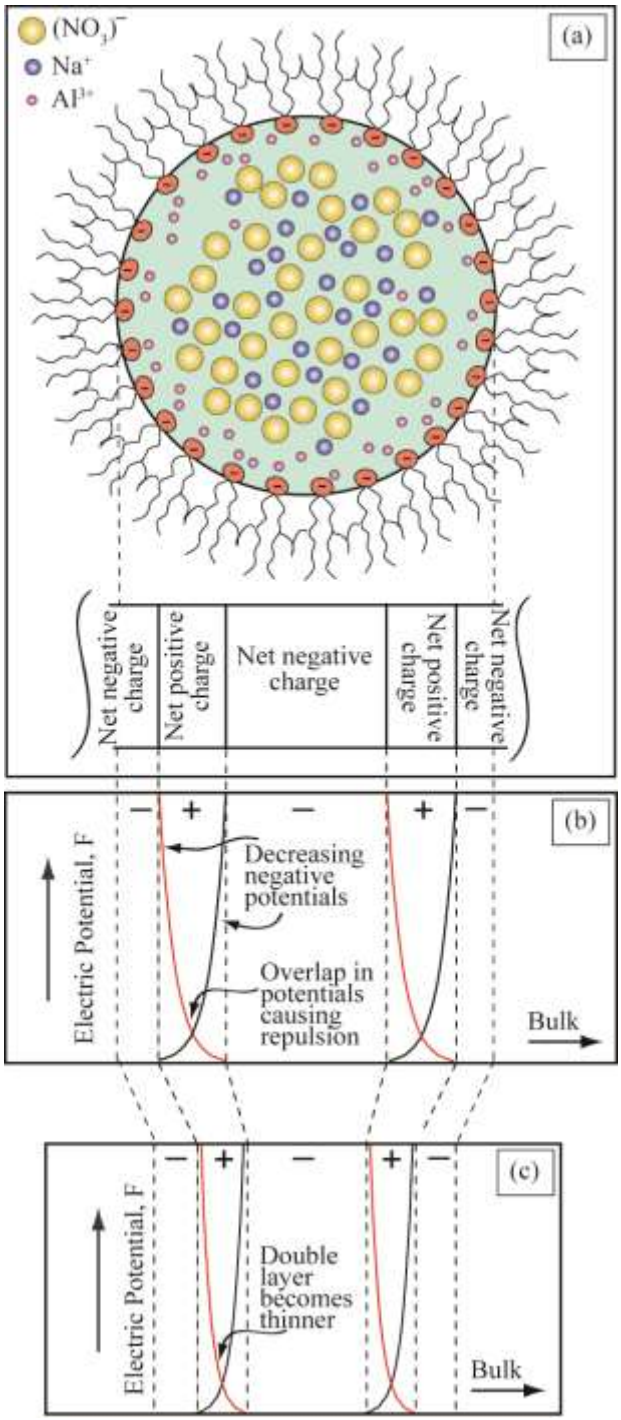

Figure 2 - 4. Schematic demonstrating (a) ion distribution of an electrolyte-filled reverse micelle, (b) the set of electrical potentials that might be expected for such a distribution, and (c) reduction in the electrical double layer that leads to a size reduction of the reverse micelle.

micelle behavior observed in this study, it may at least provide insight into what modifications need to be made to make a more relevant theoretical interpretation. In any case, the Gouy-Chapman theory is expected to apply to the reverse micellar systems because the electrolyte concentrations are fairly dilute.

For the boundary conditions outlined in Figure 2-4a, a set of potentials might be expected as illustrated in Figure 2-4b. The overlapping of these potentials generates a repulsive force that balances the attractive forces maintaining reverse micelle stability. With a higher salt concentration, there is more effective shielding of the charged surface by the electrolyte solution resulting in steeper decay of the electrical potentials. This is known as compression of the electrical double layer. In other words, in the presence of a higher positive charge density close to the surfactant surface, the influence of this negatively charged surface extends over shorter distances. This effect explains the reduction in reverse micelle size with increase in salt molarity. At the lower molarities up to 0.4 M for the $Al(NO_3)_3$ system, in which the reverse micelle systems are stable, the gradual increase in counterion concentration results in compression of the electrical double layers, allowing them to move into closer proximity to each other before a similar overlap in the potentials and repulsion is achieved to form a smaller equilibrium size, schematically represented in Figure 2-4c. This reduction, however, cannot be sustained indefinitely. There will be a molarity at which the concentration of ions is so high that the negative co-ions in the core undergo significant electrostatic repulsion between them. In consequence, the core would require a larger volume to accommodate the increasing numbers of co-ions. This could be achieved by elongation of the inner core of the reverse micelles, for example, but this would result in an increase in repulsion between the

electrical double layers along the elongated axis. Forming a two-phase system rather than accommodating further additions of salt avoids excess repulsion and represents the point of instability.

On the basis of the qualitative model of Figure 2-4, the electrical double layer thickness is what defines the average reverse micelle size, which is the length at which forces between overlapping potentials become relevant.[29] This thickness is a mathematical construct that defines the distance away from a charged surface for which the potential at the surface is reduced by 1/e and is usually on the scale of a few nanometers. This thickness, κ^{-1}, also known as the Debye screening length, is defined by[29]

$$\frac{1}{\kappa} = \left(\frac{\varepsilon_r \varepsilon_o k_B T}{1000 q^2 N_A \sum_i z_i^2 c_{io}} \right)^{1/2} \tag{1}$$

where ε_r is the relative dielectric permittivity, ε_o is the electrical permittivity of vacuum, k_B is Boltzmann's constant, T is the temperature, q is the elementary charge, N_A is Avogadro's number, z_i is the valence of the counterions, and c_{io} is the concentration of counterions. For a given system at constant temperature, the electrical double layer depends only on counterion concentration and the valence of ions. Considering the system, equation 1 can be modified such that

$$RMS \propto \left(\frac{\varepsilon_r \varepsilon_o k_B T}{1000 q^2 N_A} \right)^{1/2} \left(z_e^2 c_{e)} \right)^{-1/2} \tag{2}$$

where RMS is the reverse micelle size. Equation 2 results in an expression that can be plotted with $\eta = (z_e^2 c_e)^{-1/2}$ on the x-axis and RMS on the y-axis. In this expression, z_e is

the valence of the salt counterions and c_e is the concentration of the salt counterions. The surfactant counterions (i.e., Na^+) are not considered in this equation because they are not believed to contribute to the formation of the electrical double layer, as they are located in the reverse micelle core to shield the co-ions and not in the immediate vicinity of the surfactant headgroups. Figure 2-5 demonstrates that a very strong linear correlation exists, providing compelling support for the model depicted in Figure 2-4, despite the simplicity of the model. Equation 2 demonstrates that reverse micelle size is dependent on at least two parameters (z_e and c_e) and confirms that the Gouy-Chapman theory is useful for interpretation of reverse micelle behavior as salts are incorporated into these systems. The lines in Figure 2-5 do not predict the size of the parent reverse micelles without salt additions because at extremely low concentrations, the surfactant counterions are not fully displaced from the surfactant interface, thus making the model less valid from the perspective of the net charge close to the surfactant headgroups.

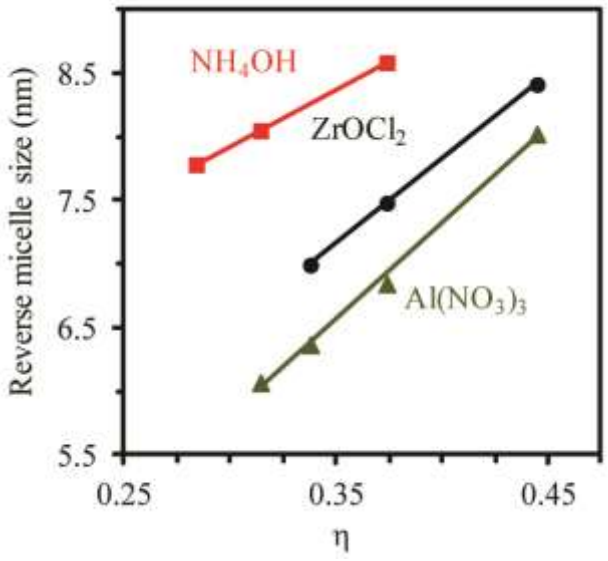

Figure 2 - 5. Average reverse micelle size with respect to $\eta = (z_e^2 c_e)^{-1/2}$.

In preparing Figure 2-5, z_e values of +2, +3, and +4 were used for NH_4OH, $Al(NO_3)_3$, and $ZrOCl_2$ systems, respectively. In fact, any value of valence for each of the systems can be used and there would still be a linear relationship, since z_e is a constant for a given system. Nonetheless, the values used are a preview to arguments that will be made in the next section. Figure 2-5 provides a framework under which one can understand the behavior of reverse micelles before loss of stability, when the reverse micelle size is controlled by the thickness of the electrical double layer.

2. Effect of Cation Valence on Reverse Micelle Stability

So far, the effect of salt on reverse micelle size and the mechanism causing instability has been explained. For completion, the effect of valence of the salt counterions also needs to be accounted for in the stability of these systems. From evaluating equation 2, the valence of the salt counterions is known as a variable that results in a decrease in the reverse micelle size as the value increases, but it does not provide a means to predict the point of instability in these systems.

The equilibrium reverse micelle size depends on the overlap of the electrical double layers, resulting in compression as salt concentration is increased. This allows the potentials to move into closer proximity to each other before they generate an equilibrium force that balances the forces conditional for reverse micelle formation. At the point of instability, it is assumed that the minimum potential at the center of the overlapping potentials is a constant value, proportional to a constant repulsive force between them. The Boltzmann equation[29] is considered for describing the local concentration of the ions that generate the decaying potentials in order to determine the effect of valence of the salt counterions on the critical concentration.

The electrostatic energy for an ion of valence z_e at a point where the potential is ϕ can be represented by $z_e q\phi$. This leads to the following form of the Boltzmann equation:

$$c = c_o \exp\left(-\frac{z_e q\phi}{k_B T}\right) \tag{3}$$

where c is the local concentration distribution and c_o is the bulk ion concentration (i.e., the concentration of salt added to the system). If the critical salt concentration for reverse micelle destabilization, c_c, is related to the minimum potential ϕ_c, then equation 3 takes the form

$$c_c = c_o \exp\left(-\frac{z_e q\phi_c}{k_B T}\right) \tag{4}$$

Rearranging this equation gives

$$\ln c_c = \frac{q\phi_c}{k_B T} z_e + \ln c \tag{5}$$

which relates the natural logarithm of the critical concentration to the salt valence.

Plotting the natural logarithm of the experimentally determined critical ‘concnetration at which destabilization occurs with respect to the salt cation valence, a linear fit is obtained, as illustrated in Figure 2-6. The data provides a linear relationship that takes the form

$$\ln c_c = -0.35 z_e + 0.16 \tag{6}$$

which can also be written as follows:

$$c_c = \exp(-0.35 z_e + 0.16) \tag{7}$$

Thus, if one knows the valence of the counterions in a reverse micelle solution of water/AOT/isooctane, a prediction of the concentration at which destabilization occurs can be reliably obtained for ω_o = 10. A similar relationship is expected for other ω_o values and other reverse micelle systems. For example, Calandra et al.'s[33] data for a $NiCl_2$ system at ω_o = 9, a value close to thte value of ω_o = 10, is in reasonable agreement with the data presented in Figure 2-6.

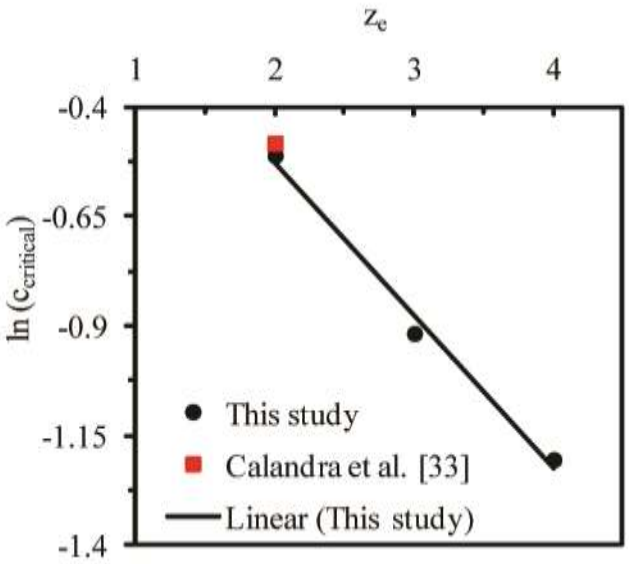

Figure 2 - 6. Relationship between the critical concentration and salt cation valence in water/AOT/isooctane reverse micelle systems with ω_o = 10.

By comparing equation 5 and equation 6, one can see that the slope may be interpreted in the following way:

$$-0.35 = \frac{q\phi_c}{k_B T} \tag{8}$$

which can be rearranged as follows:

$$\phi_c = -\frac{0.35 k_B T}{q} \tag{9}$$

Thus, the critical potential can be calculated from the linear fit obtained in Figure 2-6. This corresponds to ϕ_c = -8.8 mV at room temperature. Additionally, comparison of equations 5 and 6 gives ln c = 0.16, which relates the local concentration in the ion distribution at the point where $\phi = \phi_c$ and results in c = 1.2 M. This concentration is higher than the bulk concentration, justifying the assumption that the core of the reverse micelles must contain the coions. Equation 9 also demonstrates that there is an effect of temperature on stability.

Figure 2-6 utilizes counterion oxidation states of +2 for the NH_4OH system, +3 for the $Al(NO_3)_3$ system, and +4 for the $ZrOCl_2$ system. This requires some elaboration. For the case of NH_4OH, it has been demonstrated that the hydrogen-bond donor ability of water in AOT reverse micelles can be enhanced by a factor of up to 65 compared to bulk water.[34] Such an effect could lead to increased dissociation of NH_4OH inside the reverse micelle water cores. As a reminder, most of the NH_4OH is expected to migrate into the isooctane phase by forming NH_4OH pairs. Nonetheless, some NH_4OH molecules will stay inside the reverse micelles and, in the proximity of the negatively charged surfactant heads, will dissociate into NH_4^+. Furthermore, the charged surfactant film could also lead to dissociation of the NH_4OH on the outside of the reverse micelle, near the surfactant film, as depicted in Figure 2-7. The paired charges symmetric about the surfactant film can explain why it is necessary to consider an oxidation state of +2 for the NH_4OH system. The valence of NH_4^+ remains +1, but a factor of two must be applied to account for a factor of 2x the electrostatic screening at the surfactant interface, from both inside and outside of the interface. The effect is a direct consequence of the solubility of the ammonium hydroxide in the bulk oil phase. The NH_4^+ ions inside the water cores will

shrink the reverse micelles, whereas the NH_4^+ ions outside the water cores will expand the reverse micelles. This is supported by the experimental reverse micelle sizes found for this system. The average size of reverse micelles at the point of instability for the $Al(NO_3)_4$ system is about 6 nm, whereas for the $ZrOCl_2$ system it is about 7 nm, just slightly larger. For these two salts, which are only soluble in the water core, the change in the average reverse micelle size from 0 M to the molarity at the point of instability is as much as 4.4 nm. In contrast, the change in size for the NH_4OH is about 2.4 nm. The change in size is almost a factor of 2 between the $Al(NO_3)_3$ system and the NH_4OH system, supporting the notion that there are competing forces that contract and expand the reverse micelles. However, specific ion effects have not been evaluated and could explain the size differences. Specific ion effects will be explored in another chapter.

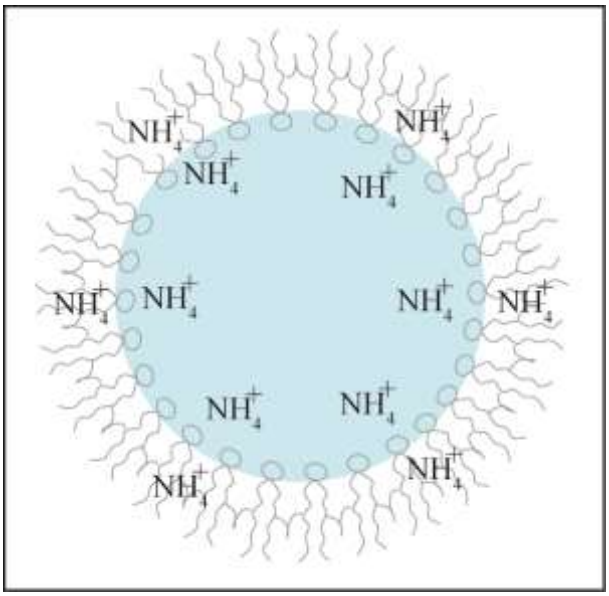

Figure 2 - 7. Given the solubility of ammonium hydroxide in the oil phase, an NH_4^+ ion distribution just outside of the surfactant film will also exist.

For the case of the $Al(NO_3)_3$ and $ZrOCl_2$ systems, oxidation states of +3 and +4 are utilized in the model. High valency ions, such as Al^{3+} and Zr^{4+}, have a very strong

tendency to hydrolyze in water, leading to the formation of polynuclear species with oxygen. For example, it is known that a tetramer complex, $[Zr_4(OH)_8(H_2O)_{16}]^{8+}$, exists for $ZrOCl_2$ when dissolved in water.[35-37] Other Zr^{4+} hydrolyzed species, including a $[Zr_2(O)_2(H_2O)_{12}]^{4+}$ dimer with oxygen bridges, have also been shown to exhibit stability.[38] For the case of Al^{3+}, the polynuclear species $[Al(H_2O)_6]^{3+}$ is the most common.[39] These complexes could all be present inside the water domains of the reverse micelles. However, the model assumes that each zirconium ion contributes a charge of +4. If instead, zirconium is assumed to be present in the dimer form, the concentration and charge no longer fit equation 6, as the concentration of zirconium ions with respect to the +4 charge will be lowered by half. That is, for every two zirconium ions there will be net charge of +4, instead of maintaining a 1:1 relationship. This leads to the conclusion that the configuration of the polynuclear species inside the water domains does not influence the behavior of the solutions and that it is only the charge of the cation in a specific species that dictates the behavior. It is also possible that the polynuclear species close to the charged surfactant heads are no longer stable and the Zr^{4+} and Al^{3+} ions become independent of their waters of hydration.[28]

Nonetheless, the assumed +4 oxidation state for zirconium does not account for the larger size of the reverse micelles for the $ZrOCl_2$ system as compared to the $Al(NO_3)_3$ system. If the electrical double layer thickness depends on the counterion valence, a thinner layer is expected for higher valence counterions. This should result in small reverse micelles for the $ZrOCl_2$ system, which is clearly not the case. This can be resolved by taking into consideration the presence of the co-ions. Assuming that dissociation of polynuclear species can occur in reverse micelles, for each Zr^{4+}

counterion there will be two OH^- and two Cl^- co-ions introduced into the system. For the case of the $Al(NO_3)_3$ system, there will be three NO_3^- co-ions. Thus, although the electrical double layer thickness will be reduced by the higher valence for Zr^{4+} compared to Al^{3+} counterions, the size of the negatively charged core must be larger for the $ZrOCl_2$ system.

In summary, the addition of salts in reverse micelle systems causes a reduction in size of the reverse micelles and has been attributed to the ion distribution and formation of electrical double layers in the water core of the reverse micelles. With the addition of significant amounts of salts, the inability to further compress the co-ions in the central core of the reverse micelles causes destabilization of the reverse micelles. Destabilization results in a two-phase system, evident by large features observed in dynamic light scattering measurements, opacity of the solutions, and the observation of water coalescence for systems having concentrations above a critical concentration. There is a strong relationship between the critical concentration of a salt and the cation valence for the reverse micelle systems with added salts. Interpretation of the data uncovers two features not previously considered. The first is that ammonium hydroxide is soluble in the oil phase, with notable consequences in regards to the effective valence of this salt. The second is that for reverse micelles formed using ionic surfactants, dissociation reactions of polynuclear species due to the charged surfactant film should be considered.

G. Conclusions

This chapter describes a model for the mechanisms of reverse micelle stability with systematic additions of salts using dynamic light scattering. This approach results in

a model for defining reverse micelle stability based on the development of a pair of electrical double layers within the reverse micelle structures. Salt additions cause a decrease in the average reverse micelle size. This decrease in size is a direct consequence of the electrical double layer thickness for the potentials that develop in the interior of the reverse micelles. As salt concentration is increased, the electrical double layers become thinner and allow the potentials to move into closer proximity to each other. However, there is a limit at which this can occur, defined by the greater concentration of co-ions in the core with increasing salt additions.

H. References

1. B.L. Cushing, V.L. Kolesnichenko, C.J. O'Connor, "Recent Advances in the Liquid-phase Syntheses of Inorganic Nanoparticles," *Chem. Rev.*, **104** [9] 3893-946 (2004).

2. K. Holmberg, "Surfactant-templated Nanomaterials Synthesis," *J. Colloid Interface Sci.*, **274** [2] 355-64 (2004).

3. I. Capek, "Preparation of Metal Nanoparticles in Water-in-oil (W/O) Microemulsions," *Adv. Colloid Interface Sci.*, **110** [1-2] 49-74 (2004).

4. M.A. López-Quintela, "Synthesis of Nanomaterials in Microemulsions: Formation Mechanisms and Growth Control," *Curr. Opin. Colloid Interface Sci.*, **8** [2] 137-44 (2003).

5. M.P. Pileni, "The Role of Soft Colloidal Templates in Controlling the Size and Shape of Inorganic Nanocrystals," *Nat. Mater.*, **2** [3] 145-50 (2003).

6. V.R. Vasquez, B.C. Williams, and O.A. Graeve, "Stability and Comparative Analysis of AOT/Water/Isooctane Reverse Micelle System Using Dynamic Light Scattering and Molecular Dynamics," *J. Phys. Chem. B*, **115** [12] 2979-87 (2011).

7. A. Gardner, V.R. Vasquez, A. Clifton, and O.A. Graeve, "Molecular Dynamics Analysis of the AOT/Water/Isooctane System: Effect of Simulation Time, Initial Configuration, and Model Salts," *Fluid Phase Equilib.*, **262** [1-2] 264-70 (2007).

8. A. Nanni and L. Dei, "$Ca(OH)_2$ Nanoparticles from W/O Microemulsions," *Langmuir*, **19** [3] 933-8 (2003).

9. X. Li, C.K. Loong, P. Thiyagarajan, G.A. Lager, and R. Miranda, "Small-angle Neutron Scattering Study of Nanophase Zirconia in a Reverse Micelle Synthesis," *J. Appl. Cyrstallogr.*, **33** [3-1] 628-31 (2000).

10. X. Fang and C. Yang, "An Experimental Study on the Relationship between the Physical Properties of CTAB/Hexanol/Water Reverse Micelles and ZrO_2-Y_2O_3 Nanoparticles Prepared," *J. Colloid Interface Sci.*, **212** [2] 242-51 (1999).

11. W. Härtl, Ch. Beck, M. Roth, F. Meyer, and R. Hemelmann, "Nanocrystalline Metals and Oxides II: Reverse Microemulsions," *Ber. Bunsenges. Phys. Chem.*, **101** [11] 1714-17 (1997).

12. I. Lisiecki and M.P. Pileni, "Synthesis of Copper Metallic Clusters Using Reverse Micelles as Microreactors," *J. Am. Chem. Soc.*, **115** [10] 3887-96 (1993).

13. F.J. Arrigada and K. Osseo-Asare, "Controlled Hydrolysis of Tetraethoxysilane in a Nonionic Water-in-oil Microemulsion: A Statistical Model of Silica Nucleation," *Colloids Surf., A*, **154** [3] 311-26 (1999).

14. F. Debuigne, J. Cuisenaire, L. Jeunieau, B. Masereel, and J.B. Nagy, "Synthesis of Nimesulide Nanoparticles in the Microemulsion Epikuron/Isopropyl Myristate/Water/n-butanol (or Isopropanol)," *J. Colloid Interface Sci.*, **243** [1] 90-101 (2001).

15. D. Chen and S. Wu, "Synthesis of Nickel Nanoparticles in Water-in-oil Microemulsions," *Chem. Mater.*, **12** [5] 1354-60 (2000).

16. B.J. Nagy, I. Bodart-Ravet, and E.G. Derouane, "Preparation Characterization and Catalytic Activity of Monodisperse Colloidal Metal Borides," *Faraday Discuss. Chem. Soc.*, **87**, 189-98 (1989).

17. E. Sheu, K.E. Göklen, T.A. Hatton, and S.H. Chen, "Small-angle Neutron Scattering Studies of Protein-reversed Micelle Complexes," *Biotechnol. Prog.*, **2** [4] 175-86 (1986).

18. J.B. Nagy, "Multinuclear NMR Characterization of Microemulsions: Preparation of Monodisperse Colloidal Metal Boride Particles," *Colloids Surf.*, **35** [2] 201-20 (1989).

19. J. Henle, P. Simon, A. Frenzel, S. Scholz, S. Kaskel, "Nanosized BiOX (X = Cl, Br, I) Particles Synthesized in Reverse Microemulsions," *Chem. Mater.*, **19** [3] 366-73 (2007).

20. P.J. Missel, N.A. Mazer, M.C. Carey, and G.B. Benedek, "Influence of Alkali-metal Counterion Identity on the Sphere-to-rod Transition in Alkyl Sulfate Micelles," *J. Phys. Chem.,* **93** [26] 8354-66 (1989).

21. G. Porte and J. Appell, "Growth and Size Distributions of Cetylpyridinium Bromide Micelles in High Ionic Strength Aqueous Solutions," *J. Phys. Chem.,* **85** [17] 2511-19 (1981).

22. P.J. Missel, N.A. Mazer, G.B. Benedek, C.Y. Young, and M.C. Carey, "Thermodynamic Analysis of the Growth of Sodium Dodecyl Sulfate Micelles," *J. Phys. Chem.,* **84** [9] 1044-57 (1980).

23. N.A. Mazer, G.B. Benedek, and M.C. Carey, "An Investigation of the Micellar Phase of Sodium Dodecyl Sulfate in Aqueous Sodium Chloride Solutions Using Quasielastic Light Scattering Spectroscopy," *J. Phys. Chem.,* **80** [10] 1075-85 (1976).

24. N.J. Chang and E.W. Kaler, "The Structure of Sodium Dodecyl Sulfate Micelles in Solutions of Water and Deuterium Oxide," *J. Phys. Chem.,* **89** [14] 2996-3000 (1985).

25. O. Bayer, H. Hoffman, W. Ulbricht, and H. Thurn, "The Influence of Solubilized Additives on Surfactant Solutions with Rodlike Micelles," *Adv. Colloid Interface Sci.*, **26**, 177-203 (1986).

26. R.G. Alargova, V.P. Ivanova, P.A. Kralchevsky, A. Mehreteab, and G. Broze, "Growth of Rod-like Micelles in Anionic Surfactant Solutions in the Presence of Ca^{2+} Counterions," *Colloids Surf., A*, **142** [2-3] 201-18 (1998).

27. R.G. Alargova, K.D. Danov, P.A. Kralchevsky, G. Broze, and A. Mehreteab, "Growth of Giant Rodlike Micelles of Ionic Surfactant in the Presence of Al^{3+} Counterions," *Langmuir*, **14** [15] 4036-49 (1998).

28. R. Alargova, J. Petkov, D. Petsev, I.B. Ivanov, G. Broze, and A. Mehreteab, "Light Scattering Study of Sodium Dodecyl Polyoxyethylene-2-sulfate Micelles in the Presence of Multivalent Counterions," *Langmuir*, **11** [5] 1530-6 (1995).

29. R.J. Stokes and D. Fennell Evans. *Fundamentals of Interfacial Engineering*, pp. 130-4, 143-55. Wiley-VCH, New York, 1996.

30. P.P. Sethna, H.D. Downing, L.W. Pinkley, and D. Williams, "Infrared Band Intensities in Ammonium Hydroxide and Ammonium Salts," *J. Opt. Soc. Am.,* **68** [4] 429-31 (1978).

31. D.R. Lide, *CRC Handbook of Chemistry and Physics*, pp. 8-37. CRC Press, Boca Raton, FL, 1990.

32. J.J. Rack, T.M. McCleskey, and E.R. Birnbaum, "Perturbing the Sequestered Water-pool in Microemulsions: The Role of the Probe in Affecting Reverse Micelle Equilibria," *J. Phys. Chem. B*, **106** [3] 632-6 (2002).

33. P. Calandra, G. Di Marco, A. Ruggirello, and V.T. Liveri, "Physico-chemical Investigation of Nanostructures in Liquid Phases: Nickel Chloride Ionic Clusters Confined in Sodium Bis(2-ethylhexyl) Sulfosuccinate Reverse Micelles," *J. Colloid Interface Sci.*, **336** [1] 176-82 (2009).

34. M.-F. Ruasse, I.B. Blagoeva, R. Ciri, L. Garcia-Rio, J.R. Leis, A. Marques, J. Mejuto, and E. Monnier, "Organic Reactions in Micro-organized Media: Why and How?" *Pure Appl. Chem.*, **69** [9] 1923-32 (1997).

35. G.M. Muha and P.A. Vaughan, "Strucutre of the Complex Ion in Aqueous Solutions of Zirconyl and Hafnul Oxyhalides," *J. Chem. Phys.*, **33** [1] 194-9 (1960).

36. T.C.W. Mak, "Refinement of the Crystal Structure of Zirconyl Chloride Octahydrate," *Can. J. Chem.*, **46** [22] 3491-7 (1968).

37. C. Hagfeldt, V. Kessler, I. and I. Persson, "Structure of the Hydrated, Hydrolysed and Solvated Zirconium(IV) and Hafnium(IV) Ions in Water and Aprotic Oxygen Donor Solvents. A Crystallographic, EXAFS Spectroscopic and Large Angle X-ray Scattering Study," *Dalton Trans.*, **2004** [14] 2142-51 (2004).

38. N. Rao, M.N. Holerca, and V. Pophristic, "Computational Study of the Small Zr(IV) Polynuclear Species," *J. Chem. Theory Comput.*, **4** [1] 145-55 (2008).

39. A. Singhal and K.D. Keefer, "A Study of Aluminum Speciation in Aluminum Chloride Solutions by Small Angle X-ray Scattering and ^{27}Al NMR," *J. Mater. Res.*, **9** [8] 1973-83 (1994).

CHAPTER 3: ANALYTICAL EVALUATION OF THE EFFECTS OF ELECTROLYTE ADDITION ON REVERSE MICELLE SIZE IN THE AOT-WATER-ISOOCTANE SYSTEM

A. Introduction

In Chapter 2, a qualitative model of the effect that salts have on reverse micelle size and stability is described.[1] The model is based on the concept of two overlapping electrical double layers that develop in the confines of the reverse micelle and, more specifically, between the surfactant-lined interface and a central core with displaced co-ions (relative to the surfactant headgroup charge). According to the model, a direct proportionality between the reverse micelle size and the electrical double layer thickness exists and was observed. In the analysis, it was assumed that Na^+ counterions were not significantly contributing to the electrical double layer thickness and instead were displaced to the central core because of the higher cation valence of the added salt.[2-4] Furthermore, the sodium ions would screen the electrostatic repulsion between the co-ions in the central core. This is justified by evaluating local concentrations according to the Gouy-Chapman theory. However, while the sodium ions can be displaced from the interface, they can still participate in the electrical double layer thickness, either entirely or partially and depends on the fidelity of the model. Even if the sodium were contributing to the electrical double layer, the previous arguments used to develop the model are still valid since the contribution of the sodium ions are constant and only shift the curves. Nevertheless, the position of sodium ions in the reverse micelle interior with electrolyte ions having higher cation valence is still unknown.

The position of sodium ions in the base system has been studied without added salt.[5] Nuclear magnetic resonance (NMR) indicates two types of sodium in the interior of the reverse micelle, those bound to the surfactant interface and those dissociated into the interior of the reverse micelle. The differences in the relaxation rates between the two types of sodium states was used to estimate the amount of dissociated sodium ions and resulted in an upper limit of 28%. This strongly supports the concept of a Stern layer, or bound layer immediately adjacent the surfactant interface.[6] The surface potential is reduced across the Stern layer and the diffuse electrical double layer develops according to this reduced potential. In addition to establishing dissociated states, the position of sodium ions in the electrical double layer or in a core environment described in Chapter 2 could also be established by NMR due to the difference in interactions with the local environment in the electrical double layer (with other counterions) and in the core (with co-ions). However, NMR is a relatively expensive characterization technique. Less costly analysis is beneficial to establish support for such a study or to determine that it is unnecessary, for example.

The purpose of this work is to further investigate the validity of the previously developed model. More specifically, the validity of the core concept in the model is investigated, that is, whether or not a core can exist based on analytical results of the electrical double layer concept and whether or not sodium ions are displaced into the core or reside in the electrical double layer instead. Determining the location and configuration of co-ions inside of reverse micelles can have important implications on establishing a fundamental theory for templated crystal growth in reverse micelles because the type of co-ion has been shown to influence particle development when

preparing nanoparticles, including transfer dynamics of precursors and controlling morphology, for example.[7-9] Furthermore, the core described in the model can have fundamental implications on reverse micelle destabilization because of the inability to compress the core as the reverse micelle shrinks and core expands with increasing salt concentration in the polar phase.[1] This can explain the different destabilization sizes that were observed for different systems. However, an alternate explanation also exists. As the average reverse micelle size decreases, and more reverse micelles form to preserve volume, the interfacial area between the water and oil phases increases. The increased interfacial area and associated increase in the average surfactant headgroup area would increase the interfacial tension and could destabilize the reverse micelle structure because a minimum interfacial tension is conditional for the spontaneous formation of reverse micelles.[10-12] This would suggest a similar destabilization size with varying salt unless there were other specific interactions and clarification of the mechanism is necessary.

Four scenarios are evaluated here: (i) the qualitative model as described in Chapter 2 with sodium ions excluded from the electrical double layer, (ii) the qualitative model as described in Chapter 2 with sodium ions included in the electrical double layer, (iii) a slightly modified model (incorporating a Stern layer into the electrical double layer) with sodium ions excluded from the electrical double layer, and (iv) the Stern model with sodium ions included in the electrical double layer.

B. Computational Methods

The average reverse micelle sizes that were measured for Chapter 2 are summarized in Table 3 - I. The sizes, measured by dynamic light scattering (DLS), are the hydrodynamic radii that include the drag effects associated with the reverse micelle

interface structure, affecting Brownian motion and resulting in overestimating size. The reverse micelle interface contains AOT surfactant molecules. The length of the AOT surfactant molecule is approximately 1.1 nm.[5,13] The surfactant headgroup is typically considered to reside at or inside the interface between the polar and organic phases, with the surfactant tail extending into the polar phase, like the model first described by Hoar and Schulman in 1942.[8,13-19] Although considered conceptually, the amount of bound oil in the surfactant tails is often unknown and ignored.[13,17] Considering that the surfactant tails can also lay down on the interface and the organic phase can penetrate through and be bound, or remain mobile, an assumption that approximately one third of the overall AOT length contributes to the hydrodynamic radius was made for this work so that the polar domain size is 0.7 nm less than the measured hydrodynamic diameter.

Table 3 - I. Average Reverse Micelle Diameter (Hydrodynamic) with Salt Additions in the Water/AOT/Isooctane System with Water/Surfactant of Ten[1]

System	0.1 M	0.2 M	0.3 M	0.4 M	0.5 M	0.6 M
NH_4OH	--	8.6	--	8.0	--	7.8
$Al(NO_3)_3$	8.0	6.8	6.4	6.1	--	--
$ZrOCl_2$	8.4	7.5	7.0	--	--	--

The average number of reverse micelles in solution, $\overline{N}_{RM}$, was calculated by dividing the total water volume (in nm) by the volume of an average water phase domain size that is calculated by correcting the average hydrodynamic radius, $\overline{d}_h$ (in nm), for the hydrodynamic effects and assuming a spherical reverse micelle morphology:

$$N_{RM} = \frac{3.6 \times 10^{21}}{\frac{4}{3}\pi\left(\frac{\overline{d}_h - 0.7}{2}\right)^3} \quad (1)$$

The morphology of reverse micelles is dynamic, but expected to be spherical on average for the current system with added salt.[20-24] The average number of surfactant molecules per reverse micelle, $\overline{N}_S$, was calculated using:

$$\overline{N}_S = \frac{n_s N_A}{N_{RM}} \quad (2)$$

where n_s is the number of moles of surfactant, N_A is Avogadro's constant, and assuming that the surfactant molecules are homogeneously distributed .

The average surface charge density, $\overline{\sigma}_0$, was estimated by assuming that the surfactant molecules are distributed evenly amongst $\overline{N}_{RM}$ reverse micelles of average size. The surface area, *A*, of an average reverse micelle is given by:

$$A = 4\pi\left(\frac{\overline{d}_h - 0.7}{2}\right)^2 \quad (3)$$

and the average surface charge density is given by:

$$\overline{\sigma}_0 = \frac{\overline{N}_S z_h e}{A} \quad (4)$$

where z_h is the valence of the headgroup and *e* is the elementary charge constant. For further computations, it is assumed that the surfactant, and surface charge density, is distributed over a planar surface so that the Gouy-Chapman theory applies.[6] A solution of the Poisson-Boltzmann equation leads to the relationship between surface charge density and potential at a charged surface according to the Gouy-Chapman theory and is given by:

$$s_0 = e_r e_0 k f_0 \quad (5)$$

where ε_r is the relative dielectric permittivity for water, ε_o is permittivity of vacuum, κ is the inverse of the electrical double layer thickness, and f_0 is the surface potential. Furthermore, the potential as a function of distance from the surface, $f(d)$, can also be derived from the Poisson-Boltzmann equation and is given by:

$$f(d) = f_0 \exp(-kd) \quad (6)$$

The model from Chapter 2 can be used to describe the reduction in reverse micelle size with increased salt concentration as a consequence of compression of a pair of electrical double layers that allow the respective surfaces to move in closer proximity to each other to balance forces.[1] The concept of a critical potential, f_c, or the potential at half of the distance across the two electrical double layers, $d_{/2}$, was described as a consequence of this model. Analysis of this concept results in a critical potential of -9 mV for the system. Considering $f(d_{/2})$, then equation 6 becomes:

$$f(d_2) = f_c = f_0 \exp(-kd_{/2}) \quad (7)$$

Rearranging equation 7 and substituting in the solution of equation 5 for f_0 gives:

$$d_{/2} = \frac{1}{\kappa} \ln\left(\frac{2\sigma_o}{\varepsilon_r \varepsilon_o \kappa \phi_c}\right) \quad (8)$$

A factor of 2 is included in equation 8 to account for the two electrical double layers so that the critical potential is reduced in half for only one potential. Equation 8 is now in a form that can be used to evaluate the proposed model because the polar phase diameter would be the sum of $4d_{/2}$ and the size of a central core, d_c, so that the following relationship can be defined:

$$d_h - 0.7 = 4d_{/2} + d_c \tag{9}$$

Rearranging equation 9 results in an equation that can be used to verify the feasibility of a core and estimate the core size:

$$d_c = d_h - 0.7 - 4d_{/2} \tag{10}$$

To properly evaluate the model according to equation 8 and equation 10, the electrical double layer thickness κ^{-1} must be defined:

$$\frac{1}{\kappa} = \left(\frac{\varepsilon_r \varepsilon_o k_B T}{1000 e^2 N_A \sum_i z_i^2 c_{io}} \right)^{1/2} \tag{11}$$

where k_B is Boltzmann's constant, T is temperature, z_i is the valence of the counterions of solute i, and c_{io} is the bulk concentration of solute i. Some of the analysis in this work was performed assuming that the sodium counterions are completely displaced from the EDL by counterions of higher valence. To check the validity of this assumption, the relative amounts of sodium counterions compared to other counterions, R, was evaluated using the following relationship:

$$R = \frac{c_j = c_{jo} \exp\left(-\frac{z_j e\phi}{kT} \right)}{c_k = c_{ko} \exp\left(-\frac{z_k e\phi}{kT} \right)} \tag{12}$$

where c_j is the local concentration of the salt counterion and c_k is the local concentration of the sodium counterion in the electrical double layer. Displacement from the surfactant headgroup was evaluated by considering the ratio given by equation 12 when $f = f_o$ and the extent of sodium displaced from the electrical double layer was evaluated by

considering equation 12 when $f = f_c$. Equation 5 was used to estimate ϕ_o, assuming all sodium counterions are in fact present in the electrical double layer.

To incorporate the Stern model,[6] the following relationship will be used:

$$\sigma_S = \sigma_o Q \tag{13}$$

where σ_S is the reduced surface charge density across the Stern layer and Q is the fraction of dissociated sites. Assuming Q = 0.5, then σ_S becomes:

$$\sigma_S = 0.5\sigma_o \tag{14}$$

A value of Q = 0.5 is assumed just to demonstrate the effect of the Stern layer and would indicate a greater extent of headgroup dissociation than the upper limit of dissociated sites estimated in the study by Wong *et al.*[5] The diffuse electrical double layer extending from a surface with charge density of σ_S was analyzed with equation 8, equation 10, and equation 12 to critically evaluate the Stern model and compare the results to those obtained by only considering the Gouy-Chapman theory. The constants used in all analyses are summarized in Table 3 - II.

Table 3 - II. Symbols, Constants, and Units Used in Analytical Model

Symbol	Constant	SI Unit	*Symbol*	Constant	SI Unit
π	3.14	--	f_c	-9.00×10^{-3}	V
n_s	0.02	mol	ε_r	78.5	--
N_A	6.02×10^{23}	/mol	ε_o	8.85×10^{-12}	F/m
z_h	1	--	k_B	1.38×10^{-23}	$m^2kgs^{-2}K^{-1}$
e	1.60×10^{-19}	C	T	298	K

C. Results and Discussion

Table 3 - III, Table 3 - IV, and Table 3 - V contain the computational steps and values used to obtain the surface charge density of reverse micelles containing varying amounts of NH_4OH, $Al(NO_3)_3$ and $ZrOCl_2$, respectively. The diameter of the polar phase is reduced and a corresponding increase in the number of reverse micelles is observed as the concentration of any salt increases because of the assumption that the water volume is preserved. This size-number dependence agrees with the assessment of Spirin *et al*.[25] The number of surfactant molecules per reverse micelle decreases because of the increased interface area between the oil and water phases when salt concentration is increased and the increased interfacial area reduces the surface charge density of the surfactant film. Reduced surface charge density with decreasing reverse micelle size agrees with the works of Lemyre *et al*. and Pileni.[26,27] The estimated surface charge density ranges from 0.49-0.70 C/m^2 and is about twice as large as the values reported or used by other researchers or assumed from geometrical models (~0.20-0.37 C/m^2), which can be the result of different assumptions than those used in this study or different experimental conditions.[13,18,27]

Table 3 - III. Diameter of Polar Phase, Number of Reverse Micelles, Number of Surfactant Per Reverse Micelle, and Surface Charge Density Calculated for Additions of NH_4OH

NH_4OH (M)	0.2	0.4	0.6
d_h - 0.7 (nm)	7.9	7.3	7.1
N_{RM} (x 10^{19})	1.4	1.8	1.9
N_S	860	680	630
σ_o (-C/m^2)	0.70	0.65	0.64

Table 3 - IV. Reduced Diameter, Number of Reverse Micelles, Number of Surfactant Per Reverse Micelle, and Surface Charge Density Calculated for Additions of $Al(NO_3)_3$

$Al(NO_3)_3$ (M)	0.1	0.2	0.3	0.4
d_h - 0.7 (nm)	7.3	6.1	5.7	5.4
N_{RM} (x 10^{19})	1.7	3.0	3.7	4.4
N_S	680	400	330	280
σ_o (C/m^2)	0.65	0.55	0.52	0.49

Table 3- V. Reduced Diameter, Number of Reverse Micelles, Number of Surfactant Per Reverse Micelle, and Surface Charge Density Calculated for Additions of $ZrOCl_2$

$ZrOCl_2$ (M)	0.1	0.2	0.3
d_h - 0.7 (nm)	7.7	6.8	6.3
N_{RM} (x 10^{19})	1.5	2.2	2.7
N_S	800	550	440
σ_o (C/m^2)	0.68	0.61	0.57

The calculated surface charge densities as a function of the added salt concentrations are demonstrated in Figure 3 - 1, which also includes the points of instability. The points of instability correspond to different surface charge densities for the different salts. Previously, the inability to further compress co-ions into the core of the reverse micelle was suggested as the mechanism for destabilization.[1] Alternatively, a mechanism known as salting out has been described for which the reduced surfactant density at the interface increases interfacial tension until single phase reverse micelles are no longer supported.[28,29] The change in interfacial tension with salt concentration, like reverse micelle size, is also proportional to the electrical double layer thickness.[30] Thus, the relationship to the electrical double layer thickness cannot rule out either mechanism.

The strong dependence of surface charge density on the electrical double layer thickness does suggest that the interfacial tension is a balancing force. However, the differences in surface charge density at the points of instability suggests that the surface charge density and interfacial tension are not the controlling mechanism by which destabilization occurs or destabilization would occur at the same surface charge density unless the change in interfacial tension with added salt decreases in the order of NH_4OH, $ZrOCl_2$, and $Al(NO_3)_3$ so that a lower surface charge density can be accommodated in that respective order. However, the change in interfacial tension is not readily available to make any definite conclusions. Resolving this issue can provide valuable insight into the destabilization mechanism, validating or discrediting the destabilization mechanism that is proposed in Chapter 2.

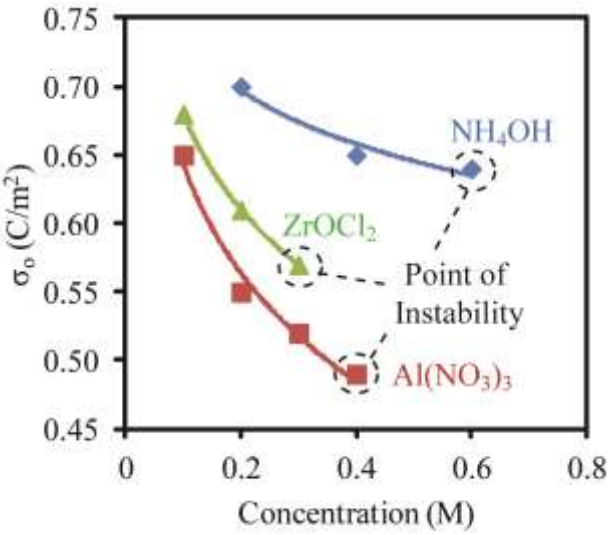

Figure 3 - 1. The surface charge density of AOT reverse micelles in isooctane as a function of added salt concentration. Lines are drawn as a guide for the eye.

The computational steps and values used to evaluate the validity of the model developed in Chapter 2, assuming that sodium counterions do not participate in the electrical double layer, are given in Table 3 - VI. The results indicate that the core size at the point of instability is 3.5 nm, 3.4 nm, and 4.7 nm for NH_4OH, $Al(NO_3)_3$, and $ZrOCl_2$ containing reverse micelle solutions, respectively, and confirms the feasibility of a central core containing both sodium counterions and electrolyte co-ions.

Table 3 - VI. Point of Instability, Surface Charge Density of Surfactant Film, Electrical Double Layer Thickness, Distance from Surfactant Film to Point of Critical Potential, Polar Phase Diameter, and Core Size Using a Gouy-Chapman Based Model

Electrolyte	NH_4OH	$Al(NO_3)_3$	$ZrOCl_2$
P.O.I. (M)	0.6	0.4	0.3
σ_o (C/m^2)	0.64	0.49	0.57
κ^{-1} ($x10^{-9}$ m)	0.28	0.23	0.2
$d_{/2}$ ($x10^{-9}$ m)	0.9	0.5	0.4
d_h-0.7 ($x10^{-9}$ m)	7.1	5.4	6.3
d_c ($x10^{-9}$ m)	3.5	3.4	4.7

The relative concentrations of sodium ions relative to the salt counterions was calculated by equation 12, using the maximum (surface) and minimum (critical) potentials, and the results are given in Table 3 - VII. The value of *R* at the surface is 25.2, 174, and 206,000 for NH_4OH, $Al(NO_3)_3$, and $ZrOCl_2$ electrolyte solutions, resepectively and demonstrates the displacement of sodium from the surfactant interface because of the higher valence of the additive and agrees well with the model. However, the *R* values at the minimum potential are 0.15 for the analysis of all three electrolytes, suggesting surplus sodium ions (~7x) when compared to the electrolyte counterion. Given that there is more than nine times higher sodium concentration than the salt

counterion concentration, some of the sodium ions must be displaced outside of the two overlapping electrical double layers according to this analysis. The problem with the analysis is that it was assumed that the sodium counterions are in fact in the electrical double layer and neglects the possibility that there is another sodium position that is more energetically favorable, such as the displacement into the core to screen the electrostatic repulsion between displaced co-ions. Co-ions can also be present in the electrical double layer.[4] Reality is likely to be somewhere in between, that is, some of the co-ions and sodium counterions participate in the electrical double layer and some of them are displaced to the core. Thus, an analysis excluding sodium counterions from the electrical double layer and including them represent two extremes.

Table 3 - VII. Ratio of Salt Counterion to Sodium Counterion Concentration at the Maximum and Minimum Potential in the Electrical Double Layer

Electrolyte	Potential (V)	*R*
NH_4OH	-0.14	25.2
	-0.01	0.15
$Al(NO_3)_3$	-0.10	174
	-0.01	0.15
$ZrOCl_2$	-0.11	206,000
	-0.01	0.15

The computational steps and values that were used to evaluate the validity of the model, but assuming that all sodium counterions and co-ions are included in the electrical double layer, are demonstrated in Table 3 - VIII. In this scenario, the sodium counterions further reduce the electrical double layer thickness and the estimated core size is 5.9 nm, 4.2 nm, and 5.5 nm for the NH_4OH, $Al(NO_3)_3$, and $ZrOCl_2$ electrolyte solutions,

respectively, which are all larger core sizes than when sodium is assumed to be excluded from the electrical double layer. In this case, the core would consist of water instead of a net-negatively charged core. Two overlapping potentials can still be assumed by considering a slight modification to the model based on the results of Biswas *et al.* in which the net negative surface is generated by the local orientation of the hydrogen bond network (water molecules).[31] Alternatively, the intermediate condition in which some of the sodium counterions and the electrolyte co-ions are separated into the core can still generate the net negative surface in the core.

Table 3 - VIII. Point of Instability, Surface Charge Density of Surfactant Film, Electrical Double Layer Thickness (EDL), Distance from Surfactant Film to Point of Critical Potential, Polar Phase Diameter, and Core Size Using a Gouy-Chapman Based Model and Assuming Sodium Counterions Contribute to the Electrical Double Layer

Electrolyte	NH_4OH	$Al(NO_3)_3$	$ZrOCl_2$
P.O.I. (M)	0.6	0.4	0.3
σ_o (C/m^2)	0.64	0.49	0.57
κ^{-1} ($x10^{-9}$ m)	0.15	0.14	0.13
$d_{/2}$ ($x10^{-9}$ m)	0.3	0.3	0.2
d_h-0.7 ($x10^{-9}$ m)	7.1	5.4	6.3
d_c ($x10^{-9}$ m)	5.9	4.2	5.5

A similar analysis was performed, but assuming a reduced potential because of the development of a Stern layer. The results, either without or with sodium counterions in the electrical double layer, are presented in Table 3 - IX. Including the Stern model further reduces the electrical double layer thickness and increases the calculated sizes of the core, demonstrated by comparing the results in Table 3 - IX to the results in Table 3 - VI and Table 3 - VIII.

Table 3 - IX. Point of Instability, Surface Charge Density of Surfactant Film, Surface Charge Density at the Stern Layer, Electrical Double Layer Thickness (EDL), Distance from Surfactant Film to Point of Critical Potential, and Core Size Using a Stern-Based Model Without and With Sodium Counterions Contributing to the Electrical Double Layer

Condition	Electrolyte	NH_4OH	$Al(NO_3)_3$	$ZrOCl_2$
	P.O.I. (M)	0.6	0.4	0.3
	σ_o (C/m^2)	0.64	0.49	0.57
	σ_S (C/m^2)	0.32	0.25	0.29
Without	κ^{-1} ($x10^{-9}$ m)	0.28	0.23	0.20
	$d_{/2}$ ($x10^{-9}$ m)	0.35	0.19	0.16
	d_c ($x10^{-9}$ m)	5.7	4.6	5.7
With	κ^{-1} ($x10^{-9}$ m)	0.15	0.14	0.13
	$d_{/2}$ ($x10^{-9}$ m)	0.10	0.05	0.06
	d_c ($x10^{-9}$ m)	6.7	6.9	6.9

D. Conclusions

Analysis of the electrical double layer thickness and distance from the surface potential to the critical potential supports the qualitative model that was developed in Chapter 2. Specifically, the length of the two overlapping electrical double layers supports the formation of a central core. A core size of 3.4-6.9 nm is estimated for the three systems analyzed at the respective points of instability, depending on the assumptions that are made. The core size is larger if sodium counterions, dissociated from the surfactant headgroups, are incorporated into the electrical double layer. However, the amount of sodium counterions in the electrical double layer cannot be determined from this analysis. The core size is also increased by the incorporation of a Stern layer. However, the extent by which the surface potential is reduced is unclear.

The analysis supports further development of the model to understand the precise location of the sodium counterions and extent of occupied states in the Stern layer.

E. References

1. H. Fathi, J.P. Kelly, V.R. Vasquez, and O.A. Graeve, "Ionic Concentration Effects on Reverse Micelle Size and Stability: Implications for the Synthesis of Nanoparticles," *Langmuir,* **28** [25] 9267-74 (2012).

2. R. Alargova, J. Petkov, D. Petsev, I.B. Ivanov, G. Broze, and A. Mehreteab, "Light Scattering Study of Sodium Dodecyl Polyoxyethylene-2-sulfate Micelles in the Presence of Multivalent Counterions," *Langmuir*, **11** [5] 1530-6 (1995).

3. R.D. Falcone, J.J. Silber, and N.M. Correa, "What are the Factors that Control Non-aqueous/AOT/n-heptane Reverse Micelle Sizes? A Dynamic Light Scattering Study," *Phys. Chem. Chem. Phys.,* **11** [47] 11096-100 (2009).

4. Stokes, R. J.; Fennell Evans, D. *Fundamentals of Interfacial Engineering*; pp. 130-140. Wiley-VCH, New York, 1996.

5. M. Wong, J.K. Thomas, and T. Nowak, "Structure and State of H_2O in Reversed Micelles. 3," *J. Am. Chem. Soc.,* **99** [14] 4730-6 (1977).

6. Stokes, R. J.; Fennell Evans, D. *Fundamentals of Interfacial Engineering*; pp. 152-62. Wiley-VCH, New York, 1996.

7. J.H. Adair, T. Li, K. Havey, J. Moon, J. Mecholsky, A. Morrone, D.R. Talham, M.H. Ludwig, and L. Wang, "Recent Developments in the Preparation and Properties of Nanometer-size Spherical and Platelet-shaped Particles and Composite Particles," *Mater. Sci. Eng., R,* **23** [4-5] 139-242 (1998).

8. S.P. Moulik and B.K. Paul, "Structure, Dynamics and Transport Properties of Microemulsions," *Adv. Colloid Interface Sci.,* **78** [2] 99-195 (1998).

9. M.P. Pileni, "Mesostructured Fluids in Oil-rich Regions: Structural and Templating Approaches," *Langmuir,* **17** [24] 7476-86 (2001).

10. G. Gillberg, H. Lehtinen, and S. Friberg, "NMR and IR Investigation of the Conditions Determining the Stability of Microemulsions," *J. Colloid Interface Sci.,* **33** [1] 40-53 (1970).

11. V. Pillai, P. Kumar, M.J. Hou, P. Ayyub, and D.O. Shah, "Preparation of Nanoparticles of Silver Halides, Superconductors and Magnetic Materials Using

Water-in-oil Microemulsions as Nano-reactors," *Adv. Colloid Interface Sci.*, **55**, 241-69 (1995).

12. S.P. Moulik and B.K. Paul, "Structure, Dynamics and Transport Properties of Microemulsions," *Adv. Colloid Interface Sci.*, **78** [2] 99-195 (1998).

13. H.B. Bohidar and M. Behboudnia, "Characterization of Reverse Micelles by Dynamic Light Scattering," *Colloids Surf., A*, **178** [1-3] 313-23 (2001).

14. N.E. Levinger and L.A. Swafford, "Ultrafast Dynamics in Reverse Micelles," *Annu. Rev. Phys. Chem.*, **60**, 385-406 (2009).

15. V. Uskoković and M. Drofenik, "Synthesis of Materials within Reverse Micelles," *Surf. Rev. Lett.*, **12** [2] 239-77 (2005).

16. M.J. Castagnola and P.K. Dutta, "Crystal Growth of Zincophosphates from Conventional Media and Reverse Micelles: Mechanistic Implications," *Microporous Mesoporous Mater.*, **20** [1-3] 149-59 (1998).

17. S. Brunetti, D. Roux, A.M. Bellocq, G. Fourche, and P. Bothorel, "Micellar Interactions in Water-in-oil Microemulsions. 2. Light Scattering Determination of the Second Virial Coefficient," *J. Phys. Chem.*, **87** [6] 1028-34 (1983).

18. E. Sheu, K.E. Göklen, T.A. Hatton, and S.-H. Chen, "Small-angle Neutron Scattering Studies of Protein-reversed Micelle Complexes," *Biotechnol. Prog.*, **2** [4] 175-86 (1986).

19. T.P. Hoar and J.H. Schulman, "Transparent Water-in-oil Dispersions: the Oleopathic Hydro-micelle," *Nature*, **152** [3847] 102-3 (1943).

20. P.D.I. Fletcher, A.M. Howe, and B.H. Robinson, "The Kinetics of Solubilisate Exchange between Water Droplets of a Water-in-oil Microemulsion," *J. Chem. Soc., Faraday Trans. 1*, **83** [4] 985-1006 (1987).

21. C. Petit, P. Lixon, and M.-P. Pileni, "In Situ Synthesis of Silver Nanocluster in AOT Reverse Micelles," *J. Phys. Chem.*, **97** [49] 12974-83 (1993).

22. K.E. Marchand, M. Tarret, J.P. Lechaire, L. Normand, S. Kasztelan, and T. Cseri, "Investigation of AOT-based Microemulsions for the Controlled Synthesis of MoS_x Nanoparticles: An Electron Microscopy Study," *Colloids Surf., A*, **214** [1-3] 239-48 (2003).

23. A. Gardner, V.R. Vásquez, A. Clifton, and O.A. Graeve, "Molecular Dynamics Analysis of the AOT/Water/Isooctane System: Effect of Simulation Time, Initial Configuration, and Model Salts," *Fluid Phase Equilib.*, **262** [1-2] 264-70 (2007).

24. V.R. Vasquez, B.C. Williams, and O.A. Graeve, "Stability and Comparative Analysis of AOT/Water/Isooctane Reverse Micelle System Using Dynamic Light Scattering and Molecular Dynamics," *J. Phys. Chem. B,* **115** [12] 2979-87 (2011).

25. M.G. Spirin, S.B. Brichkin, and V.F. Razumov, "Gold Clusters and Nanoparticles in Reverse Micelles Formed by Tritons X-100, X-114, and X-45," *Colloid J.,* **73** [3] 384-8 (2011).

26. J.-L. Lemyre, S. Lamarre, A. Beaupré, and A.M. Ritcey, "A New Approach for the Characterization of Reverse Micellar Systems by Dynamic Light Scattering," *Langmuir,* **26** [13] 10524-31 (2010).

27. M.P. Pileni, "Reverse Micelles as Microreactors," *J. Phys. Chem.*, **97** [27] 6961-73 (1993).

28. E. Ruckenstein and R. Krishnan, "Effect of Electrolytes and Mixtures of Surfactants on the Oil-water Interfacial Tension and Their Role in Formation of Microemulsions," *J. Colloid Interface Sci.,* **76** [1] 201-11 (1980).

29. J.A. Beunen and E. Ruckenstein, "The Effect of Salting out and Micellization on Interfacial Tension," *Adv. Colloid Interface Sci.,* **16** [1] 201-31 (1982).

30. P.K. Weissenborn and R.J. Pugh, "Surface Tension of Aqueous Solutions of Electrolytes: Relationship with Ion Hydration, Oxygen Solubility, and Bubble Coalescence," *J. Colloid Interface Sci.*, **184** [2] 550-63 (1996).

31. R. Biswas, T. Chakraborti, B. Bagchi, and K.G. Ayappa, "Non-monotonic, Distance-dependent Relaxation of Water in Reverse Micelles: Propagation of Surface Induced Frustration along Hydrogen Bond Networks," *J. Chem. Phys.*, **137** [1] 014515 9pp. (2012).

CHAPTER 4: SPECIFIC ION EFFECTS ON REVERSE MICELLE SIZE AND STABILITY IN THE ELECTROLYTE-AOT-ISOOCTANE SYSTEM

A. Introduction

Although the basic structure of a water-in-oil microemulsion was described in literature as early as 1943 and has been used for synthesis of novel nanomaterials since 1982, the effect of precursors on reverse micelles has received little attention.[1-28] Stable reverse micelles are of particular interest for nanoparticle formation and the synthesis should be performed without breaking the microemulsion. This is especially true if the nanoparticles are to be made by a multi-step process. Not breaking the microemulsion represents a primary challenge of reverse micelle synthesis and a few key requirements have been suggested, but stability is generally not accurately predicted or controlled. Requirements for stability are that the water phase should form well-defined and closed water domains, which is facilitated by dilute water concentrations, geometry of the surfactant, length of an added cosurfactant, and additives.[29-36]

In contrast to the titration method, recent work has begun to evaluate reverse size and stability in the AOT/water/isooctane system with systematic additions of electrolyte without changing the water content.[37] The results of this previous work suggests that electrostatic interactions between the surfactant head groups and electrolyte solution cause the average reverse micelle size to decrease with an increase in the electrolyte concentration, which can be understood by considering compression of overlapping electrical double layers according to the Gouy-Chapman theory of ion ordering at a

charged surface. A critical electrolyte concentration can no longer accommodate these structural changes and the reverse micelles become unstable.

A core-shell model of structuring in reverse micelles conceptually similar to the work in previous chapters has been experimentally explored and debated based on recent advances in ultrafast spectroscopic techniques.[38-40] However, the analysis has been focused primarily on simple systems without salt additions and more specifically on the structure of water in the reverse micelles. Layer-wise decomposition of water structure indicated that a pseudo-ordered hydrogen-bond network is formed, but still dynamic because of collective motions caused by fluctuations in reverse micelle morphology.[41] Furthermore, the hydrogen bond network is similar for varying water-to-surfactant ratio (ω_o), but the surfactant counterion distribution changes.[39] At ω_o = 2, most of the counterions are not dissociated, but the counterions exist mostly as an asymmetric bimodal distribution between two water surfaces dominated by negative water poles when ω_o = 7.5. While this arrangement varies from the original model proposed in Chapter 2, the consequences are exactly the same: a negative surface layer, an intermediate layer where counterions reside, and a central core layer that provides a secondary negative surface. Furthermore, the two water layers create a highly symmetric well. Despite the assumptions made in the model presented in Chapter 2, such as a symmetric bimodal distribution of counterions within a symmetric well, the effect of electrolyte concentration on reverse micelle size was strongly correlated to the model and encourages further development.

A more extensive set of electrolytes were studied for this chapter to evaluate specific counterion (cation) and co-ion (anion) effects with respect to the headgroup of

the anionic surfactant. The study is also extended to include monovalent counterions. Extension of the electrical double layer concept developed in Chapter 2 to low concentrations cannot produce the reverse micelle size without electrolyte additions. Therefore, low concentrations were also evaluated. A special case, for which there is not a size decrease, but a size increase with increasing electrolyte concentration, was found and discussed. This work has important implications for developing a fundamental understanding of reverse micelle behavior in the presence of electrolyte solutions, which are precursors for reverse micelle synthesis. A broader goal is to develop a model to predict stable and unstable reverse micelle synthesis parameters in the electrolyte/AOT/isooctane system and then be able to extend this model to other systems. Thus, understanding the importance of specific ion effects is of critical importance.

B. Experimental Methods

All reverse micelle solutions were prepared and characterized by methods previously established.[37] The only differences were the type and amount of electrolyte added. To prepare the reverse micelle solutions, 8.891 g of sodium bis(2-ehtylhexyl) sulfosuccinate (AOT, 98+%, Sigma-Aldrich, St. Louis, MO) was mixed with 69.0 g of 2,2,4-trimethylpentane (isooctane, 99+%, Sigma-Aldrich, St. Louis, MO). A separate solution containing 3.6 g of water and the appropriate amount of electrolyte were prepared. The types and amount of electrolytes for the prepared solutions are provided in Table 4-I. The isooctane solution and water solution were allowed to mix separately for 30 minutes before mixing them together to make the reverse micelle solutions having ω_o = 10. The reverse micelle solution was mixed for 2 hours before characterization. At least three solutions of each composition were prepared and characterized.

Table 4 - I. Electrolyte Reactant Information

Counterion valence	Electrolyte	Purity, Manufacturer (A1, B2, or C3)	Concentration range (M)	Step size (M)	Equivalent amounts (g)
Monovalent	$NaBH_4$	98%, A	0.1-0.5	0.1	0.014-0.068
	$HAuCl_4$	99.9+%, A	0.1-0.5	0.1	0.142-0.709
Divalent	$CuCl_2$	99+%, B	0.1-0.6	0.1	0.061-0.368
	$FeSO_4$	99+%, A	0.1-0.6	0.1	0.111-0.665
	$Mg(NO_3)_2$	98%, B	0.1-0.6	0.1	0.092-0.554
	$MgCl_2$	99+%, C	0.1-0.6	0.1	0.073-0.439
Trivalent	$Al(NO_3)_3$	99.99%, B	0.1-0.4	0.1	0.118-0.471
	$Fe(NO_3)_3$	98+%, B	0.1-0.4	0.1	0.145-0.582
	$Y(NO_3)_3$	99.9%, B	0.1-0.4	0.1	0.138-0.552
Tetravalent	$ZrOCl_2$	99.9985%, B	0.01-0.30	0.01	0.012-0.348

[1]Sigma-Aldrich, St. Louis, MO, [2]Alfa Aesar, Ward Hill, MA, [3]Thermo Fisher Scientific, Waltham, MA

The size of the reverse micelles were measured by dynamic light scattering (DLS) using either a Nanotrac Ultra instrument (Microtrac, Montgomeryville, PA) or a Nanotrac Wave instrument (Microtrac, Montgomeryville, PA. A correlation factor is applied when using the Nanotrac Wave, determined by measuring and comparing the average sizes of reverse micelles containing $Mg(NO_3)_2$ using both instruments. The average of five runs was considered one measurement, each performed for 15 s. Five of these measurements were made for each sample and at least three samples were prepared for each composition, except for reverse micelle solutions containing $HAuCl_4$, which were only prepared once. The isooctane fluid constants used for analysis are an index of refraction of 1.40, low temperature viscosity of 0.542 cP at 20°C, and a high temperature viscosity of 0.389 cP at 50°C. An index of refraction of 1.48 was utilized for the reverse micelles,

although the index of refraction does not significantly affect the computation. DLS does not produce an absolute size value and the distributions are only suitable for comparison purposes, such as for observing size changes. The interest of this chapter was to observe size changes resulting in observable trends. As such, and in addition to the relative ease of measuring and analyzing data, DLS is particularly suitable for experimentally observing the effects that electrolytes have on reverse micelle sizes.

C. Results and Discussion

Chapter 2 demonstrated that the average reverse micelle size when salts are added to the water/AOT/isooctane system is directly proportional to the electrical double layer thickness, which is defined by

$$\frac{1}{\kappa} = \left(\frac{\varepsilon_r \varepsilon_o k_B T}{1000 q^2 N_A \left(z^2 c \right)} \right)^{1/2} \tag{1}$$

where κ^{-1} corresponds to the electrical double layer thickness, ε_r is the relative dielectric permittivity of the solvent, ε_o is the electrical permittivity of vacuum, k_B is Boltzmann's constant, T is the temperature, q is the elementary charge, N_A is Avogadro's number, z is the valence of the counterion, and c is the bulk concentration of the counterion. The only relevant variables in the EDL thickness with respect to changing the type and amount of electrolyte are the counterion valence and bulk concentration. Thus, previous results demonstrate a linear relationship exists between the average reverse micelle size and $(z^2c)^{-1/2}$. The size is controlled by the interaction between two overlapping electrical double layers, according to Chapter 2. Compression of the electrical double layers, by increasing electrolyte valence or concentration, causes the average reverse micelle size to decrease. The reverse micelle size continues to decrease with increasing electrolyte

concentration up to the point of instability, at which the single phase reverse micellar phase is no longer supported and a two-phase system forms instead. The two-phase system consists of the reverse micellar phase and a coalesced water phase. It is proposed that the second phase forms because of the inability to compress an unlimited amount of co-ions into the core of the reverse micelle. Furthermore, the point of instability corresponds to $1.2/z$ for the systems presented in Chapter 2. Analysis of specific ion effects is performed here based on this concept.

1. Effect of Monovalent Counterions

Figure 4-1 confirms that the average reverse micelle size is proportional to the electrical double layer thickness when monovalent counterions were introduced, which contains data for electrolyte concentrations up to 0.5 M (the point at which the solutions became turbid). While the transition from transparent to turbid represents the point of instability for the $NaBH_4$ system, the transition does not capture instability for the $HAuCl_4$ system. In addition to the reverse micellar phase, the presence of an additional size distribution at larger sizes in the DLS results indicate the presence of a coalesced phase and is demonstrated in Figure 4-1b.[42] Thus, all solutions were unstable when $HAuCl_4$ was added although the solutions were transparent when less than 0.5 M $HAuCl_4$ was added.

The points of instability are at concentrations much lower than expected from the relationship developed in Chapter 2 (1.2 M) and might be explained by the longer electrical double layer thickness of monovalent ions compared to higher valence ions such that they cannot be fully accommodated into the confined space of the reverse micelle structures. Furthermore, monovalent electrolytes are considered special cases in

the model because the Na^+ counterion is identical to the counterion of the surfactant molecules and therefore do not displace the surfactant counterions as is expected for higher valence counterions.[37,43] The results demonstrate that the average reverse micelle size decreases linearly as $(z^2c)^{-1/2}$ is decreased (i.e. as electrolyte concentration is increased) when $NaBH_4$ is added to the reverse micelle system, which can be expected from the work in Chapter 2. However, the average reverse micelle size increases linearly as $(z^2c)^{-1/2}$ is decreased when $HAuCl_4$ is added to the reverse micelle system. This result is unique from all other data collected in this study and may be used to explain the lack of stability for this system.[37,42]

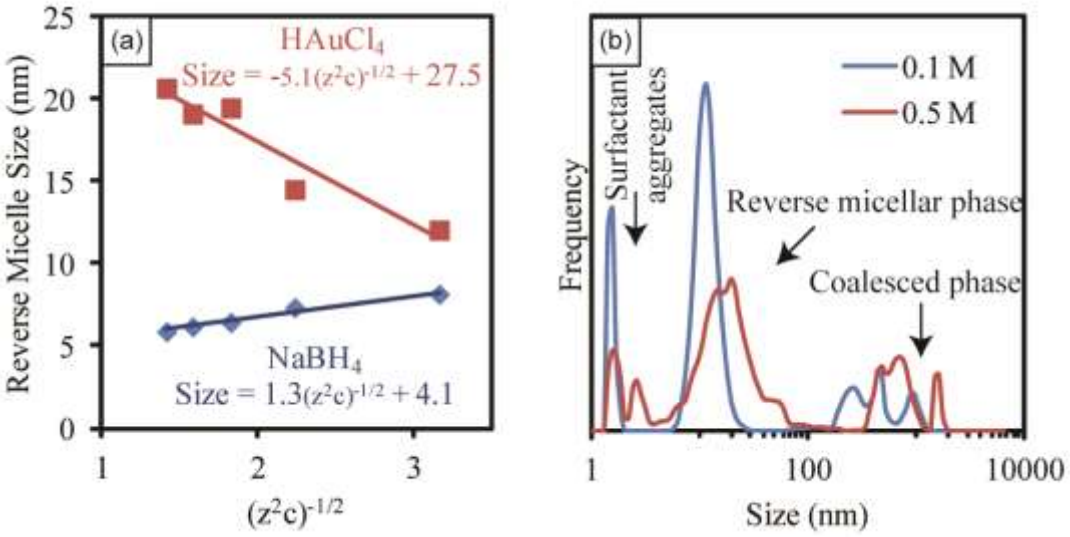

Figure 4 - 1. (a) Average reverse micelle size with respect to counterion valence and concentration of $NaBH_4$ and $HAuCl_4$ in water/AOT/isooctane reverse micelle solutions with ω_o =10. (b) Size distributions of water/AOT/isooctane reverse micelle solutions with ω_o =10 and varying amount of $HAuCl_4$ added.

Reverse micelle growth with $HAuCl_4$ additions cannot be directly accounted for in the qualitative model developed in Chapter 2. The proposed mechanism for reverse

micelle size changes, compression of the electrical double layers with increasing counteiron valence or electrolyte concentration, only predicts size decreases with increasing compression of the EDLs. Three possible explanations for the reverse micelle growth discrepancy are described here. The first explanation is that the size of the $(AuCl_4)^-$ co-ion complex is too large to be effectively accommodated into the core of the reverse micelle. Hydrated ion sizes are considered to investigate this argument. An ion in water will form a hydration complex because of ion-dipole interactions. An example of a hydration complex is demonstrated by the schematic given in Figure 4-2, where the negative dipole of coordinating water molecules (i.e. the oxygen poles) orient towards the sodium cation. The average radial distance of the water coordination shell is given as r_{Na-O} and can be written more generally as r_{M-O} for any metal ion, M, in solution. A summary of r_{M-O} values has been given by Ohtaki and Radnai.[44] In three dimensions, tetrahedral, octahedral, or no specific symmetry can be assumed for the water coordination around Na^+ ions and r_{Na-O} is in the range of 230-250 pm for a dilute electrolyte solution. The coordination complex is expected to be perturbed by the local electric field effects of other ions and the surfactant headgroups in the confined space of a reverse micelle. Nevertheless, the local field effects should be similar for varying types of ions and the structure of the dilute coordination complex is assumed to be a representative measure of the ion interaction with water in a reverse micelle since the actual structure is unknown. Thus, r_{M-O} values will be used to describe the size of the ion hydration complexes with respect to behavior in reverse micelles. The validity of using this assumption to establish effects within reverse micelles will be highlighted in a

subsequent section by demonstrating a relationship between reverse micelle sizes and ion hydration sizes.

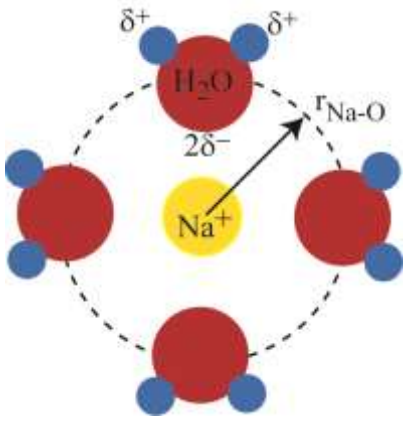

Figure 4 - 2. Schematic demonstrating a hydrated ion complex in dilute solution.

Chapter 2 demonstrated that NH_4OH, $Al(NO_3)_3$, or $ZrOCl_2$ cause a decrease in the average reverse micelle size. The sizes of the ion hydration complexes for these electrolytes are estimated to range from 187-365 pm, with hydrated Al^{3+} and Cl^- ions being at small and large extremes, respectively. Thus, ion sizes within this range cannot be used to justify average reverse micelle growth. The size of the $(BH_4)^-$ anion complex in $NaBH_4$ is estimated to be between 192-395 pm, assumed by considering the range of distances with coordinated metals because $r_{M\text{-}O}$ is unknown for this complex.[45,46] The structure of the $(AuCl_4)^-$ anion complex is also unknown, but expected to be more than 357-400 pm based on considering distances with coordinated metals and larger than that for all other ions studied in this work.[44,47]

An alternate explanation of the anomalous reverse micelle size trend with $HAuCl_4$ additions is considered by slight modifications to the model from Chapter 2 based on the results of Biswas *et al.*[39] If the negative surface charge and net negatively charged core

developed in the model are replaced by a frustrated hydrogen bond network that forms a symmetric well containing counterions, then it is possible that H^+ ions react with water molecules to form hydronium ions and become part of the hydrogen bond network when $HAuCl_4$ is added to the reverse micelle system. The high reactivity of H^+ with water molecules would make it the potential-determining ion in the well. Thus, the well in the hydrogen bond network could be positively charged and contain the $(AuCl_4)^-$ complex counterion that decays from the resulting positive surface potentials. The interaction between the negatively charged complex in the well and the AOT surfactant at the reverse micelle interface results in Coulombic repulsion and can be used to explain the expansion in reverse micelle size. A revised model describing this is demonstrated in Figure 4-3. Also incorporated into the new model is a Stern layer, which is a strongly bound layer immediately in contact with the charged surface. The Stern layer is considered to be a capacitor and reduces the surface potential in a linear manner to the ζ-potential at the shear plane (edge of the Stern layer). In the Stern model, the Gouy-Chapman diffuse layer extends from the shear plane and the potential decays according to the ζ-potential instead of the surface potential.

Alternatively, a combination of large ion complex size and effects of the hydrogen bond network may be responsible for the reverse micelle growth when $HAuCl_4$ is added since neither of these effects can be ruled out. The large $(AuCl_4)^-$ ion size could also be the driving force for it to selectively reside at the interface because of the already disrupted hydrogen bond network near the AOT headgroups, accommodating large ions more readily, and the need to maximize water-water and ion-water interactions in the system.[47] An analysis of pH effects on electrolyte accommodation in reverse micelles

may provide insight for determining if changing the hydrogen bond network or ion size is causal because potential determining ions H^+ and OH^- could be used to switch the effect of the hydrogen bond network to cause either size decrease or increase for the same electrolyte solution, depending on the pH, if the hydrogen bond network is causal. Some pH studies on reverse micelle behavior or reverse micelle synthesis exist, but not in a systematic way that establishes the effect on reverse micelle size changes with added salt.[6,48-51] At least one study establishes improved solubility in reverse micelles by addition of an acid, which can be a result of changes to the hydrogen bond network.[4]

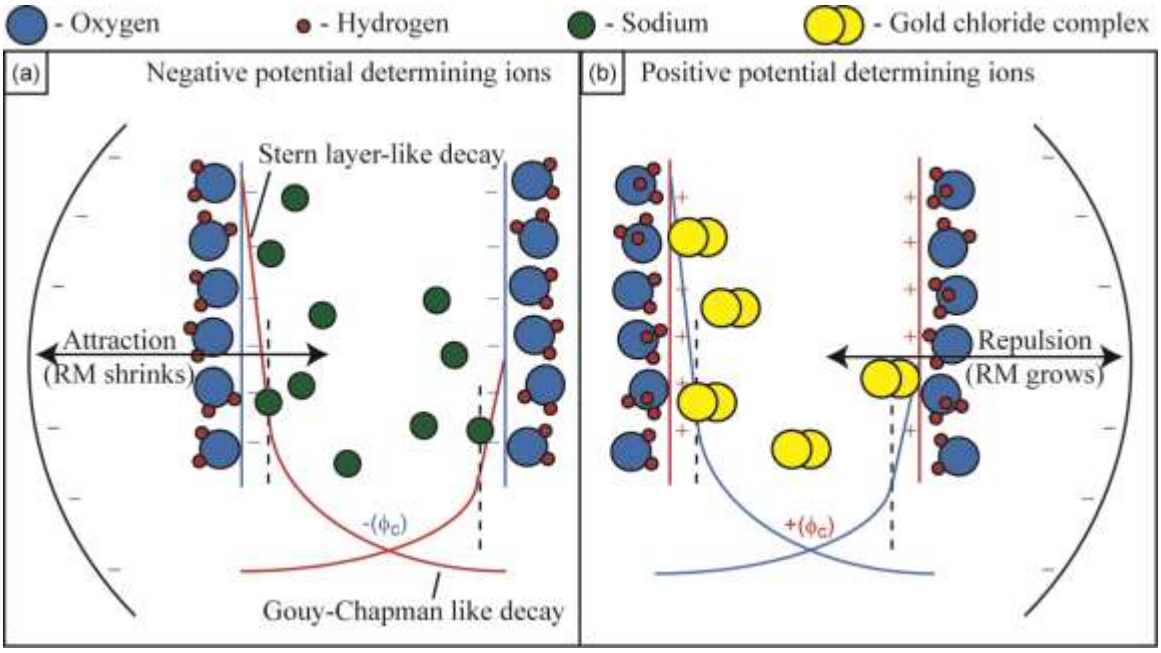

Figure 4 - 3. Qualitative model for opposite reverse micelle size changes as a result of structural changes to the hydrogen bond network from negative or positive potential determining ions.

2. Effect of Divalent and Trivalent Counterions

The average reverse micelle sizes with electrolytes containing multivalent counterions are demonstrated in Figure 4-4. The average sizes of the reverse micelles

containing divalent counterions as a function of electrical double layer thickness are given in Figure 4-4a and the linear fits demonstrate the dependence on the electrical double layer thickness. The linear dependence on the electrical double layer thickness and similar slope can be expected from the compression of the electrical double layer thickness with increasing electrolyte concentration and because there are no changing variables in the electrical double layer thickness (equation 1). However, the size intercept of the linear fits cannot be accounted for using the electrical double layer thickness and can be considered a specific ion effect. This is demonstrated in Figure 4-4b, which shows a linear dependence of the size intercept from the fits given in Figure 4-4a on the hydrated ion complexes (cation and anion) for the four electrolytes, assuming that $r_{M\text{-}O}$ is a representative measure.[44] Thus, the size of the reverse micelles can be fully described using the electrolyte concentration and size of the ion hydration complexes. The analysis allows the average reverse micelle size to be predicted for other electrolytes using the sizes of the associated ion hydration complexes.

An interesting feature of Figure 4-4 is that the slopes of the linear fits in Figure 4-4b and Figure 4-3d have opposite sign, which could indicate that the effect of ion hydration sizes are different for the electrolytes with divalent counterions when compared to the effect when electrolytes with trivalent counterions are added. The electrolytes having divalent counterions follow expectations that larger average reverse micelle sizes are obtained with larger hydrated ion sizes. However, the opposite is true of electrolytes with trivalent counterions; smaller reverse micelles are obtained with larger ion hydration sizes. Thus ion size cannot be the only important consideration. This could also be a unique consequence of specific ions, because trivalent counterions provide a greater

extent of electrostatic screening and result in a greater difference between the surface potential and the ζ-potential. Furthermore, smaller counterions also provide a greater

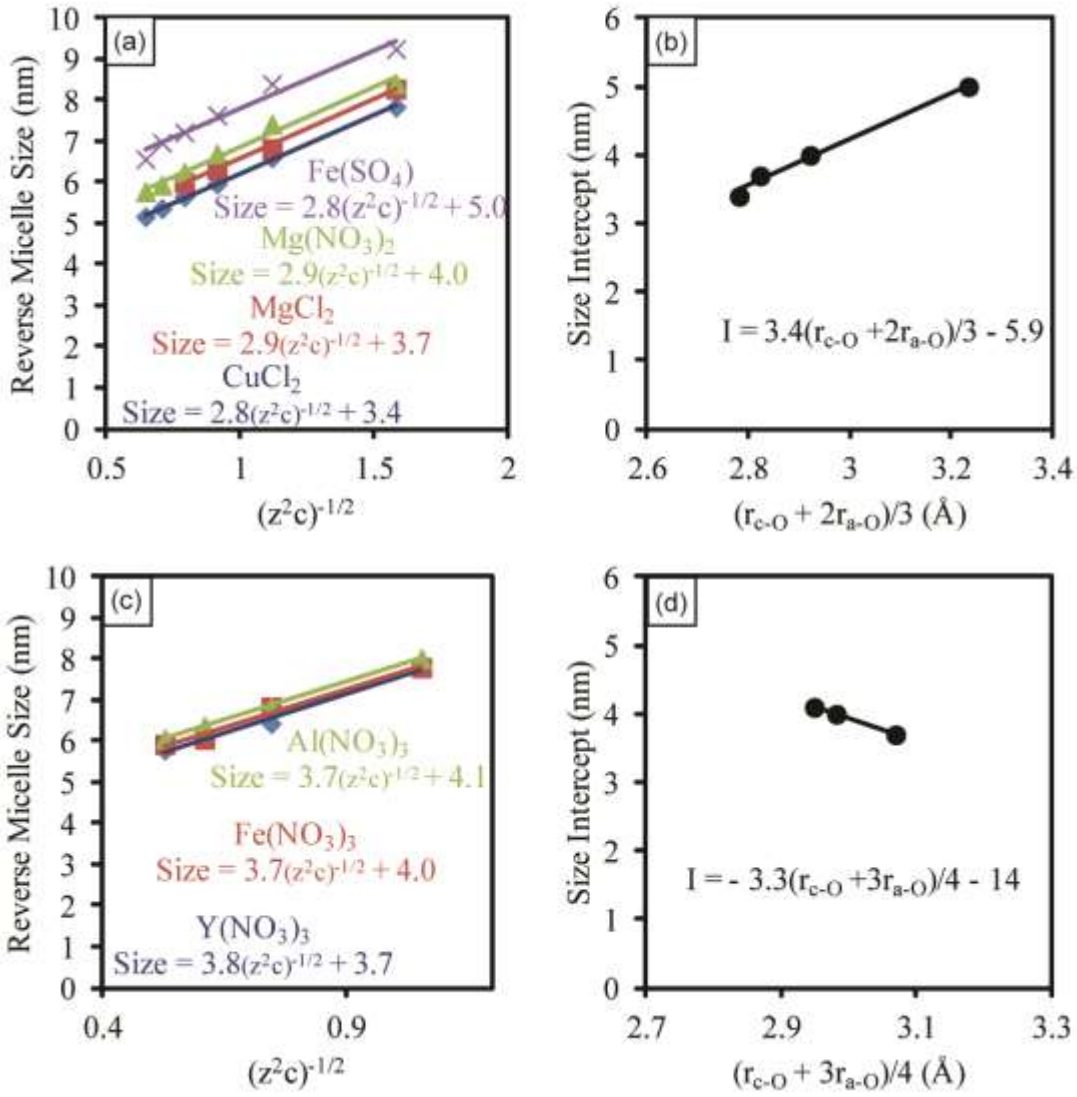

Figure 4 - 4. (a) Effect of electrolytes with divalent counterions on average reverse micelle size. (b) Effect of average ion hydration radii on reverse micelle size intercept of linear fits when electrolytes with divalent counterions are added. (c) Effect of electrolytes with trivalent counterions on average reverse micelle size. (d) Effect of average ion hydration radii on reverse micelle size intercept when electrolytes with trivalent counterions are added.

extent of electrostatic screening. In the model presented in Chapter 2, the inner potential is generated by the co-ion core. Thus, when the ζ-potential is reduced, then the surface charge density of the core must also be reduced. Reduced surface potential of the core could be accommodated by additional ordering within the core or by swelling of the core size. The increased size with smaller counterions might be a consequence of core swelling, but the exact mechanism has not been resolved.

The point of instability with $Fe(SO_4)$, $Mg(NO_3)_2$, $MgCl_2$, and $CuCl_2$ additions occurred at 0.2 M, 0.5 M, 0.4 M and 0.3 M, respectively. The point of instability of $Mg(NO_3)_2$ is in reasonable agreement with the results from Chapter 2. However, the points of instability when $Fe(SO_4)$, $MgCl_2$, or $CuCl_2$ are added are lower than would be expected. Figure 4-5 depicts a possible explanation for the discrepancy. The edges of the two shaded regions connect the points of instability. The point of instabilities for the $Mg(NO_3)_2$, $MgCl_2$, and $CuCl_2$ systems occur at concentrations for which the average reverse micelle size is similar. Thus, the lower point of instability of $MgCl_2$ and $CuCl_2$ when compared to $Mg(NO_3)_2$ is likely to be a reverse micelle size effect. The destabilization at similar sizes suggests a salting out mechanism, where the surface tension is increased to a point where a single phase reverse micelle solution is no longer supported because of increased interfacial area and reduced surfactant coverage with decreasing reverse micelle size. A similar analysis can demonstrate why the points of instability for $Fe(NO_3)_3$ and $Y(NO_3)_3$ were 0.3 M, less than the point of instability of 0.4 M for $Al(NO_3)_3$. The reverse micelle sizes with dissolved $Fe(SO_4)$ are not small enough to justify a salting out mechanism. Thus, this is a specific ion effect. The hydrated iron and sulfate ion complexes are both greater in size than the respective ions for the other

electrolytes. This specific ion size effect leading to destabilization is also in agreement with the instability of $HAuCl_4$ containing reverse micelles, because the size of the hydrated $(AuCl_4)^-$ ion complex is too large and manifests as larger reverse micelles (average size of 21 nm was measured for $(z^2c)^{-1/2} = 1.5$). The shaded region in Figure 4-5 corresponding to instability as a result of ion size effect was generated using only two data points. It would be beneficial to evaluate a greater number of electrolytes having large ion hydration complexes to establish a more accurate boundary. The effect of counterion valence on these boundaries also needs to be established.

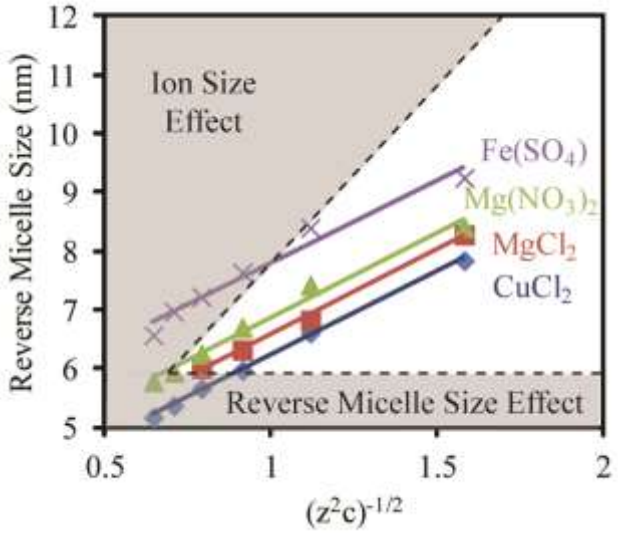

Figure 4 - 5. The shaded regions demonstrate unstable reverse micellar solutions as a result of reverse micelles that are too small and hydrated ion sizes that are too large.

3. Low Concentrations and Estimate of Stern Layer Occupation

The natural progression of applying the Gouy-Chapman theory is to use the Stern model, which is more commonly used in colloidal science because it can describe

behavior at higher concentrations, effects of ion specificity due to size and valence, as well as other important implications of surface chemistry.[52] For example, there is an upper limit on the number of ions that can be held at the charged surface of the Stern layer depending on ion size, which can also affect bonding or the formation of charge transfer complexes dictated by the specific ion-surface interaction. Instead of considering only the surface charge density in the Gouy-Chapman theory, the ζ-potential also has relevant consequences. Smaller ions can pack more efficiently at a charged surface, resulting in enhanced electrostatic screening and a lower ζ-potential. Thus, greater overlap of two electrical double layers would be allowed and result in smaller reverse micelles compared to larger ions of the same valence because of the overall reduction in the potential caused by the Stern layer. The Stern model is expected to give further qualitative insight into reverse micelle structure and stability. Thus, it is useful to estimate the Stern layer occupancy.

In Chapter 2, the linear relationship developed between the average reverse micelle size and the electrical double layer thickness can not be extrapolated back to the average reverse micelle size without added salt. It is possible that the sodium ions are not fully displaced at low concentrations, making the model invalid for low concentrations. This also provides inspiration to study the effect of low concentrations in this work and the results are presented in Figure 4-6. Low $ZrOCl_2$ concentrations (regime 1) result in a different slope as a function of the electrical double layer thickness than higher concentrations (regime 2). The same is true of NH_4OH concentration (regimes 3 and 4, respectively).

In the absence of added salt, the sodium counterions in AOT reverse micelles have been studied by ^{27}Na and ^{1}H NMR.[53] Two types of hydrated sodium were identified, either strongly bound to the surfactant interface or dissociated and the obtained ^{27}Na spectra were used to estimate the fraction of dissociated sodium. Such a study is not yet performed to estimate the binding of multivalent counterions to the surfactant interface. Assuming that the different slopes at low concentrations when compared to higher concentrations in Figure 4-6 correspond to the development of the strongly bound Stern layer, then the concentration at which the slope changes can be used to estimate the extent of dissociated surfactant headgroups. The slope transition occurs at approximately 0.12 M for NH_4OH and 0.04 M for $ZrOCl_2$. The estimated average reverse micelle sizes at these concentrations (extrapolated from the linear fits in Figure 4-6) are 9.7 nm and 7.9 nm, respectively, and can be considered an estimate of the upper size limit. Assuming AOT length of 1.1 nm and that the water phase resides inside the surfactant molecules, an estimate of the lower size limit gives 7.5 nm and 5.7 nm average sizes for $ZrOCl_2$ and NH_4OH, respectively.[53] The actual reverse micelle size is most likely between these two extreme size estimates. An estimate range for the extent of dissociated sites in the Stern layer based on the two size extremes will be made.

The estimated water volume for the average reverse micelle sizes is 220-490 nm^3 for the $ZrOCl_2$ slope transition and 96-260 nm^3 for the NH_4OH slope transition. Based on the 3.6 mL water volume and size of the average $ZrOCl_2$ and NH_4OH reverse micelles, there are between 0.7-1.6 $\times 10^{19}$ reverse micelles and 1.4-3.8 $\times 10^{19}$, respectively. Assuming that the surfactant is evenly distributed amongst the number of reverse micelles, there are between 330-680 surfactant molecules per reverse micelle containing

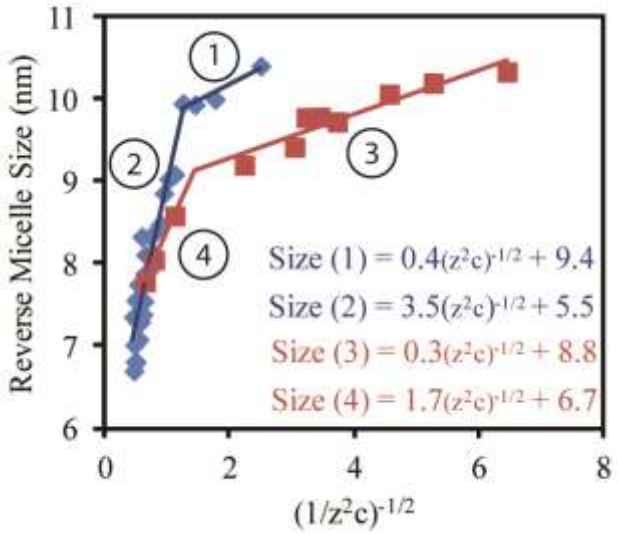

Figure 4 - 6. Effect of $ZrOCl_2$ (blue) and NH_4OH (red) concentration on average reverse micelle size (linear fits and equations are provided for the four designated regimes).

$ZrOCl_2$ and 280-400 surfactant molecules per reverse micelle containing NH_4OH. Based on the concentration of $ZrOCl_2$ and NH_4OH at the slope transition, there are 5-12 hydrated Zr^{4+} ions and 7-19 hydrated NH_4^+ pairs that occupy the Stern layer. The justification for pairs was described in Chapter 2. Accounting for the effective valences, approximately 93-94% of the surfactant headgroups are dissociated for $ZrOCl_2$ containing reverse micelles and 90-95% of the surfactant headgroups are dissociated for the NH_4OH containing reverse micelles. For comparison, Wong *et al*. estimated that an upper limit of 28% of the sodium ions dissociated in RMs without added salts.[53] The greater extent of dissociation from the Stern layer with salts can be a result of introducing co-ions with the electrolyte and the need to screen these co-ions.

4. Relative Permittivity of Confined Electrolyte Solution

Efforts have been made to measure or estimate the relative permittivity of confined water, but no general consensus has been reached.[53-57] In general, these reports find relatively small changes to the relative permittivity in confined space. Recently, anomalous dielectric behavior of nanoconfined electrolyte solutions was found by molecular dynamic simulations.[58] The relative permittivity decreases with increasing salt concentration in bulk water, but was found to increase in confined space with increasing salt concentration until a critical concentration is reached. The explanation that was given is that the dielectric behavior results from the interplay between the effect of confinement and the effect that ions have on the hydrogen bond network of the water molecules in the confined space. Thus, it can be expected that the relative permittivity in reverse micelles is influenced by the added salt.

If there are changes to the relative permittivity in the confined space of the reverse micelles with salt additions, then the change can be evaluated according to equation 1, because the electrical double layer thickness will only depend on three variables (ε_r, z, and c). The analysis of the average reverse micelle size with electrical double layer thickness, given in Figure 4-1, Figure 4-4, and Figure 4-6, is such that the dependence on z and c can be removed because the slope of average reverse micelle size with the added salt is given by:

$$m = \left(\frac{\varepsilon_r \varepsilon_o k_B T}{1000 q^2 N_A} \right)^{1/2} \qquad (2)$$

assuming that the reverse micelle size does not depend on any other variable except the hydrated ion sizes, which do not affect the slope anyway. Rearranging equation 2 gives an expression for the relative permittivity as a function of the slope presented in the

analysis and is given by equation 3, which represents a unique way to experimentally assess the relative permittivity of confined water.

$$\varepsilon_r = \frac{1000\, q^2 N_A m^2}{\varepsilon_o k_B T} \tag{3}$$

It is possible that the varying slopes of the average reverse micelle size changes because the sodium counterions from the AOT molecules are neglected from the electrical double layer thickness. It remains unclear whether or not the sodium ions are completely displaced from the electrical double layer, although all of the work in this study assumes (with arguments) that the sodium is fully displaced from the electrical double layer or at least negligible in the analysis. An analysis of the slopes as presented and by refitting the data to find the slopes with sodium counterions from the AOT included in the electrical double layer analysis is provided in Figure 4-7. The slopes change with electrolyte counterion valence in different ways, depending on whether or not sodium counterions from the AOT are included in the electrical double layer or not, which is demonstrated in Figure 4-7a. Thus, it is of critical importance to establish the location of the sodium counterions resulting from surfactant headgroup dissociation. The results in Figure 4-7b show that the calculated relative permittivity is also highly dependent on excluding or including the sodium counterions from surfactant headgroup dissociation and is further evidence that the sodium ions are likely to be excluded from the electrical double layer. When including the sodium counterions in the analysis, the resulting ε_r values are unreasonably large. The calculated result in Figure 4-7b that excludes the sodium counterions agrees well with the assessment of other researchers. For example, it appears that the relative permittivity for confined water, estimated by roughly extrapolating the data set back to zero valence, is similar in magnitude to that of bulk water.[54] A

remarkable feature is that the estimated relative permittivity calculated for the electrolyte solutions are 1-2 orders of magnitude greater. Such changes in relative permittivity can significantly alter equilibrium and reaction kinetics.

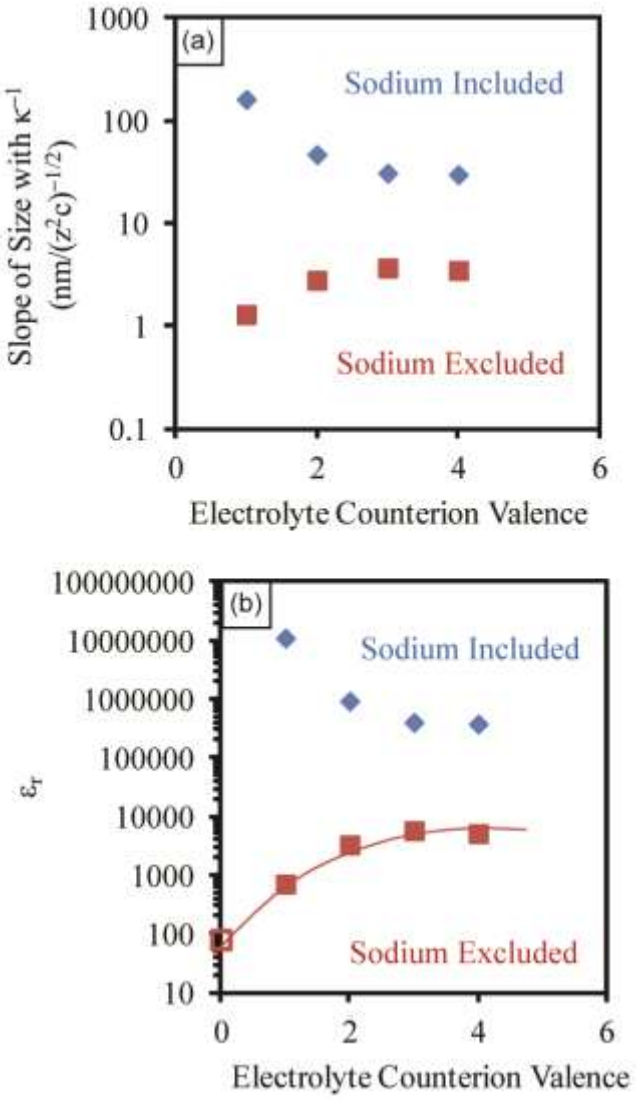

Figure 4 - 7. (a) Effect of slope of reverse micelle size with electrical double layer thickness on electrolyte counterion valence assuming that that sodium from the AOT is either excluded or included in the electric double layer analysis. (b) Calculated relative permittivity in the confined reverse micelle environemtn on electrolyte counterion valence assuming that that sodium from the AOT is either excluded or included in the electric double layer analysis.

It has been demonstrated above that the average reverse micelle sizes, when salts having monovalent counterions with respect to the surfactant headgroups are added, are proportional to the electrical double layer thickness. The addition of $HAuCl_4$ is a special case in which average reverse micelle size increased with increasing concentration. The size increase can be a result of the large anion complex, effects of the hydrogen bond network, or a combination of these two effects. Analysis of multiple electrolytes having divalent and trivalent counterions allows one to determine that the average reverse micelle size is proportional to the electrical double layer thickness and the average size of the electrolyte ion hydration complexes. Furthermore, the analysis provides two mechanisms for instability, one based on the reverse micelle size and the other based on the ion hydration complex sizes. Having established the size dependencies and mechanisms for instability, prediction of average reverse micelle size and the points of instability can be made for the encapsulation of other electrolyte solutions. Further analysis of the size changes provides an estimate of the relative permittivity of the reverse micelle interior phase and ε_r is found to increase by one or two orders of magnitude, which can have significant consequences for reactions performed within reverse micelles. Low ion occupancy of the Stern layer in reverse micelles is estimated by studying low concentrations, which can be caused by the need to screen co-ions or a consequence of the hydrogen bond network.

D. Conclusions

A number of specific ion effects are demonstrated in this work. Additions of $NaBH_4$ and $HAuCl_4$, having monovalent counterions relative to the AOT surfactant headgroup, result in an opposite average reverse micelle size dependence with increasing

electrolyte concentration. The reverse micelle sizes of $NaBH_4$ decrease while those of $HAuCl_4$ increase. The effect of $NaBH_4$ is typical of salt additions to the reverse micelles, but the effect of $HAuCl_4$ is anomalous. One possible explanation is the large size of the co-ion complex of the $HAuCl_4$, which is also supported by the low destabilization concentration that is observed when adding $FeSO_4$ into the reverse micelle solution. However, more complex interactions, such as the nature of the hydrogen bond network and corresponding interactions, cannot be ruled out. Thus, there is a need to establish the precise distribution of all the components in the reverse micelle interior.

When adding salts that introduce divalent counterions with respect to the surfactant headgroup, the slopes obtained by the linear fits that establish the dependence of reverse micelle size on the electrical double layer thickness are similar. However, the size intercepts for the fits are different and can be directly correlated to the average hydrated ion size for the added salt. The size intercepts for the fits to size data of reverse micelles containing salts with trivalent counterions also correlate with the average hydrated ion sizes for the added electrolyte, but indirectly. The point of instability for the various salts can be described by two effects: (i) the traditional salting out mechanism by which surface tension increases with increasing interfacial area and reduced surfactant headgroup coverage can explain most of the points of instability and (ii) a sufficiently large co-ion size can also cause a lower point of instability.

Stern layer occupation is estimated by studying a slope transition for the reverse micelle size dependence on the electrical double layer thickness. Approximately 90 to 95% of the surfactant headgroups are dissociated. This value is higher than counterion dissociation from headgroups without added salt and can be attributed to the need to

screen co-ions that are also introduced by the salt. The relative permittivity of the salt solution in the confined space of the reverse micelles is also estimated when assuming that the slopes of the linear reverse micelle size only depends on the electrical double layer thickness and reasonable results are obtained compared to other researchers. Electrolyte solutions confined in reverse micelles is found to increase the relative permittivity by one or two orders of magnitude depending on the counterion valence.

E. References

1. T.P. Hoar and J.H. Schulman, "Transparent Water-in-oil Dispersions: the Oleopathic Hydro-micelle," *Nature*, **152** [3847] 102-3 (1943).

2. J.H. Schulman and D.P. Riley, "X-ray Investigation of the Structure of Transparent Oil-water Disperse Systems I," *J. Colloid Sci.*, **3** [4] 383-405 (1948).

3. J.H. Schulman and J.A. Friend, "Light Scattering Investigation of the Structure of Transparent Oil-water Disperse Systems II," *J. Colloid Sci.*, **4** [5] 497-509 (1949).

4. M. Boutonnet, J. Kizling, P. Stenius, and G. Maire, "The Preparation of Monodisperse Colloidal Metal Particles from Microemulsions," *Colloids Surf.*, **5** [3] 209-25 (1982).

5. J.H. Adair, T. Li, T. Kido, K. Havey, J. Moon, J. Mecholsky, A. Morrone, D.R. Talham, M.H. Ludwig, and L. Wang, "Recent Developments in the Preparation and Properties of Nanometer-size Spherical and Platelet-shaped Particles and Composites," *Mater Sci. Eng., R*, **23** [4-5] 139-242 (1998).

6. K.S.N. Reddy, L.M. Salvati, P.K. Dutta, P.B. Abel, K.I. Suh, and R.R. Ansari, "Reverse Micelle Based Growth of Zincophosphate Sodalite: Examination of Crystal Growth," *J. Phys. Chem.*, **100** [23] 9870-80 (1996).

7. M.L. Curri, A. Agostiano, L. Manna, M.D. Monica, M. Catalano, L. Chiavarone, V. Spagnolo, and M. Lugara, "Synthesis and Characterization of CdS Nanoclusters in a Quaternary Microemulsion: the Role of Cosurfactant," *J. Phys. Chem. B*, **104** [35] 8391-7 (2000).

8. K. Homberg, "Surfactant-templated Nanomaterials Synthesis," *J. Colloid Interface Sci.*, **274** [2] 355-64 (2004).

9. S.A. Morrison, C.L. Cahill, E.E. Carpenter, S. Calvin, R. Swaminathan, M.E. McHenry, and V.G. Harris, "Magnetic and Structural Properties of Nickel Zinc Ferrite Nanoparticles Synthesized at Room Temperature," *J. Appl. Phys.*, **95** [11] 6392-5 (2004).

10. Y. Lee, J. Lee, C.J. Bae, J.-G. Park, H.-J. Noh, J.-H. Park, and T. Hyeon, "Large-scale Synthesis of Uniform and Crystalline Nanoparticles Using Reverse Micelles as Nanoreactors under Reflux Conditions," *Adv. Funct. Mater.*, **15** [3] 503-9 (2005).

11. J.-L. Lemyre and A.M. Ritcey, "Synthesis of Lanthanide Fluoride Nanoparticles of Varying Shape and Size," *Chem. Mater.*, **17** [11] 3040-3 (2005).

12. S. Ohkoshi, S. Sakurai, J. Jin, and K. Hashimoto, "The Addition of Alkaline Earth Ions in the Chemical Synthesis of ε-Fe_2O_3 Nanocrystals that Exhibit a Huge Coercive Field," *J. Appl. Phys.*, **97** [10] 10K312 3pp. (2005).

13. V. Uskoković and M. Drofenik, "Synthesis of Materials within Reverse Micelles," *Surf. Rev. Lett.*, **12** [2] 239-77 (2005).

14. J.P. Kelly and O.A. Graeve. "Effect of Powder Characteristics on Nanosintering," pp. 57-95 in Engineering Materials, Vol. 35, *Sintering*. Edited by R.H.R. Castro and K. Van Benthem. Springer Science, New York, 2013.

15. M. Yadav, A.K. Singh, N.Tsumori, and Q. Xu, "Palladium Silica Nanosphere-catalyzed Decomposition of Formic Acid for Chemical Hydrogen Storage," *J. Mater. Chem.*, **22** [36] 19146-50 (2012).

16. C.G.S. Souza, W. Beck Jr., and L.C. Varanda, "Multifuntional Luminomagnetic FePt@Fe_3O_4/SiO_2/Rhodamine B/SiO_2 Nanoparticles with High Magnetic Emanation for Biomedical Applications," *J. Nanopart. Res.*, **15** [4] 1545 11pp. (2013).

17. S. Wang, C. Li, P. Yang, M. Ando, and N. Murase, "Silica Encapsulation of Highly Luminescent Hydrophobic Quantum Dots by Two-step Microemulsion Method," *Colloids Surf., A*, **395**, 24-31 (2012).

18. Z.-H. Lu, H.-L. Jiang, M. Yadav, K. Aranishi, and Q. Xu, "Synergistic Catalysis of Au-Co@SiO_2 Nanospheres in Hydrolytic Dehydrogenation of Ammonia Borane for Chemical Hydrogen Storage," *J. Mater. Chem.*, **22** [11] 5065-71 (2012).

19. C.-S. Lee, H.H. Chang, J. Jung, N.A. Lee, N.W. Song, and B.H. Chung, "A Novel Fluorescent Nanoparticle Composed of Fluorene Copolymer Core and Silica Shell with Enhanced Photostability," *Colloids Surf., B*, **91**, 219-25 (2012).

20. X. Cao, J. Yu, Z. Zhang, and S. Liu, "Bioactivity of Horseradish Peroxidase Entrapped in Silica Nanospheres," *Biosens. Bioelectron.*, **35** [1] 101-7 (2012).

21. H. Qu, L. Cao, W. Liu, G. Su, B. Dong, and H. Zhai, "Photoluminescence Properties of ZnS/CdS/ZnS Quantum Dot-quantum Wells Doped with Ag^{+} Ions," *J. Nanopart. Res.*, **13** [10] 5157-61 (2011).

22. G. Bhakta, R.K. Sharma, N. Gupta, S. Cool, V. Nurcombe, and A. Maitra, "Multifunctional Silica Nanoparticles with Potentials of Imaging and Gene Delivery," *Nanomed. Nanotechnol.*, **7** [4] 472-9 (2011).

23. F.N. Radwan, K.J. Carroll, and E.E. Carpenter, "Dual Mode Nanoparticles: CdS Coated Iron Nanoparticles," *J. Appl. Phys.*, **107** [9] 09B515 3pp. (2010).

24. T. Jafari, A Simchi, and N. Khalpash, "Synthesis and Cytotoxicity Assessment of Superparamagnetic Iron-gold Core-shell Nanoparticles Coated with Polyglycerol," *J. Colloid Interface Sci.*, **345** [1] 64-71 (2010).

25. H.T. Xue and P.Q. Zhao, "Synthesis and Magnetic Properties from Mn-doped CdS/SiO_2 Core-shell Nanocrystals," *J. Phys. D: Appl. Phys.*, **42**, 015402 5pp. (2009).

26. N. Hagura, W. Widiyastuti, F. Iskandar, and K. Okuyama, "Characterization of Silica-coated Silver Nanoparticles Prepared by a Reverse Micelle and Hydrolysis-condensation Process," *Chem. Eng. J.*, **156** [1] 200-5 (2010).

27. S.K. Basiruddin, A. Saha, N. Pradhan, and N.R. Jana, "Functionalized Gold Nanorod Solution via Reverse Micelle Based Polyacrylate Coating," *Langmuir*, **26** [10] 7475-81 (2010).

28. V. Dandavate, H. Keharia, and D. Madamwar, "Ethyl Isovalerate Synthesis Using *Candida rugosa* Lipase Immobilized on Silica Nanoparticles Prepared in Nonionic Reverse Micelles," *Process Biochem.*, **44** [3] 349-52 (2009).

29. D.J. Mitchell and B.W. Ninham, "Micelles, Vesicles and Microemulsions," *J. Chem. Soc., Faraday Trans. 2*, **77** [4] 601-29 (1981).

30. M.P. Pileni, "Reverse Micelles as Nanoreactors," *J. Phys. Chem.*, **97** [2] 6961-73 (1993).

31. B. Lindman, P. Stilbs, and M.E. Moseley, "Fourier Transform NMR Self-diffusion and Microemulsion Structure," *J. Colloid Interface Sci.*, **83** [2] 569-582 (1981).

32. J.H. Fendler, "Atomic and Molecular Clusters in Membrane Mimetic Chemistry," *Chem. Rev.*, **87** [5] 877-99 (1987).

33. X. Fang and C. Yang, "An Experimental Study on the Relationship between the Physical Properties of CTAB/Hexanol/Water Reverse Micelles and ZrO_2-Y_2O_3 Nanoparticles Prepared," *J. Colloid Interface Sci.*, **212**, 242-51 (1999).

34. A. Nanni and L. Dei, "$Ca(OH)_2$ Nanoparticles from W/O Microemulsions," *Langmuir*, **19** [3] 933-8 (2003).

35. F. Porta, C. Bifulco, P. Fermo, C.L. Bianchi, M. Fadoni, and L. Prati, "Synthesis of Spherical Nanoparticles of $Cu_2L_2O_5$ (L = Ho, Er) from W/O Microemulsions," *Colloids Surf., A*, **160** [3] 281-90 (1999).

36. D. Makovec, A. Košak, and M. Drofenik, "The Preparation of MnZn-ferrite Nanoparticles in Water-CTAB-hexanol Microemulsions," *Nanotechnology*, **15** [4] S160-6 (2004).

37. H. Fathi, J.P. Kelly, V.R. Vasquez, and O.A. Graeve, "Ionic Concentration Effects on Reverse Micelle Size and Stability: Implications for the Synthesis of Nanoparticles," *Langmuir*, **28** [25] 9267-74 (2012).

38. N.E. Levinger and L.A. Swafford, "Ultrafast Dynamics in Reverse Micelles," *Annu. Rev. Phys. Chem.*, **60**, 385-406 (2009).

39. R. Biswas, T. Chakraborti, B. Bagchi, and K.G. Ayappa, "Non-monotonic, Distance-dependent Relaxation of Water in Reverse Micelles: Propagation of Surface Induced Frustration along Hydrogen Bond Networks," *J. Chem. Phys.*, **137** [1] 014515 9pp. (2012).

40. B. Bagchi, "From Anomalies in Neat Liquid to Structure, Dynamics and Function in the Biological World," *Chem. Phys. Lett.*, **529**, 1-9 (2012).

41. E.E. Fenn, D.B. Wong, and M.D. Fayer, "Water Dynamics in Small Reverse Micelles in Two Solvents: Two-dimensional Infrared Echoes with Two-dimensional Background Subtraction," *J. Chem. Phys.*, **134** [5] 054512 11pp. (2011).

42. O.A. Graeve, H. Fathi, J.P. Kelly, M.S. Saterlie, K. Sinha, G. Rojas-George, R. Kanakala, D.R. Brown, and E.A. Lopez, "Reverse Micelle Synthesis of Oxide Nanopowders: Mechanisms of Precipitate Formation and Agglomeration Effects," *J. Colloid Interface Sci.*, **407**, 302-9 (2013).

43. R.G. Alargova, J. Petkov, D. Petsev, I.B. Ivanov, G. Broze, and A. Mehreteab, "Light Scattering Study of Sodium Dodecyl Polyoxy-ethylene-2Sulfate Micelles in the Presence of Multivalent Counterions," *Langmuir*, **11** [5] 1530-6 (1995).

44. H. Ohtaki and T. Radnai, "Structure and Dynamics of Hydrated Ions," *Chem. Rev.*, **93** [3] 1157-1204 (1993).

45. Y. Filinchuk, D. Chernyshov, and V. Dmitriev. "Crystal Chemistry of Light Metal Borohydrides," pp. 1-16 in Boron Hydrides, High Potential Hydrogen Storage Materials. Edited by U.B. Dmirci and P. Miele. Nova Publishers, New York, 2010.

46. Y. Filinchuk, A.V. Talyzin, H. Hagemann, V. Dmitriev, D. Chernyshov, and B. Sundqvist, "Cation Size and Anion Anisotropy in Structural Chemistry of Metal Borohydrides. The Peculiar Pressure Evolution of $RbBH_4$," *Inorg. Chem.*, **49** [11] 5285-92 (2010).

47. B. Chu, D.C. Whitney, and R.M. Diamond, "On Anion-exchange Resin Selectivities," *J. Inorg. Nucl. Chem.*, **24** [11] 1405-15 (1962).

48. T. Kawai, A. Fujino, K. Kon-No, "Synthesis of Monodisperse ZrO_2 Particles in Polyoxyethylated Nonionic Reversed Micelles," *Colloids Surf., A*, **109**, 245-53 (1996).

49. S. Santra, R. Tapec, N. Theodoropoulou, J. Dobson, A. Hebard, and W. Tan, "Synthesis and Characterization of Silica-coated Iron Oxide Nanoparticles in Microemulsion: The Effect of Nonionic Surfactants," *Langmuir*, **17** [10] 2900-6 (2001).

50. C.J. Barbé, R. Graf, K.S. Finnie, M. Blackford, R. Trautman, and J.R. Bartlett, "Sol-gel Synthesis of Complex Titanates in Micro-emulsions," *J. Sol-Gel Sci. Technol.*, **26** [1-3] 457-62 (2003).

51. A. Nanni and L. Dei, "$Ca(OH)_2$ Nanoparticles from W/O Microemulsions," *Langmuir*, **19** [3] 933-8 (2003).

52. R. J. Stokes and E. D. Fennell, *Fundamentals of Interfacial Engineering*; pp. 152-63. Wiley-VCH: New York, 1996.

53. M. Wong, J.K. Thomas, and T. Nowak, "Structure and State of H_2O in Reversed Micelles. 3," *J. Am. Chem. Soc.*, **99** [14] 4730-6 (1977).

54. S. Senapati and A. Chandra, "Dielectric Constant of Water Confined in a Nanocavity," *J. Phys. Chem. B*, **105** [22] 5106-9 (2001).

55. A. Ghoufi, A. Szymczk, R. Renou, and M. Ding, "Calculation of Local Dielectric Permittivity of Confined Liquids from Spatial Dipolar Correlations," *Europhys. Lett.*, **99** [3] 37008 6pp. (2012).

56. J. Martí, G. Nagy, E. Guàrdia, and M.C. Gordilla, "Molecular Dynamics Simulation of Liquid Water Confined inside Graphite Channels: Dielectric and Dynamical Properties," *J. Phys. Chem B.,* **110** [47] 23987-94 (2006).

57. B. Zhou, A. Kobayashi, H.-B. Cui, L.-S. Long, H. Fujimori, and H. Kobayashi, "Anomolous Dielectric Behavior and Thermal Motion of Water Molecules Confined in Channels of Porous Coordination Polymer Crystals," *J. Am. Chem. Soc.,* **133** [15] 5736-9 (2011).

58. H. Zhu, A. Ghoufi, A. Szymczyk, B. Balannec, and D. Morineau, "Anomalous Dielectric Behavior of Nanoconfined Electrolytic Solutions," *Phys. Rev. Lett.,* **109** [10] 107801 5pp. (2012).

CHAPTER 5: PROCESS CONTROL DIAGRAM FOR THE REVERSE MICELLE SYNTHESIS OF ZIRCONIUM HYDROXIDE IN THE WATER-AOT-ISOOCTANE SYSTEM

A. Introduction

Water-in-oil microemulsions are used for precipitation synthesis in what has come to be known as reverse micelle synthesis since Boutonnet first demonstrated in 1982 that metal nanoparticles can be made and transferred to supports without agglomeration.[1] This was done in three different microemulsion systems: water/cetyltrimethylammonium bromide/octanol, water/pentaethyleneglycol dodecyl ether/hexane, and water/pentaethyleneglycol dodecyl ether/hexadecane. Only extremely small amounts of the metal precursors could be added (~0.1-2.6 mM) to the ionic surfactant system. Hydrogen or hydrazine (2-3% of the total volume) was added directly to the microemulsion to trigger the reduction of the precursors. Reduction with hydrogen was slow compared to reduction with hydrazine, which was also more complete. The system with as little as 2.6 mM of H_2PtCl_4 precursor was not stable and flocculated after reduction and reaction for 72 hours. All precipitates settled slowly and completely over the period of several days. Up to 0.1 M H_2PtCl_4 could be added to the nonionic surfactant systems. Reactions using microemulsions with up to 6.1 mM H_2PtCl_4 were stable without settling for months and could be transferred to supports without agglomeration. Under certain conditions, lower surfactant (4.2-4.94%) and higher hydrazine amounts (30-40 μL), the microemulsion were not stable with as little as 4.4 mM H_2PtCl_4 and demonstrates the potential for unstable colloidal suspensions even when within the precursor solubility limits. It was reported and is still generally accepted that

the limits of the method are associated with particle nucleation and growth rather than the properties of the microemulsion.

The reverse micelle method has been used to produce all types of materials and there are several review articles on the topic.[2-11] The general methods for forming nanoparticles by the reverse micelle synthesis technique include mixture of microemulsions containing different reactants, direct addition of a precipitating agent to a reactant containing microemulsion, or bubbling a reactive gas through a reactant containing microemulsion. Reactants can be dissolved in the microemulsion by the addition of a soluble salt or by an exchange reaction with surfactant counterions prior to mixing the microemulsions when using ionic surfactants.

Particles can be left in solution, transferred to a substrate, or removed from suspension to form a powder, depending on the application. Adding excess water, heating, adding alcohol, or adding acetone are techniques that have been used to disrupt the microemulsion and flocculate the particles so that they can be removed by settling or centrifuging.[12-17] Alternatively, synthesis conditions that do not produce stable microemulsions do not require a step to break the microemulsion before centrifuging and can also increase particle yields.[18,19] Freeze drying with supercritical drying has also been used for particle removal to prevent particle agglomeration.[20] Redispersing the particles after flocculation can be challenging depending on the state of the agglomerates, the cleaning procedure, and effects of surface chemistry such as the interaction between particle surfaces and the surfactant molecules.[21]

Precursors are often added in very dilute concentrations, on the scale of 1 mM, to the reverse micellar systems to produce stable dispersions.[1,22,23] However, precipitation

has also been performed using concentrations a few order of magnitudes greater, on the scale of 1 M.[14,24-26] Highly concentrated solutions often turn turbid upon reacting, indicating that the particles have grown to large sizes or flocculated because the microemulsion is unstable. Large and non uniform particle sizes are often found when the microemulsion is destroyed in comparison with the small and uniform sizes that can be obtained when the microemulsion remains stable. However, unstable microemulsions can also improve polydispersity depending on the particle nucleation and growth conditions.[27] Coagulation can also occur for particles prepared using very dilute precursors in the absence of surfactant adsorption onto the surface or the addition of a capping agent and indicates that surface chemistry must also be well controlled for complete dispersion.[28,29] Well controlled particle development and an appropriate capping agent can be used for self-assembly of nanoparticles into 2-D and 3-D particle superlattices.[30-33] Thus, it is of interest to understand the limits for producing a stable dispersion after a precipitation reaction in reverse micelles, which are found to be extremely sensitive to the preparation procedure.[34]

Previous analysis in Chapter 2 and Chapter 4 demonstrated that reverse micelles with various electrolytes are stable up to a critical salt concentration.[35] For example, additions of $ZrOCl_2$ and NH_4OH are stable up to 0.3 M and 0.6 M, respectively, in the water phase that has been mixed with an isooctane phase with 0.2 M dioctyl sodium sulfosuccinate (AOT) and water to surfactant ratio of ten. Li *et al.* performed synthesis of zirconium hydroxide using $ZrOCl_2$ and NH_4OH in water/AOT/toluene reverse micelles.[36] The $ZrOCl_2$ concentration was 0.2 M and the NH_4OH concentration varies because of the preparation procedure. Small angle neutron scattering (SANS) was used

to investigate the size of the reverse micelles before mixing the two reverse micelle solutions and after mixing them. The reverse micelles with $ZrOCl_2$ were smaller than the parent system without electrolyte and the system with NH_4OH added. Mixtures of $ZrOCl_2$ and NH_4OH resulted in intermediate sizes, but it is unclear whether or not the system was stable after the precipitation reaction. Many precipitation reactions are performed within precursor limits assuming that these are also suitable limits for the precipitation reaction, but it is not clear if these are sufficient criteria for obtaining dispersed precipitates.[37,38]

In this study, stability of three separate reverse micellar systems is presented. The first system consists of mixtures of $ZrOCl_2$ and NH_4OH containing reverse micelles to precipitate zirconium hydroxide. The concentration limits suitable for stable precipitate formation are lower than the precursor limits. The second system is similar to the system exploited by Jiao *et al.* to produce nanoparticles of the perovskite $CaRuO_3$.[39] The third system is similar to the system used by Aragón *et al.* to produce a form of $MnCO_3$ for use as an anode for lithium-ion batteries.[40] The purpose is not to reproduce the work in the aforementioned studies, but to add to them by characterizing the microemulsions used for the precipitation reactions because like many studies, the focus provided by the respective authors is on the characterization of the resulting particles after removing them from the microemulsion and not on the microemulsions used to produce the particles.

B. Experimental Methods

1. System I

Reverse micellar solutions were prepared by first mixing 100 mL of 2,2,4-trimethylpentane (99.8%, Sigma-Aldrich, Inc., St. Louis, MO) with 8.891 g of anionic

surfactant sodium 1,4-bis(2-ehtylhexoxy)-1,4-dioxobutane-2-sulfonate (99.0-100.5%, Sigma-Aldrich, Inc., St. Louis, MO). A separate electrolyte solution with 0.05-0.20 M was prepared by mixing 3.6 mL of distilled water with either 0.058 g, 0.116 g, 0.174 g, or 0.232 g of $ZrOCl_2 \cdot 8H_2O$ (99.9985%, Alfa Aesar, Ward Hill, MA), assuming that the water of hydration for the salt is negligible in comparison to the total water content. For each precipitation experiment, the organic phase and water phase were allowed to mix for at least 30 minutes before combining them to form a microemulsion (M1). A second microemulsion was prepared in a similar way (M2), but contained 0.34 mL of NH_4OH (28-30% NH_3, Alfa Aesar, Ward Hill, MA) in 3.48 mL of distilled water. The water content was reduced according to the amount of water introduced by the NH_4OH and to prepare a 0.05 M solution in the microemulsion when accounting for solubility in the isooctane phase.[35] M1 and M2 solutions were magnetically stirred separately for 2 hours. Precipitation reactions were initiated by mixing the corresponding M1 and M2 solutions, which were allowed to mix using magnetic stirring for 30 minutes prior to characterization.

The experiments described above involve systematic variation of the $ZrOCl_2$ concentration within the precursor limits of both $ZrOCl_2$ and NH_4OH. A second set of experiments was performed to systematically vary the NH_4OH concentration. In this case, the $ZrOCl_2$ microemulsions (M1) were prepared with 0.058 g (0.05 M). The NH_4OH microemulsions (M2) are prepared by mixing NH_4OH:distilled water amounts of 1.18:3:16 mL, 2.04:2.85 mL, and 2.89:2:54 mL. The three precipitation reactions were initiated by mixing the appropriate M1 and M2 solutions, as described above.

2. System II

This system consists of reverse micelles of identical characteristics as described by Jiao *et al.*[39] Ruthenium (III) chloride hydrate (99.9%, Alfa Aesar, Ward Hill, MA) and calcium chloride dihydrate (99% min, Alfa Aesar, Ward Hill, MA) were dissolved in water at a concentration of 0.55 M (1.260 g of $RuCl_3 \cdot xH_2O$ and 0.736 g of $CaCl_2 \cdot 2H_2O$ in 20 mL of de-ionized water). This solution was dispersed in 80 mL of n-octane (98+%, Alfa Aesar, Ward Hill, MA), 15 mL of 1-butanol (99%, Alfa Aesar, Ward Hill, MA), and 16 g of the cationic surfactant cetyltrimethylammonium bromide (High purity grade, Amresco, Solon, OH). Another reverse micellar solution was prepared at a concentration of 0.76 M (1.6 g Na_2CO_3). These two reverse micellar solutions have a ω_o = 5.34 and were mixed for 2 hours before characterization. In addition, reverse micellar solutions of $RuCl_3$ with concentrations of 0.1-0.4 M $CaCl_2$ and Na_2CO_3 with concentrations of 0.1-0.6 M were prepared and characterized.

3. System III

This system consists of reverse micelles of identical characteristics as described by Aragón *et al.*[40] Manganese (II) nitrate tetrahydrate (97.5%, Acros Organics, Geel, Belgium) was dissolved in water at a concentration of 0.3 M (0.881 g of $Mn(NO_3)_2$ in 11.67 g of de-ionized water). This solution was dispersed in 19.97 mL of 2-hexanol (99%, Acros Organics, Geel, Belgium), 69.0 g of 2,2,4-trimethylpentane (99.8%, Sigma-Aldrich, Inc., St. Louis, MO), and 19.50 g of cetyltrimethylammonium bromide (High purity grade, Amresco, Solon, OH), resulting in a ω_o = 3.65. This solution was mixed for two hours before characterization. Another reverse micellar solution of similar composition, but now with dissolved sodium hydrogen carbonate (99%, Fisher Scientific, Fair Lawn, NJ) was prepared at a concentration of 0.3 M (0.295 g of Na_2HCO_3). This

solution was also mixed for 2 hours before characterization. In addition, solutions of $Mn(NO_3)_2$ with concentrations of 0.5-0.7 M and $NaHCO_3$ with concentrations of 0.4 M were prepared and characterized.

4. Characterization

A Nanotrac Ultra Dynamic Light Scattering (DLS) instrument (Microtrac, Inc. Montgomeryville, PA) was utilized to measure the size distribution of the reverse micelles. To determine error values, each sample was measured five times, with each measurement consisting of an average of five runs of 15 s each, according to a combination of manufacturing specifications and the recommendations given in ASTM standard E2490-09.[41] Experimental constants that were used for analysis are: (i) Na-AOT refractive index of 1.48, (ii) CTAB refractive index of 1.435, (iii) isooctane and n-octane refractive index of 1.40, and (iv) isooctane and n-octane viscosity of 0.542.

C. Results and Discussion

1. System I

The results of DLS measurements on mixtures of $ZrOCl_2$ solutions with 0.05 M NH_4OH solutions are depicted in Figure 5-1. The size distributions provided in Figure 5-1a demonstrate that the reverse micellar solutions remain stable when the 0.05 M $ZrOCl_2$ is mixed with the NH_4OH solution because the size distribution is similar to that of the parent micellar systems.[35] However, when 0.10 M $ZrOCl_2$ is mixed with the NH_4OH, the solutions become turbid and agglomerates approximately 100-1000 nm in diameter are observed in the particle size distribution in addition to the size distribution of the dispersed phase. At higher concentrations, solution turbidity remains indicating that the solutions are also unstable, but the agglomerates are large enough that they are no longer

observed using DLS measurements. Figure 5-1b demonstrates that the average size of the dispersed phase decreases with increasing $ZrOCl_2$ concentration, up to 0.15 M, and follows a linear trend. The decrease appears to be associated with a narrowing of the size distribution presented in Figure 5-1a. As the $ZrOCl_2$ concentration is increased further to 0.20 M, the average size increased and is accommodated by a wider size distribution. The initial decrease in the size distribution can be associated with the added electrolyte or increased separation of the nucleation and growth processes associated with precipitate formation.[35] The latter would indicate either faster nucleation or slower growth rates with increasing $ZrOCl_2$ concentration. Overall, the concentration of $ZrOCl_2$ suitable for precipitation is lower than the precursor concentration limit (0.3 M).

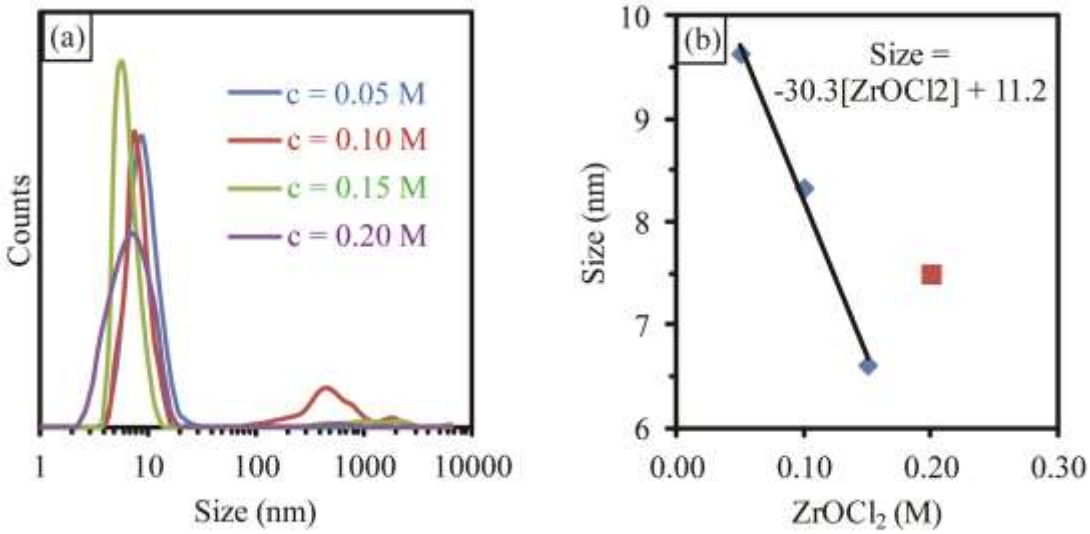

Figure 5 - 1. (a) Size distribution of precipitating solutions prepared with varying $ZrOCl_2$ concentration and 0.05M NH_4OH and (b) the average size of the dispersed phase.

The solutions mixed for precipitation remained optically transparent when varying NH_4OH concentration with constant $ZrOCl_2$ concentration (0.05 M).

Furthermore, no agglomerate structures are observed and can be demonstrated by the data given in Figure 5-1. The average size of the dispersed phase (provided in Figure 5-1b) demonstrates an initial decrease with increase in NH_4OH concentration, but followed by an increase with further addition of NH_4OH. The initial decrease is confirmed by two experiments. The NH_4OH concentration, within precursor limits, did not influence the stability of the precipitate solutions like $ZrOCl_2$ concentration does. Thus, for the experimental conditions used in this study, the NH_4OH has a negligible effect on precipitate nucleation and growth assuming that precipitates have indeed formed within the reverse micelles.

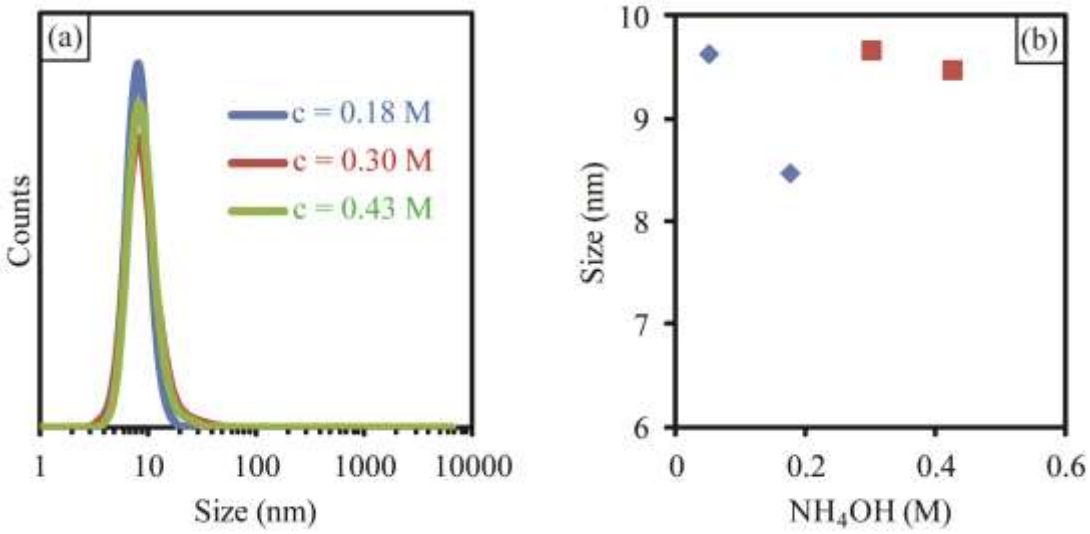

Figure 5 - 2. (a) Size distribution of precipitating solutions prepared with varying NH_4OH concentration and 0.05 M $ZrOCl_2$ and (b) the average size of the dispersed phase.

2. System II

The precursor solutions used by Jiao *et al.*[39] were not stable, which is demonstrated by the data given in Figure 5-3. The size distribution measured by DLS for

the mixture of $RuCl_3$ and $CaCl_2$ in the reverse micellar system has an average size of 14.2 nm. However, there is also a coalesced phase with sizes between 1-2 μm. Similarly, the precursor solution containing 0.76 M Na_2CO_3 was also found to be an unstable reverse micellar solution. No stable reverse micelles are observed for this concentration of Na_2CO_3. Instead, free agglomerates of 1-4 nm in size and large agglomerates with size 0.5-2 μm are observed. Small agglomerates can be attributed to free surfactant agglomerates and large agglomerates correspond to a coalesced phase.

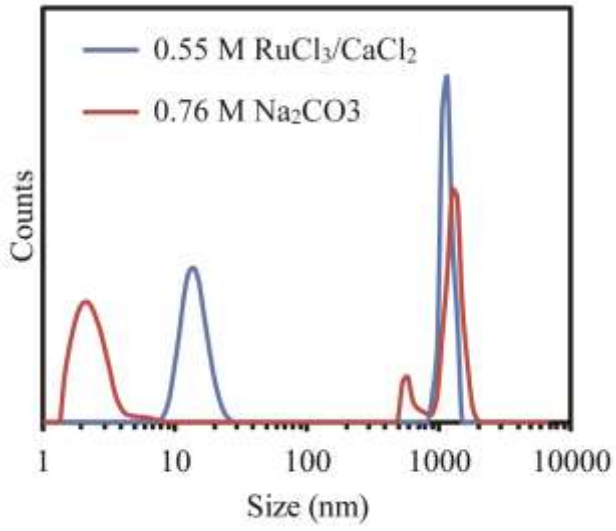

Figure 5 - 3. Dynamic light scattering measurements of precursor solutions identical to those used by Jiao *et al.*[39]

The data from a systematic investigation of the parent reverse micellar solution and with additions of $RuCl_3$ to this system is presented in Figure 5-4. The results indicate that although good stability is observed for the base system (solid curve in Figure 5-4a), the solutions with $RuCl_3$ additions are not stable. That is, the solution with no salts exhibit mostly structures that correspond to reverse micelles that have an average size of 8.3 nm, whereas the solutions with salts exhibit a greater extent of structures with sizes of

about 1 μm, corresponding to the coalesced phase. In addition to the presence of a coalesced phase with salt additions, the dispersed reverse micellar phase is found to grow in average size with increasing $RuCl_3$ concentration. The growth of the reverse micellar phase with increasing $RuCl_3$ is not expected based on the model developed in Chapter 2, but is similar to the results when adding $HAuCl_4$ to reverse micellar solutions that is presented in Chapter 4.

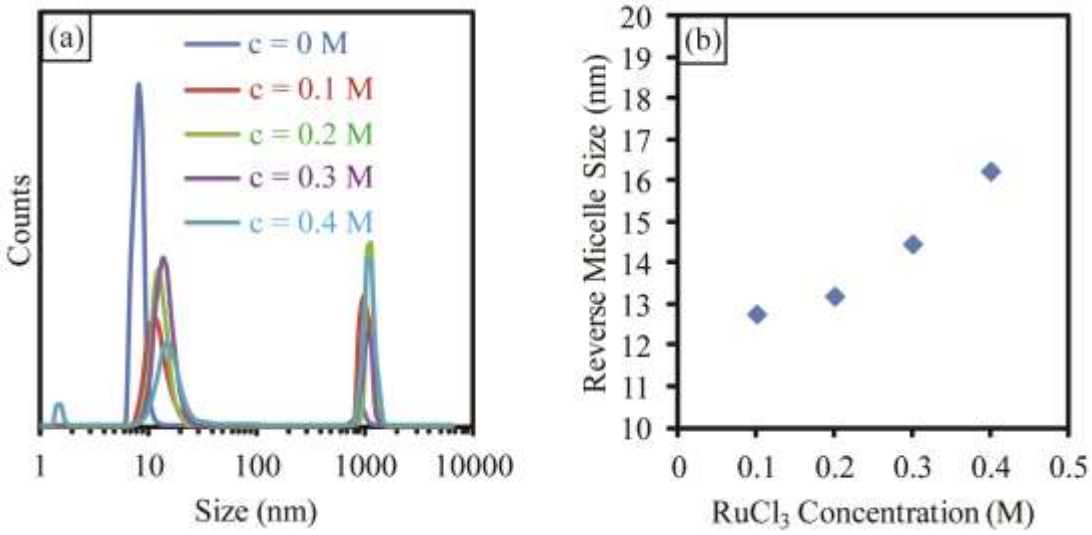

Figure 5 - 4. (a) Size distribution and (b) average size of the dispersed phase for the base system used by Jiao *et al.* when $RuCl_3$ is added.

Two possible explanations for reverse micelle growth were given in Chapter 4. The first explanation for reverse micelle growth was the large ion size of the anion complex. The size argument is unlikely based on the sizes of comparable ion hydration sizes and the results presented in Chapter 4.[42,43] The second possible cause for reverse micellar growth depended on the sign of the potential-determining ion that is introduced by adding the salt into solution, which influences the hydrogen bond network of the structured water in the reverse micelle and can explain reverse micelle growth according

to the scheme that was introduced in Chapter 4. However, this is the first example where a trivalent co-ion is introduced into the reverse micelles and cannot yet be ruled out as an important consideration.

The size distribution and average sizes of the dispersed phase when $CaCl_2$ is added to the base system of *System II* is depicted in Figure 5-5. At a concentration of 0.4 M $CaCl_2$, the dispersed phase completely disappeared and only agglomerates of surfactant are observed by DLS. $CaCl_2$, producing a divalent co-ion, also generated reverse micelle growth (though to a lesser extent then when adding $RuCl_3$) and the hydrated ion sizes are comparable to other systems that produced reverse micelle shrinkage. Thus, both hydrated ion size and being a trivalent co-ion can be ruled out as the cause for reverse micelle growth and the model presented in Chapter 4, where the configuration of the hydrogen bond network can produce reverse micelle shrinkage or growth appears to be a reasonable model, at least conceptually, for describing reverse

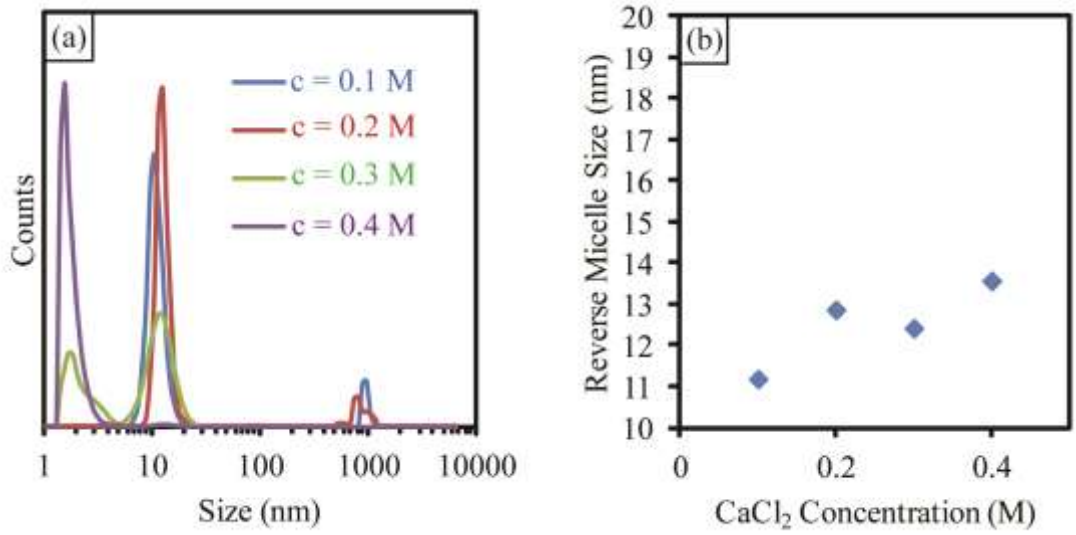

Figure 5 - 5. (a) Size distribution and (b) average size of the dispersed phase for the base system used by Jiao *et al.* when $CaCl_2$ is added.

micelle size changes with increasing electrolyte concentration. The results are similar when adding Na_2CO_3 to the base system, demonstrated by Figure 5-6. Figure 5-6a shows that the dispersed reverse micelle phase is no longer detected when the concentration of Na_2CO_3 is 0.3 M or higher, forming surfactant agglomerates and a coalesced phase only.

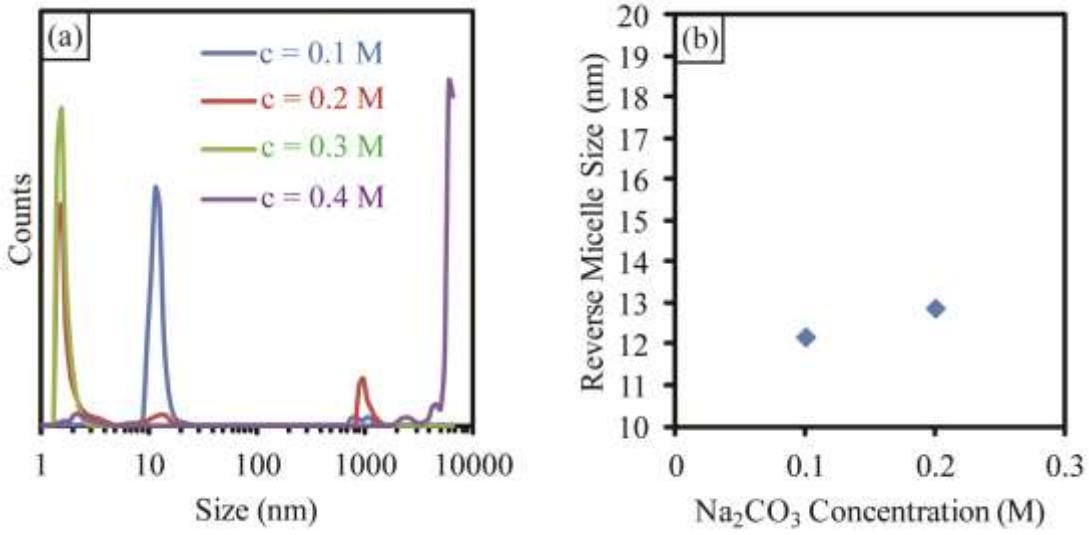

Figure 5 - 6. (a) Size distribution and (b) average size of the dispersed phase for the base system used by Jiao *et al.* when Na_2CO_3 is added.

3. System III

System III exhibits slighty different behavior compared to the other systems in that the solution with no salt additions is unstable (Figure 5-7), but becomes stable with 0.3 M $Mg(NO_3)_2$ concentration. However, as the concentration is increased, the solutions are again unstable. Thus, this system has a very specific concentration at which system stability is achieved. An analysis of how much one can deviate from the 0.3 M $Mn(NO_3)_2$ concentration is not performed, but a small level of variability centered around 0.3 M can be expected. The reverse micellar solutions of $NaHCO_3$ are compositionally very similar and they have similar effects on system stability. However, the 0.3 M

$NaHCO_3$ concentration that was used by Aragón *et al.* was not stable, having reverse micellar structures and also a coalesced phase (Figure 5-7b). Other concentrations also result in unstable solutions that form structures that are highly variable in hydrodynamic diameter. Figure 5-7b shows the signal for a concentration of 0.4 M, which results in complete destabilization of the reverse micellar phase and a wide size distribution.

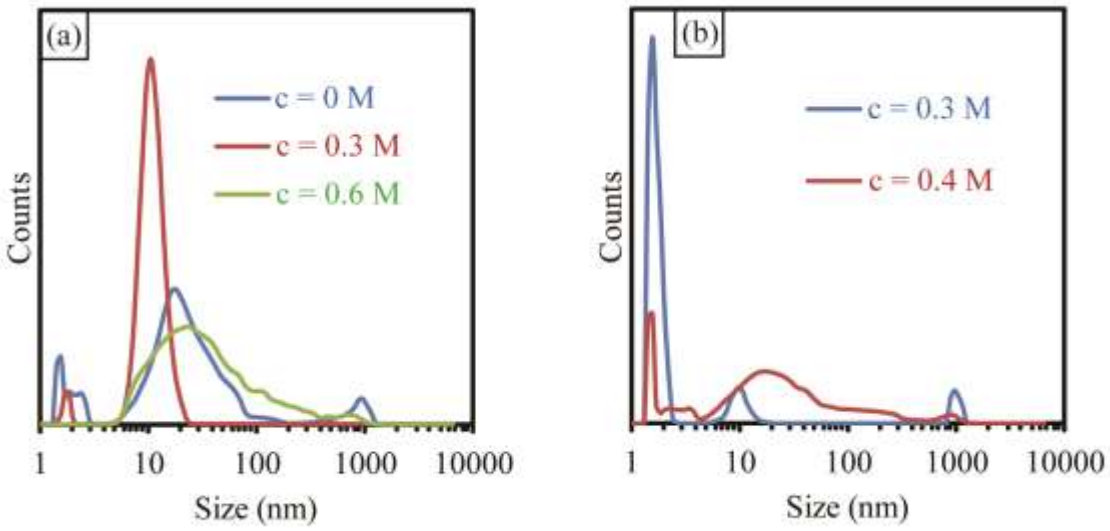

Figure 5 - 7. (a) Dynamic light scattering measurements of (a) $Mn(NO_3)_2$ and (b) $NaHCO_3$ solutions similar to those used by Aragón *et al.*[40]

4. Stability Diagram for Precipitation

Both *Systems II* and *III* eventually resulted in agglomerated powders of broad size distributions (Figure 7 from Jiao *et al.*[39]) or particles that are very large compared to the sizes of the reverse micelles (Figure 3 from Aragón *et al.*[40]). In any case, the powders are produced in the presence of destabilized microemulsions. Even under these circumstances, the presence of surfactant is useful because it can result in limited protection of the precipitates during calcination. Nonetheless, full advantage of the reverse micelle synthesis process is not occurring because the solutions consist of two

phases, that is the reverse micellar phase containing water domains and free water that is phase separated from the oil and where unconfined precipitation occurs. In further developing this process for the preparation of nanopowders, the stability of these systems with respect to the concentration of salts added to the reverse micellar solutions must be carefully considered, since destabilization of the reverse micelle synthesis process can easily occur when excess salt is added. Even under destabilized conditions, there is some usefulness connected to the process. Thus, many studies have made fortuitous use of this technique and have resulted in powders of good quality even when the synthesis methodology is flawed. However, the synthesis conditions would be considered unsuitable when multiple stage manipulations are desired. An ideal synthesis would be one that takes advantage of stable reverse micellar systems.

Precursor stability in the reverse micellar phase does not guarantee stability once precipitation occurs within the phase as was demonstrated for *System I*. This is also summarized by the stability diagram given in Figure 5-8. In the diagram, unstable suspensions result from precursor additions or from precipitates (filled symbols). Only a limited region of the diagram corresponds to stable solutions (unfilled symbols). However, it is unclear whether or not precipitates form inside of the reverse micelles or not and requires further investigation.

Prelimary results for verifying precipitation in the reverse micellar phase are provided in Figure 5-9. The transmission electron image in Figure 5-9a has white lines drawn that demonstrate agglomeration of the reverse micellar phase during sample preparation, possibly as the oil phase is evaporated and the reverse micelles become concentrated. The reverse micellar phase is observed primarily on one side of the

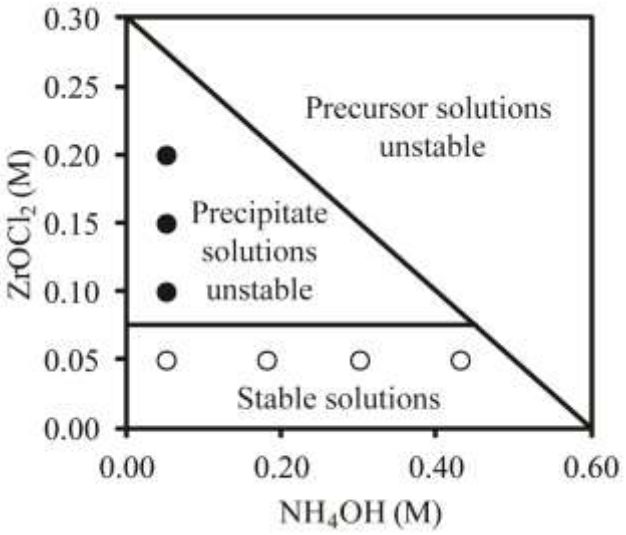

Figure 5 - 8. Stability diagram for obtaining stable solutions when mixing $ZrOCl_2$ and NH_4OH reverse micellar solutions with $\omega_o = 10$.

boundary, opposite the side that is marked with white arrows. Figure 5-9b and Figure 5-9c demonstrate progressively higher magnifications. Some individual particles having size 3-4 nm can be observed at the highest magnification, such as the particle that is highlighted by the set of red arrows. Other particles appear agglomerated into worm-like structures, which could be expected when enough of the bulk organic phase has been removed so that the percolation threshold is exceeded and an interconnected water network forms. The percolation threshold has been characterized by a dramatic increase in conductivity for reverse micellar solutions due to this type of morphology.[44] Thus, it is unlikely that TEM can accurately capture the nature of the precipitates as they exist dispersed in the original solution. Nevertheless, several similar TEM results are demonstrated in the literature.[45-49] The electron diffraction patterns for the particles from this study is provided in Figure 5-9d, which demonstrate that the particles are

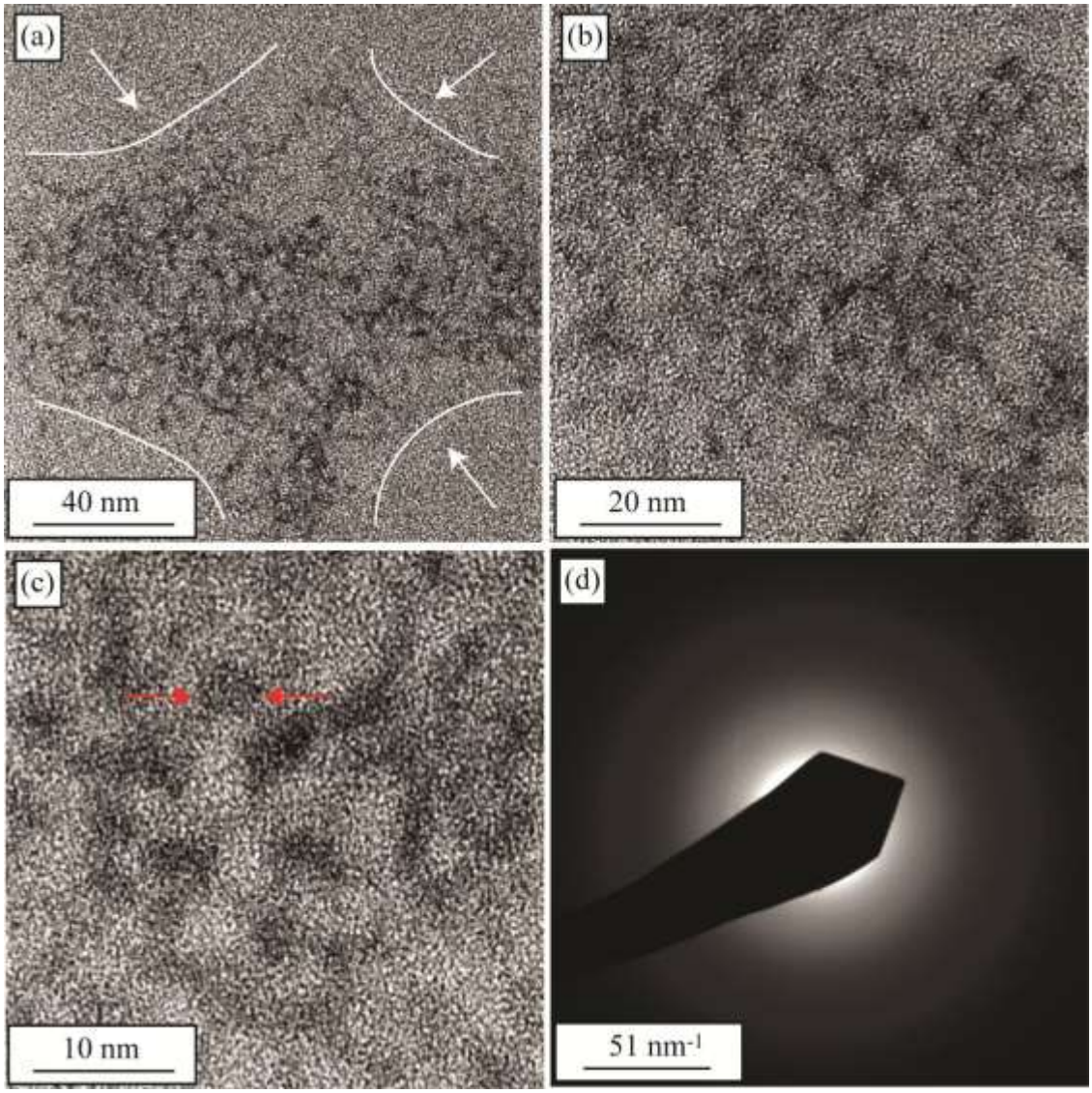

Figure 5 - 9. (a-c) Transmission electron images with progressively higher magnificaiton of precipitates formed by mixing 0.05 M $ZrOCl_2$ and 0.05 M NH_4OH reverse micellar solutions and (d) selected area electron diffraction demonstrating that the precipitates are amorphous.

amorphous. Thus, it cannot be confirmed whether or not the particles are zirconium hydroxide precipitates or the precursor precipitated upon solvent extraction during the sample preparation procedure. TEM analysis of a similar reverse micellar phase, but without NH_4OH additions, may provide further insight because the precipitation of an

amorphous precursor phase can be ruled out if the particles are not observed. Precipitation was observed for the given concentrations in bulk solution, but behavior in the reverse micelle may not be the same as in bulk solution.

Transmission electron images of an unstable precipitate solution are provided in Figure 5-10. In this case, large agglomerates are observed that are a couple of hundred nanometers in size. Several of these agglomerates are demonstrated in Figure 5-10a. A closer examination of these agglomerates is demonstrated in Figure 5-10b. The agglomerates are of low density (containing void spaces) and made up of smaller particles. The substructure has a size appearing consistent about 30-40 nm as is demonstrated by the red arrows. It is likely that these agglomerates are protected by surfactant molecules. The size of the substructure, protected by surfactant molecules, is consistent with the particle sizes that can be obtained after calcining particles produced using similar unstable conditions.[21]

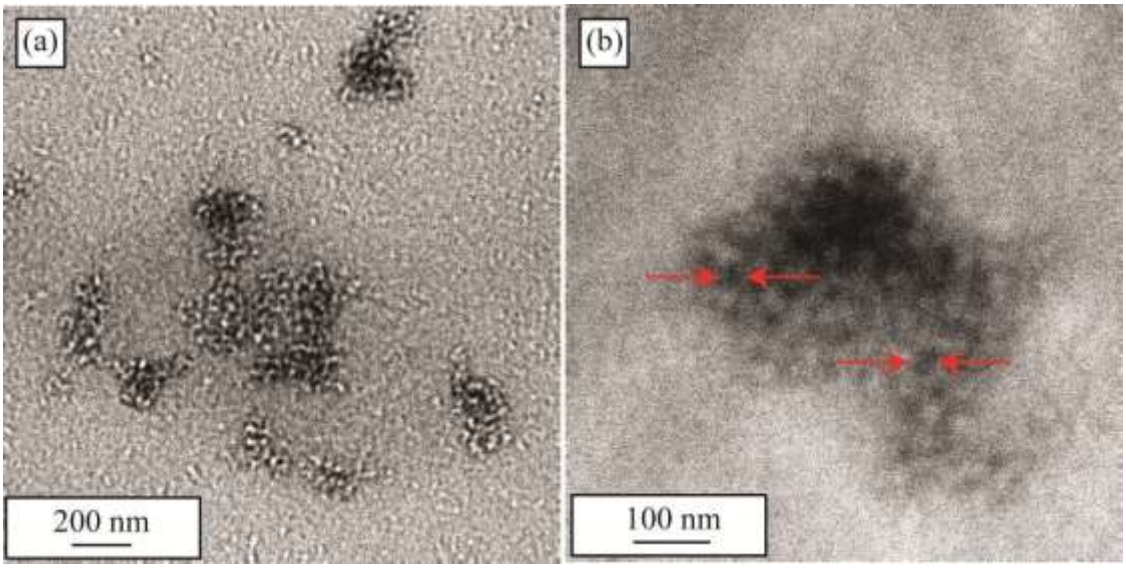

Figure 5 - 10. Transmission electron images of precipitates formed by mixing 0.1 M $ZrOCl_2$ and 0.05 M NH_4OH reverse micellar solutions.

D. Conclusions

Although up to 0.3 M $ZrOCl_2$ can be incorporated into *System I*, concentrations of 0.1 M or higher are unstable when adding NH_4OH to initiate a precipitation reaction. However, the stability is not affected by NH_4OH, all concentrations within the precursor stability limits are stable when the $ZrOCl_2$ concentration is 0.05 M. Thus, in addition to considering precursor limits, precipitation limits must also be considered to ensure system stability. Transmission electron images demonstrate particles that are about 3-4 nm in size. However, precipitates formed in unstable solutions are highly agglomerated and contain substructure that is larger than the precipitates formed under stable conditions.

Precursor salts added to microemulsions prepared with the cationic surfactant CTAB are found to cause growth of the reverse micelles and mostly produced unstable solutions. A notable exception is when $Mn(NO_3)_2$ is added to an unstable reverse micellar parent phase that results in stabilization, but eventually destabilized the reverse micellar structures at higher concentrations.

E. References

1. M. Boutonnet, J. Kizling, and P. Stenius, "The Preparation of Monodisperse Colloidal Metal Particles from Microemulsions," *Colloids Surf.,* **5** [3] 209-25 (1982).

2. J.H. Fendler, "Atomic and Molecular Clusters in Membrane Mimetic Chemistry," *Chem. Rev.*, **87** [5] 877-99 (1987).

3. V. Pillai, P. Kumar, M.J. Hou, P. Ayyub, and D.O. Shah, "Preparation of Nanoparticles of Silver Halides, Superconductors and Magnetic Materials Using Water-in-oil Microemulsions as Nano-Reactors," *Adv. Colloid Interface Sci.,* **55**, 241-69 (1995).

4. J. Eastoe and B. Warne, “Nanoparticle and Polymer Synthesis in Microemulsions,” *Curr. Opin. Colloid Interface Sci.,* **1** [6] 800-5 (1996).

5. J.H. Adair, T. Li, T. Kido, K. Havey, J. Moon, J. Mecholsky, A. Morrone, D.R. Talham, M.H. Ludwig, and L. Wang, “Recent Developments in the Preparation and Properties of Nanometer-size Spherical and Platelet-shaped Particles and Composite Particles,” *Mater. Sci. Eng., R,* **23** [4-5] 139-242 (1998).

6. W.F.C. Sager, “Controlled Formation of Nanoparticles from Microemulsions,” *Curr. Opin. Colloid Interface Sci.,* **3** [3] 276-83 (1998).

7. V.T. John, B. Simmons, G.L. McPherson, and A. Bose, “Recent Developments in Materials Synthesis in Surfactant Systems,” *Curr. Opin. Colloid Interface Sci.,* **7** [5-6] 288-95 (2002).

8. M.A. López-Quintela, “Synthesis of Nanomaterials in Microemulsions: Formation Mechanisms and Growth Control,” *Curr. Opin. Colloid Interface Sci.,* **8** [2] 137-44 (2003).

9. B.L. Cushing, V.L. Kolesnichenko, and C.J. O’Connor, “Recent Advances in the Liquid-phase Syntheses of Inorganic Nanoparticles,” *Chem. Rev.,* **104** [9] 3893-946 (2004).

10. V. Uskoković and M. Drofenik, “Synthesis of Materials within Reverse Micelles,” *Surf. Rev. Lett.,* **12** [2] 239-77 (2005).

11. J. Eastoe, M.J. Hooamby, and L. Hudson, “Recent Advances in Nanoparticle Synthesis with Reversed Micelles,” *Adv. Colloid Interface Sci.,* **128-130**, 5-15 (2006).

12. M.L. Steigerwald, A.P. Alivisatos, J.M. Gibson, T.D. Harris, R. Kortan, A.J. Muller, A.M. Thayer, T.M. Duncan, D.C. Douglass, and L.E. Brus, “Surface Derivation and Isolation of Semiconductor Cluster Molecules,” *J. Am. Chem. Soc.*, **110** [10] 3046-50 (1988).

13. P.K. Dutta and D. Robins, “Synthesis of Zeolite A from Reactants Enclosed in Reverse Micelles,” *Langmuir,* **7** [6] 1048-50 (1991).

14. N. Houyi, S. Taichenc, and L. Ganzuo, “Preparation of Monodisperse Nickel (Cobalt) Boride Catalyst Using Reversed Micellar System,” *J. Dispersion. Sci. Technol.,* **13** [6] 647-56 (1992).

15. C. Petit, P. Lixon, and M.-P. Pileni, “In Situ Synthesis of Silver Nanocluster in AOT Reverse Micelles,” *J. Phys. Chem.*, **97** [49] 12974-83 (1993).

16. M. Roth, R. Hempelmann, O. Borgmeier, T. Eifert, and H. Lueken, "Nanocrystalline NH_4MnF_3 with Controlled Grain Size: Synthesis and Antiferromagnetistm," *Nanostruct. Mater.*, **12**, 855-8 (1999).

17. E.E. Carpenter, A. Kumbhar, J.A. Wiemann, H. Srikanth, J. Wiggins, W. Zhou, and C.J. O'Connor, "Synthesis and Magnetic Properties of Gold-iron-gold NanoComposites," *Mater. Sci. Eng., A*, **286** [1] 81-6 (2000).

18. O.A. Graeve and J.O. Corral, "Preparation and Characterization of Rare-earth-doped Y_2O_3 Luminescent Ceramics by the Use of Reverse Micelles," *Optic. Mater. (Ensenada, Mexico)*, **29** [1] 24-30 (2006).

19. K. Kandori, K. Kon-No, and A. Kitahara, "Formation of Ionic Water/Oil Microemulsions and Their Application in the Preparation of $CaCO_3$ Particles," *J. Colloid Interface Sci.*, **122** [1] 78-82 (1988).

20. A.J. Zarur and J.Y. Ying, "Reverse Microemulsion Synthesis of Nanostructured Complex Oxides for Catalytic Combustion," *Nature*, **403** [6] 65-7 (2000).

21. O.A. Graeve, H. Fathi, J.P. Kelly, M.S. Saterlie, K. Sinha, G. Rojas-George, R. Kanakala, D.R. Brown, and E.A. Lopez, "Reverse Micelle Synthesis of Oxide Nanopowders: Mechanisms of Precipitate Formation and Agglomeration Effects," *J. Colloid Interface Sci.*, **407**, 302-9 (2013).

22. M. Meyer, C. Wallberg, K. Kurihara, and J.H. Fendler, "Photosensitized Charge Separation and Hydrogen Production in Reversed Micelle Entrapped Platinized Colloidal Cadmium Sulphide," *J. Chem. Soc., Chem. Commun.*, [2] 90-1 (1984).

23. C.B. Murray, D.J. Norris, and M.G. Bawendi, "Synthesis and Characterization of Nearly Monodisperse CdE (E = S, Se, Te) Semiconductor Nanocrystallites," *J. Am. Chem. Soc.*, **115** [19] 8706-15 (1993).

24. A.R. Kortan, R. Hull, R.L. Opila, M.G. Bawendi, M.L. Steigerwald, P.J. Carroll, and L.E. Brus, "Nucleation and Growth of CdSe on ZnS Quantum Crystallite Seeds, and Vice Versa, in Inverse Micelle Media," *J. Am. Chem. Soc.*, **112** [4] 1327-32 (1990).

25. R. Singh and P.K. Dutta, "Crystal Growth of Faujasitic Microporous Zincophosphate Crystals Using Reverse Micelles as Reactants," *Langmuir*, **16** [9] 4148-53 (2000).

26. E.E. Foos, R.M. Stroud, and A.D. Berry, "Synthesis and Characterization of Nanocrystalline Bismuth Telluride," *Nano Lett.*, **1** [12] 693-5 (2001).

27. I. Lisiecki and M.P. Pileni, "Synthesis of Well-defined and Low Size Distribution Cobalt Nanocrystals: The Limited Influence of Reverse Micelles," *Langmuir*, **19** [22] 9486-9 (2003).

28. T. Hirai, H. Sato, and I. Komasawa, "Mechanism of Formation of CdS and ZnS Ultrafine Particles in Reverse Micelles," *Ind. Eng. Chem. Res.*, **33** [12] 3262-6 (1994).

29. A.P. Herrera, O. REsto, J.G. Briano, and C. Rinaldi, "Synthesis and Agglomeration of Gold Nanoparticles in Reverse Micelles," *Nanotechnology*, **16** [7] S618-25 (2005).

30. L. Motte, F. Billoudet, E. Lacaze, and M.-P. Pileni, "Self-organization of Size-selected Nanoparticles into Three-dimensional Superlattices," *Adv. Mater.*, **8** [12] 1018-20 (1996).

31. M.P. Pileni, "Nanosized Particles Made in Colloidal Assemblies," *Langmuir*, **13** [13] 3266-76 (1997).

32. A. Taleb, C. Petit, and M.P. Pileni, "Synthesis of Highly Monodisperse Silver Nanoparticles from AOT Reverse Micelles: A Way to 2D and 3D Self-organization," *Chem. Mater.*, **9** [4] 950-9 (1997).

33. M. Li, H. Schnablegger, and S. Mann, "Coupled Synthesis and Self-assembly of Nanoparticles to Give Structures with Controlled Organization," *Nature*, **402** [6755] 393-5 (1999).

34. C.E. Bunker, B.A. Harruff, P. Pathak, A. Payzant, L.F. Allard, and Y.-P. Sun, "Formation of Cadmium Sulfide Nanoparticles in Reverse Micelles: Extreme Sensitivity to Preparation Procedure," *Langmuir*, **20** [13] 5642-4 (2004).

35. H. Fathi, J.P. Kelly, V.R. Vasquez, and O.A. Graeve, "Ionic Concentration Effects on Reverse Micelle Size and Stability: Implications for the Synthesis of Nanoparticles," *Langmuir*, **28** [25] 9267-74 (2012).

36. X. Li, C.-K. Loong, P. Thiyagarajan, G.A. Lager, and R. Miranda, "Small-angle Neutron Scattering Study of Nanophase Zirconia in a Reverse Micelle Synthesis," *J. Appl. Cryst.*, **33** [1] 628-31 (2000).

37. G.D. Rees, R. Evans-Gowing, S.J. Hammond, and B.H. Robinson, "Formation and Morphology of Calcium Sulfate Nanoparticles and Nanowires in Water-in-oil Microemulsions," *Langmuir*, **15** [6] 1993-2002 (1999).

38. T. Kawai, A. Fujino, K. Kon-No, "Synthesis of Monodisperse ZrO_2 Particles in Polyoxyethylated Nonionic Reversed Micelles," *Colloids Surf., A*, **109**, 245-53 (1996).

39. S. Jiao, K.T. Kilby, L. Zhang, and D.J. Fray, "A Route for Producing Nano-$CaRuO_3$ Perovskite by Combusting Precursors Prepared Using Reverse Micelle Synthesis," *Nanotechnology*, **20** [8] 085606 6pp. (2009).

40. M.J. Aragón, B. León, C.P. Vicente, and J.L. Tirado, "A New Form of Manganese Carbonate for the Negative Electrode of Lithium-ion Batteries," *J. Power Sources,* **196** [5] 2863-6 (2011).

41. "Standard Guide for Measurement of Particle Size Distribution of Nanomaterials in Suspension by Photon Correlation Spectroscopy (PCS)[1]," ASTM Designation E2490-09. ASTM International, West Conshohocken, PA.

42. I. Persson, "Hydrated Metal Ions in Aqeous Solution: How Regular are Their Structures," *Pure Appl. Chem.*, **82** [10] 1901-17 (2010).

43. H. Ohtaki and T. Radnai, "Structure and Dynamics of Hydrated Ions," *Chem. Rev.*, **93** [3] 1157-1204 (1993).

44. J.E. Puig, I. Rodríguez-Siorida, L-.I. Rangel-Zamudio, J.F. Billm-an, and E.W. Kaler, "Properties and Structures of Three- and Four-component Microemulsions," *Langmuir*, **4** [4] 806-12 (1988).

45. C.F. Yang and J.Y. Chen, "Synthesis of Stabilized Zirconia Ultrafine Powders Using AOT-isooctane-water Reverse Micelles," *J. Mater. Sci. Lett.*, **16** [11] 936-8 (1997).

46. V.T. Liveri, M. Rossi, G. D'Arrigo, D. Manno, and G. Micocci, "Synthesis and Characterization of ZnS Nanoparticles in Water/AOT/n-heptane Microemulsions," *Appl. Phys. A*, **69** [4] 369-73 (1999).

47. F.T. Quinlan, J. Kuther, W. Tremel, W. Knoll, S. Risbud, and P. Stroeve, "Reverse Micelle Synthesis and Characterization of ZnSe Nanoparticles," *Langmuir*, **16** [8] 4049-51 (2000).

48. Q. Pang, B.C. Guo, C.L. Yang, S.H. Yang, M.L. Gong, W.K. Ge, and J.N. Wang, "$Cd_{1-x}Mn_xS$ Quantum Dots: New Synthesis and Characterization," *J. Cryst. Growth,* **269** [2-4] 213-7 (2004).

49. K. Naoe, M. Kataoka, and M. Kawagoe, "Preparation of Water-soluble Palladium Nanocrystals by Reverse Micelle Method: Digestive Ripening Behavior of Mercaptocarboxylic Acids as Stabilizing Agent," Colloids Surf., A, **364** [1-3] 116-22 (2010).

CHAPTER 6: EFFECT OF MODIFIYING THE HYDROGEN BOND NETWORK OF THE POLAR PHASE ON REVERSE MICELLE SIZE, REVERSE MICELLE STABILITY, AND PRECIPITATION OF ZIRCONIUM HYDROXIDE IN THE WATER-AOT-ISOOCTANE SYSTEM

A. Introduction

Chapter 4 demonstrated the hydrogen bond network can have a decisive role in determining reverse micelle size and stability with added electrolytes. A brief summary of the relevant findings are summarized here. When $HAuCl_4$ is added to the water-AOT-isooctane reverse micellar system, the system is unstable and the average reverse micelle size is larger as electrolyte concentration is increased. Although average size with increasing electrolyte concentration is proportional to the electrical double layer thickness, compression of the electrical double layer thickness cannot explain the size increase according to the concepts originally described in Chapter 2. Two possible explanations were given: the $(AuCl_4)^-$ co-ion complex was too large or the hydrogen bond network influences the electrostatic interactions that dictate the reverse micelle sizes. However, the results presented in Chapter 5 demonstrate reverse micelle instability and growth with increasing electrolyte concentration when CTAB is used as a surfactant and the ions are not too large compared to the others that have been studied in this thesis. However, the growth can be a result of the latter explanation. Thus, it is plausible that the hydrogen bond network is an important and governing feature of reverse micelle size and stability.

A slight modification to the qualitative model presented in Chapter 2 is given in Chapter 4 to incorporate the potential effect of the hydrogen bond network. The modification is based on preferred orientation of the structured water molecules in the

reverse micelle that generates two charged surfaces, instead of the surfactant film and the core forming the surfaces described for the former model. The specific ions introduced into the reverse micelle can conceivably alter the water chemistry by donating or accepting hydrogen, for example. Ruasse *et al.* demonstrated that the hydrogen donor capability of water can be enhanced by as much as a factor of 65 in reverse micelles without added electrolyte.[1] It is unclear how added electrolytes can further influence water chemistry within a reverse micelle. The chemistry of the specific ions can cause switching of the water molecule orientation that produce the two charged surfaces and determine the type of counterions between them. The specific type of counterion, whether cationic or anionic, will define the electrostatic interaction between the surfactant interfacial layer and the counterions between the water layers that results in an attractive or repulsive force causing reverse micelle shrinkage or growth, respectively. The details are not yet fully explored to verify such a model because the characterization needed to provide direct measurements of the reverse micelle dynamics are prohibitively expensive and primarily focused on basic systems, without added electrolytes.[2] However, the concept can be further explored by performing experiments with the intention of purposefully altering the hydrogen bond network and monitoring the responses to these changes. For example, the hydrogen bond network can be altered by changing the water-to-surfactant ratio or by introducing other polar solvents besides water. Both concepts are explored here.

The water in reverse micelles is often regarded as relative contributions of a shell and core of interface and bulk-like water, respectively.[2] At or below a water-to-surfactant ratio of about 6-10, water is mostly thought of as bound to the interface in the

water-AOT-isooctane system (considered only shell water), and larger water-to-surfactant ratios also produce a core of bulk-like water.[3,4] Varying the size of the trapped polar phase, by reducing the water-to-surfactant ratio and increasing interaction with the surfactant molecules, the effective polarities of the reverse micelle environment can be substantially altered, presumably through modification of the hydrogen bond network.[5] A problem with the core-shell model is that it does not account for the evolution of the hydrogen bond network because it does not allow for the strength or length of a hydrogen bond to change.[2] More recently, layer-wise decomposition of the frustrated hydrogen bond network is being explored to provide a more accurate description of the water structure in the confined space of a reverse micelle.[6,7]

Nonaqueous polar solvents other than water or mixtures with water can affect the hydrogen bond network and a considerable effort is being made to characterize such systems.[2,8] For solvents like acetonitrile, showing no dependence on the solvation dynamics with different solvent to surfactant ratios, it is assumed that well-defined solvent pools do not form. Alternatively, the solubilization of the acetonitrile may be low and so additional acetonitrile is not incorporated into the reverse micelle phase. Despite the uncertainty of the reverse micelle structure formed with acetontrile, this system is used to encapsulate diphenylmethyl phophonium salt and found to produce enhanced yield for biomolecular reactions.[9] Solvents like glycerol have slower solvation dynamics with decreasing solvent to surfactant ratio, but to a lesser extent than when water is being confined, and is possible evidence for changes to the hydrogen bond network. Other solvents that are investigated include methanol, glycerol, formamide, and ionic liquids, such as 1-butyl-3-methyl-imadazolium $(BF_4)^-$.[2,10] The room-temperature ionic liquids

(RTIL) are an interesting class of tunable designer solvents with essentially zero volatility and the ability to tune the polarity by selection of their cationic and anionic components.

Perhaps the most significant demonstration that mixtures of nonaqeous solvents with water affect the hydrogen bond network has been summarized by Bagchi, who described recent attempts to explore chemistry and biology in binary solvent mixtures of water-dioxane, water-demthyl sulfoxide, and water-ethanol, for example.[7] The diffusion coefficients of both solute and solvent, the rotational correlation time, and local density fluctuation all exhibited anomalous non-monotonic composition dependence at surprisingly low concentrations that is thought to depend on a percolation-like transition in molecular dipole interactions, which can be thought of as a percolation threshold of the nonaqueous solvent into the hydrogen bond network.

Other significant evidence for the importance of the hydrogen bond network of reverse micelles with nonaqueous solvents in AOT/n-heptane is given by Falcone *et al*.[11] When studying the reverse micelle size of formamide, dimethylformamide, dimethylacetamide, ethylene glycol, and glycerol, the sizes as a function of solvent-to-surfactant ratio do not depend on the molar volume of the solvent. Instead the reverse micelle size depends on whether or not the solvent is an H-bond donor or not. The H-bond donor solvents (glycerol and ethylene glycol) produce sizes that are larger than the sizes of water reverse micelles and the solvents that do not donate H-bonds (dimethylformamide and dimethylacetamide) produce sizes smaller than the sizes of water reverse micelles. While formamide is an H-bond donor as a bulk solvent, it is found not to be within reverse micelles, making it a unique solvent.

A potentially important consequence of confinement inside reverse micelles is that the dissociation of ion complexes in the reverse micelles can be enhanced.[12,13] In the case of certain iron complexes, a two- to ten-fold increase in the rate of dissociation was measured in comparison to pure aqueous phase.[14] Alternatively, ion pairs (undissociated counteiron/co-ion pairs) are more likely to form in solvents with less hydrogen bonding.[15] If the extent of dissociation is influenced by the hydrogen bond network, then changing the water-to-surfactant ratio or substitution of other polar solvents for water can affect molecular dissociation and as a consequence may affect the size and stability of reverse micelles to a different extent depending on how the modification impacts the specific interactions in the reverse micelles.

Varying the water-to-surfactant ratio is common for reverse micelle synthesis and is even thought to be the most important variable for controlling the particle size.[4,16-18] Several studies arrive at different conclusions, however, and it is generally accepted that differences arise due to specific nucleation and growth conditions for the experiment.[19] Altering the water-to-surfactant ratio is also found to alter particle morphology between elongated and spherical.[20,21] There are few reports on using nonaqeous solvents to produce nanoparticles.[22,23] The few exceptions have primarily focused on the synthesis of silver nanoparticles in reverse micelles containing methanol or RTILs. While successful in producing silver nanoparticles, the implications for particle development in these systems in comparison to aqueous reverse micelles is not yet apparent. Synthesis of MgF_2 in methanol-based reverse micelles has also been reported.[24] Another reason to study how alcohols affect structure and stability in reverse micelles is that alcohol is a byproduct during the hydrolysis of metalorganic precursors used to produce oxides.[25]

The purpose of Chapter 6 was to investigate the effects of water-to-surfactant ratio and partial substitution of other polar solvents for water, namely methanol and acetone, on reverse micelle size and stability when electrolytes are added to the aqueous phase and when precipitating particles. The results will be compared to those presented in previous chapters, namely Chapter 2 and Chapter 4 for evaluating the effects of electrolyte addition and Chapter 5 for evaluating the size and stability of the reverse micelles when performing a precipitation reaction. This study has important implications because future studies concerning the characterization of the hydrogen bond network when salts are added will need to agree with the experimental observations presented here. Thus, it is expected to help determine the validity of future models based on experiments probing the hydrogen bond network of reverse micelles containing electrolytes.

B. Experimental Methods

The preparation procedure for the reverse micellar solutions was similar to that presented elsewhere, in Chapter 4 and in Chapter 5.[25] Some of the previous experiments were repeated to further characterize the solutions, but all others were prepared with some modification, either to the water-to-surfactant ratio or substitution of nonaqeous solvents for water. Water-to-surfactant ratios of 5, 7.5, 10, and 15 were studied by keeping the water content the same and decreasing or increasing the amount of surfactant used to produce the reverse micellar solution. Thus, AOT (98+%, Sigma-Aldrich, St. Louis) amounts of 17.782, 11.855, 8.891, and 5.927 g were added to the isooctane (99+%, Sigma-Aldrich, St. Louis, MO) phase to prepare these solutions, respectively. Solutions of the base systems and the systems with added $Mg(NO_3)_2$ (98%, Alfa Aesar,

Ward Hill, MA), $Al(NO_3)_3$ (99.999%, Alfa Aesar, Ward Hill, MA), and $ZrOCl_2$ (99.9985%, Alfa Aesar, Ward hill, MA) to the 3.6 mL of the distilled water phase were prepared and characterized.

Nonaqueous polar phases were substituted for water by systematic substitution of either methanol or acetone to a system that would otherwise correspond to a water-to-surfactant ratio of ten for the pure water phase without the substitutions. The substitutions were made to preserve a constant volume (3.6 mL) so that the observed size changes are a result of molecular interactions only. Otherwise, all other quantities were held constant according to the previous work, including the weight of the salts added. Thus, for 10, 20, 30, 40, and 50 volume percent substitution, it would correspond to substituting 0.36, 0.72, 1.08, and 1.80 mL of the nonaqueous solvent for the same volume of distilled water. The additions of electrolytes were made to systems with either 50% methanol substitution or 16% acetone substitution. The amounts were chosen to correspond to similar changes to the average dipole moment below and above that of water, respectively, assuming a rule of mixtures with respect to the mole fraction of each solvent and dipole moments of 1.70, 1.85, and 2.88 for methanol, water, and acetone, respectively. Thus, the net dipole moments would correspond to 1.80, 1.85, and 1.90 for the methanol-water mixture, water, and acetone-water mixture, respectively.

Precipitation experiments were performed in Chapter 5. The stability of the reverse micelles was not affected by the amount of NH_4OH, but did depend on the amount of $ZrOCl_2$ used for the precipitation reaction. Amounts of 0.1 M $ZrOCl_2$ or more produced solutions that were not stable, as noted by the turbid appearance of the solutions. Precipitation experiments were repeated for the modified systems by mixing

solutions having amounts equivalent to the previous experiments with 0.15 M $ZrOCl_2$ and 0.05 M NH_4OH, but with additional surfactant (to achieve a water-to-surfactant ratio of 5), with 50 volume percent of the aqueous phase replaced by methanol, or with 16% of the water phase replaced by acetone. The purpose was to see if the modifications stabilize previously unstable reverse micellar solutions when initiating precipitation.

Dynamic light scattering measurements were performed on either a Nanotrac ULTRA instrument (Microtrac, Montgomeryville, PA) or a Nanotrac Wave DLS instrument (Microtrac, Montgomeryville, PA) according to previous procedures.[12] Where convenient, to make direct comparisons between the two devices, the correlation factor introduced in Chapter 4 was used and pointed out in the appropriate plots by the addition of a correlation factor (CF) to the measured size. Previously, the stability of reverse micells solutions was qualitatively determined by the observed transparency or opaque appearance of the reverse micelle solution. Turbidity measurements were made on solutions in an attempt to provide a more quantitative description of stability using a turbidity meter (Model 2020, LaMotte Chemical Products Company, Chestertown, MD). The turbidity measurements were averages of five readings and five measurements were made. All characterization was performed for two experiments.

C. Results and Discussion

1. Reverse Micelle Sizes of Base Systems (Without Salts)

The average reverse micelle size when changing the water-to-surfactant ratio (ω_o) is demonstrated in Figure 6-1. The average reverse micelle size is found to change linearly with water-to-surfactant ratio over two regimes, $\omega_o \leq 7.5$ and $\omega_o \geq 7.5$ and is demonstrated in Figure 6-1a, which also contains the average size of free surfactant

aggregates that is observed at low ω_o, representing the size of the reverse micelles without water (at $\omega_o = 0$). A linear relationship between reverse micelle size and ω_o has been found or reported by several researchers.[11,26-28] A linear change in reverse micelle size with ω_o was reported by Herrera *et al.*, covering a wide range of ω_o.[29] Their linear fit was not excellent and could indicate a transition at about $\omega_o = 8$ when considering the error in the measurements at high ω_o values of 14 and 15. A transition at $\omega_o = 8$ is in excellent agreement with the results given in Figure 6-1a. Other reports found that the size relationship is non-linear, a conclusion that can be reached because of the transition.[30,31] A linear relationship has often been assumed based on a geometric model for reverse micelles that depends on the efficient packing of surfactant molecules at the interface, but problems with the geometric model have beeen discussed in the introduction of this thesis. Instead Chapter 2, Chapter 4, and Chapter 5 have demonstrated that the reverse micelle size depends on the electrical double layer thickness and therefore ion concentration. The relationship between the ω_o and the electrical double layer thickness with sodium counterions as a function of ω_o is demonstrated in Figure 6-1b. The direct relationship between the ω_o and the electrical double layer thickness can be used to explain the observation that the reverse micelle size depends linearly on ω_o, although the electrical double layer thickness is thought to control this behavior.

The slope transition at $\omega_o = 7.5$ is reminiscent of the data presented in Chapter 4 where there was a slope transition associated with the amount of counterions introduced into the system. This was demonstrated for NH_4OH and $ZrOCl_2$ additions, where low concentrations result in a smaller slope than at high concentrations. Similarly, a lower

slope occurs at higher ω_o values, where the sodium counterion concentration is reduced because less surfactant is added. The low slope at low counterion concentration can be because only the Stern layer is occupied or because the electrical double layer thicknesses are not long enough to overlap and influence the reverse micelle size. Alternatively, phase separation of the microemulsion as ω_o is increased can be the cause for the slope transition.[32] Yet another explanation is that the high slope at low water to surfactant ratios is associated with a change in morphology, since low ω_o values are known to produce elongated reverse micelle structures.[33] The exact mechanism is unclear.

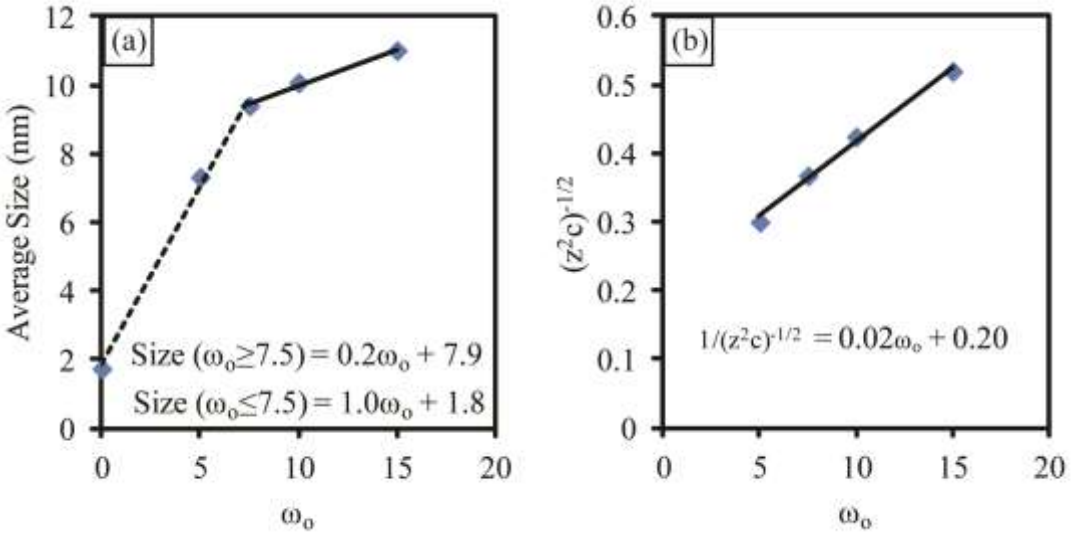

Figure 6 - 1. (a) Average reverse micelle size as a function of the water-to-surfactant ratio (ω_o) and (b) the relationship between valence and concentration of the sodium counterion and ω_o that explains the linear changes in average reverse micelle size.

The average reverse micelle size when other polar solvents were substituted for water is demonstrated in Figure 6-2. The average reverse micelle size does not change significantly when relatively low quantities of solvent are substituted, but a transition has been observed where size decreases with further substitution. The transition occurs at

20% and 30% for acetone and methanol, respectively. After the transition, the size change associated with acetone substitution is greater than the size change associated with methanol. It would be interesting to test whether or not the rate of size change can be correlated to the difference in polarity between the polar solvents, but is beyond the scope of this work because several other solvents would need to be tested. It would also be interesting to determine if the transition can be correlated to a percolation-like transition that has been observed by other researchers.[7]

Alcohols can partition to the aqueous core or reside at the reverse micelle surface as a cosurfactant.[34-36] Short chain alcohols mainly partition to the core while long chain alcohols act as cosurfactants. Furthermore, ω_o can influence where the alcohol partitions to.[37] Methanol only interacts with water at high ω_o whereas it also form a complex with AOT molecules at the reverse micelle interface when ω_o is low. It seems reasonable that the concentration of alcohol can also influence the relative quantities partitioned into the aqueous core or to the reverse micelle interfaces. Thus, the transition observed in Figure 6-2 can also be caused by dual functionality of the polar solvents being substituted.

2. Effect of Salt Additions to Base Systems

The relationship between the electrical double layer thickness and salt concentration when $\omega_o = 5$ is given in Figure 6-3. The average reverse micelle size when $Mg(NO_3)_3$ is added is given in Figure 6-3a. The point of instability when $\omega_o = 5$ is improved to 0.9 M $Mg(NO_3)_3$ in comparison to 0.5 M $Mg(NO_3)_3$ when $\omega_o = 10$ and the average size at the point of instability is decreased to 4.8 nm when $\omega_o = 5$ in comparison to 5.9 nm when $\omega_o = 10$. The relationship to the electrical double layer exists for

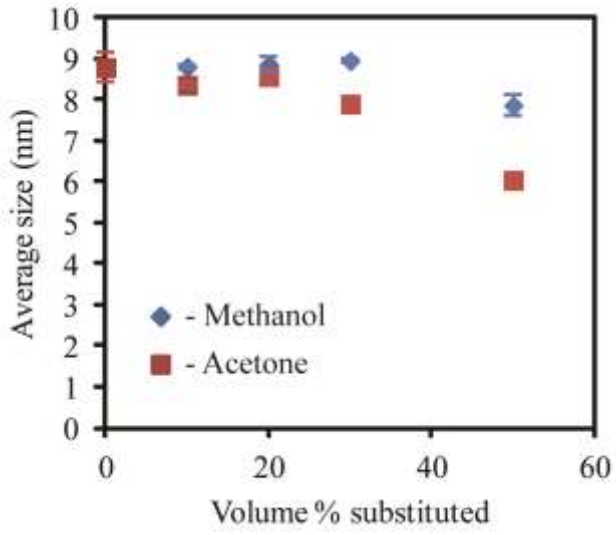

Figure 6 - 2. Average reverse micelle size in the water-AOT-isooctane system with partial substitution of other polar solvents for water.

counterions of higher valence when $\omega_o = 5$ (Figure 6-3b and Figure 6-3-c). An analysis similar to that presented in Chapter 2 to determine the critical potential at the point of instability is presented in Figure 6-3d and compared to the previous results. The critical potential did not change when changing ω_o from 10 to 5 as is indicated by the identical slope of the fitted lines. However, the intercept of the fitted lines changes from -0.2 to 0.5 and indicates that the local counterion concentration at the critical potential is doubled from 0.8 M to 1.6 M when halving ω_o (i.e. doubling the amount of surfactant and increasing the surface charge density).

An analysis of the slope similar to the analysis presented in Chapter 5 has been performed to estimate the dielectric constant of the reverse micelle interior with salt additions when $\omega_o = 5$. The estimate of the dielectric constant is increased for all the electrolytes studied, but more pronounced for $Al(NO_3)_3$ and $ZrOCl_2$, reaching estimated values of 31,000 and 37,000, respectively. The implications of the dramatic increase in

the dielectric constant by up to three orders of magnitude are unclear, but could be a possible explanation for observed differences in reaction kinetics and molecular stability in confined water versus bulk solution.

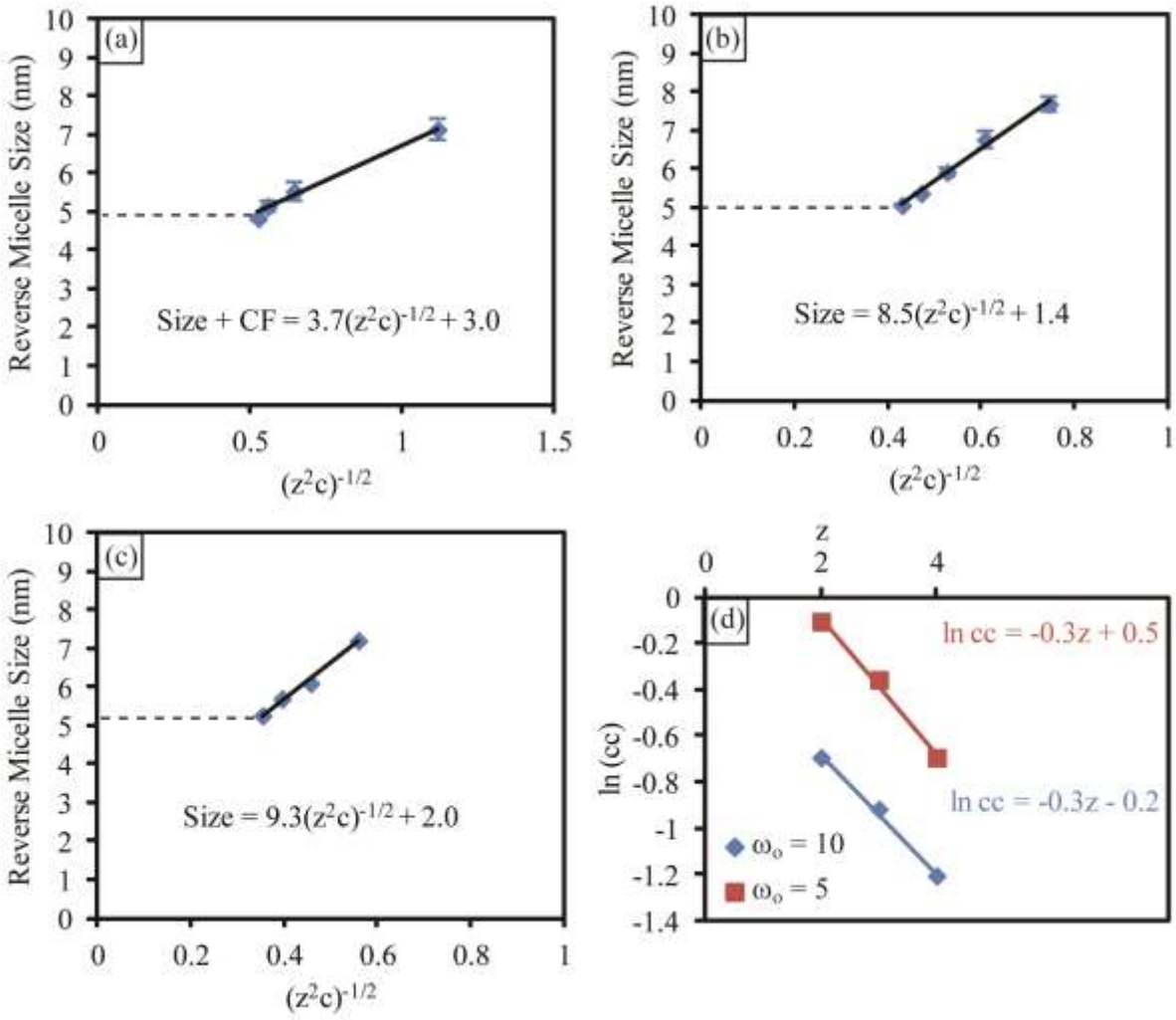

Figure 6 - 3. Average reverse micelle size as a function of the electrical double layer thickness for additions of (a) $Mg(NO_3)_3$, (b) $Al(NO_3)_3$, and (c) $ZrOCl_2$ when $\omega_o = 5$. (d) Comparison of plots used to determine critical potential when $\omega_o = 5$ or $\omega_o = 10$.

The relationship between the electrical double layer thickness and salt concentration when methanol and acetone are substituted for some of the water is

demonstrated in Figure 6-5. When $Mg(NO_3)_3$ was added, the average reverse micelle size is larger when methanol is substituted for water than when acetone is substituted (Figure 6-5a). No significant difference was observed for the average size of the reverse micelles when either methanol or acetone is substituted for water (Figure 6-5b). Opposite behavior was observed in that the average reverse micelle size is larger when acetone is substituted for water than when methanol is substituted (Figure 6-5c). An analysis similar to that presented in Chapter 2 to determine the critical potential at the point of instability is provided in Figure 6-5d. The critical potential did not change at all when acetone was substituted for water, as indicated by the similar slope to the linear fit compared to when no substitution is made. The same is true when divalent or trivalent cations were added to a system with methanol substituted for water. However, a slope transition was observed when $ZrOCl_2$ is added, but the reason is unclear. Similar to changes of ω_o, the intercept of the fitted lines also changes to 0.2 to 0.4 and indicates that the local counterion concentration at the critical potential is 1.2 M and 1.5 M when acetone and methanol were substituted for water, respectively, if divalent or trivalent counterions are added.

Analysis of the slopes for the fitted lines in Figure 6-5a, Figure 6-5b, and Figure 6-5c provides the dielectric constant of the reverse micelle interior phase when methanol and acetone are partially substituted for water and the results are given in Figure 6-6. Unlike when ω_o was changed, there does not appear to be a distinguishable effect of the polar phase substitution on the dielectric constant.

3. Turbidity Measurement of Reverse Micelle Stability

The point of instability is established qualitatively up to this point, by the visual

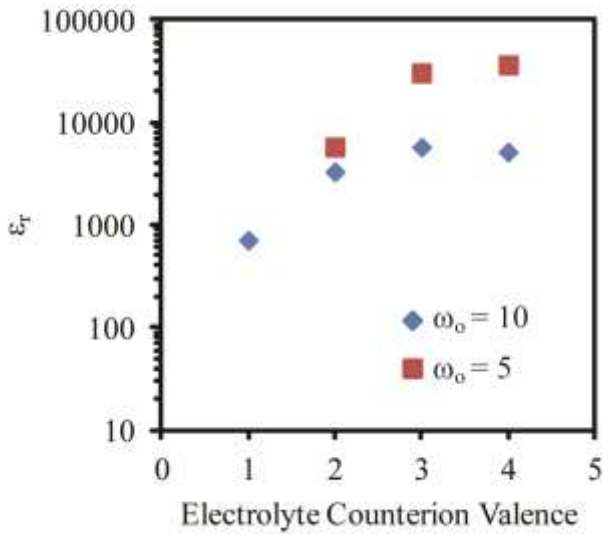

Figure 6 - 4. Comparison between the estimated dielectric constant of the reverse micelle interior with added electrolytes when $\omega_o = 5$ or $\omega_o = 10$.

observation that the solution becomes opaque. However, for systems that destabilize at relatively high electrolyte concentrations (i.e. in the $\omega_o = 5$ and methanol substituted for water in particular), the point of instability is more difficult to capture by eye. The transition to opaque appears more gradually, although coalescence is obvious by close examination. Thus, the use of turbidity measurements to provide a quantitative description that can be used to determine the points of instability is investigated.

The results of the turbidity measurements are given in Figure 6-7. All of the dotted lines in the figure are representative of points of instability determined by visual inspection. The turbidity measurements for the original system, when $\omega_o = 10$ and no substitution of the polar phase, is given in Figure 6-7a. There is an initial decrease in turbidity when increasing salt concentration in the range of stability. This can be understood by the decrease in reverse micelle size causing a decrease in scattering and thus higher optical transparency. At the points of instability, there is an increase in the

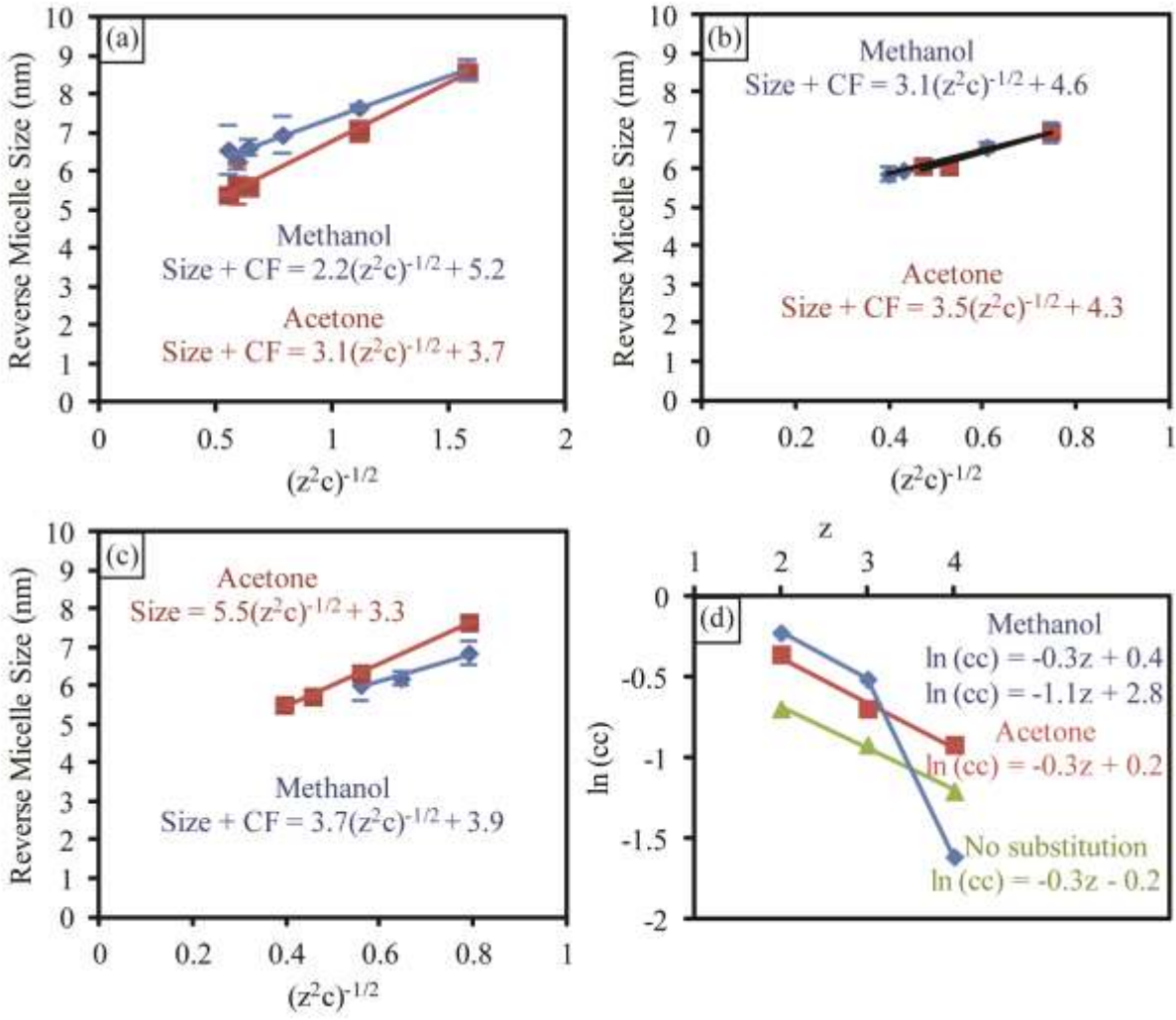

Figure 6 - 5. Average reverse micelle size as a function of the electrical double layer thickness for additions of (a) $Mg(NO_3)_3$, (b) $Al(NO_3)_3$, and (c) $ZrOCl_2$ when methanol or acetone is substituted for water. (d) Comparison of plots used to determine critical potential when substituting methanol or acetone for water.

turbidity caused by scattering of the coalesced phase. Thus, the points of instability can be accurately reproduced with turbidity measurements for the original system. The extent by which the turbidity increased with increasing salt concentration beyond the point of instability depends on the point of instability. As the point of instability increases, the extent that the turbidity increases is suppressed. The turbidity

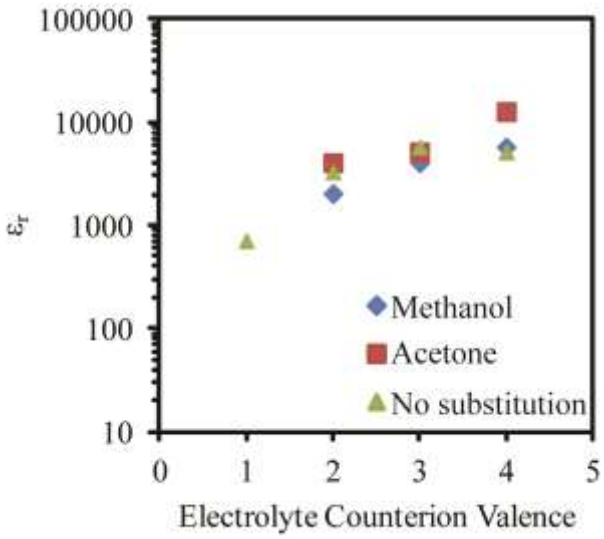

Figure 6 - 6. Estimated dielectric constant of the reverse micelle interior with partial substitution of methanol or acetone for water and without substitution for comparison.

measurements when electrolytes were added to the system having ω_o = 5 are demonstrated in Figure 6-7b. A similar decrease in turbidity was observed with increasing electrolyte addition within the range of stability, as is observed in the system with ω_o = 10. However, the increase in turbidity at the point of instability is subtle enough that it is not accurately represented when $Al(NO_3)_3$ or $ZrOCl_2$ was added to the system with ω_o = 5 because a significant increase in turbidity was not observed. An increase in turbidity was observed at the point of instability when $Mg(NO_3)_3$ was added, but the increase is not significant when considering the variability that was observed for the point of instability in this system. Thus, it appears that turbidity measurements do not capture the point of instability for this system. The point of instability with added electrolyte for the system with methanol substituted for water was reproduced reasonably well, as is demonstrated by Figure 6-7c, but with less significance when $Mg(NO_3)_2$ or

$Al(NO_3)_3$ is added. When acetone is substituted for water, the points are reproduced relatively well by turbidity measurements as is demonstrated by Figure 6-7d. The ease of using turbidity measurements to quantify the point of instability corresponds well with the solubility limit of the salt added. It becomes difficult to distinguish the point of instability for systems with high solubility limits.

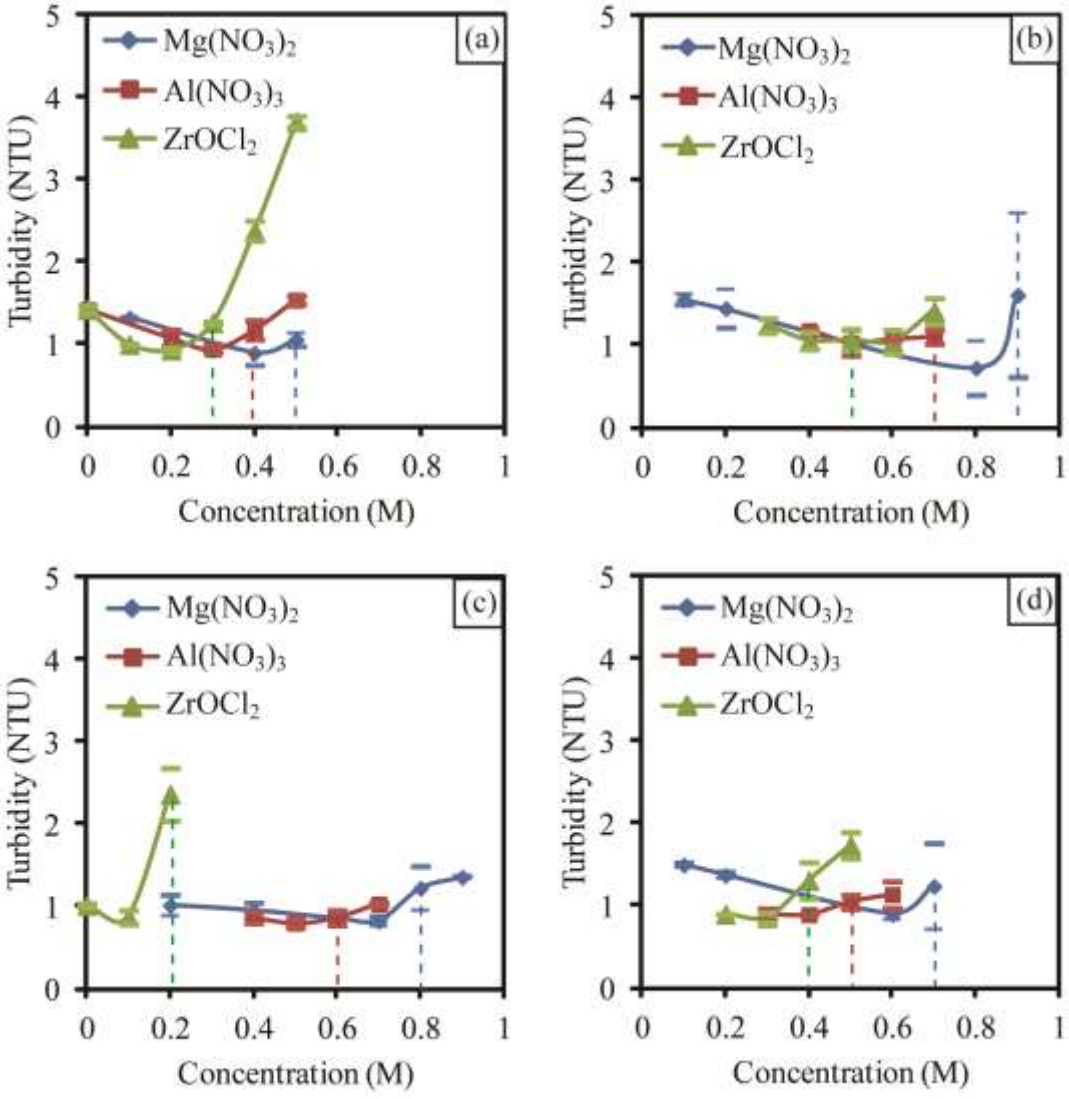

Figure 6 - 7. Turbidity measurements as a function of electrolyte concentration in reverse micellar solutions having (a) $\omega_o = 10$, (b) $\omega_o = 5$, (c) partial substitution of methanol for water, and (d) partial substitution of acetone for water.

4. Precipitation Reactions in the Modified Systems

When precipitation reactions were performed by mixing reverse micellar solutions with 0.05 M NH_4OH and 0.1 M $ZrOCl_2$, the systems with methanol or acetone substituted for water produced unstable solutions. Thus, solution stability after initiating a precipitation reaction was not improved when compared to the system without partial substitution of the polar phase that is presented in Chapter 5. These systems were no longer pursued for precipitation reactions. However, the reverse micellar solution produced with 0.05 M NH_4OH and 0.1 M $ZrOCl_2$ was stable and so this system is investigated further. A stability diagram for precipitation with the ω_o = 5 system is provided in Figure 6-8, assuming that NH_4OH does not contribute to instability within precursor limits. Precipitation reactions using as much as 0.30 M $ZrOCl_2$ could be performed without breaking the microemulsion and is a six-fold increase in $ZrOCl_2$ concentration compared to when precipitation reactions were initiated in the ω_o = 10 system. Furthermore, a greater extent of the stable precursor concentrations were suitable for precipitation reactions overall when compared to the ω_o = 10 system. Thus, decreasing ω_o increases precursor solubility and improves the stability for precipitation reactions.

It is interesting to note that although all of the changes to the reverse micelle interior improved the solubility of precursors in solution compared to the base system with ω_o = 10 (except for the $ZrOCl_2$ system added to methanol), reverse micelle stability when a precipitation reaction was only significantly improved when ω_o was decreased. Similarly, change to the dielectric constant of the reverse micelle interior with added salts was only significantly influenced by ω_o and not by the partial substitution of the polar

phase. While the consequences of dielectric constant on the precipitation are not yet understood, it seems possible that the dielectric constant of the polar phase may have important consequences on precipitation reactions in reverse micelles.

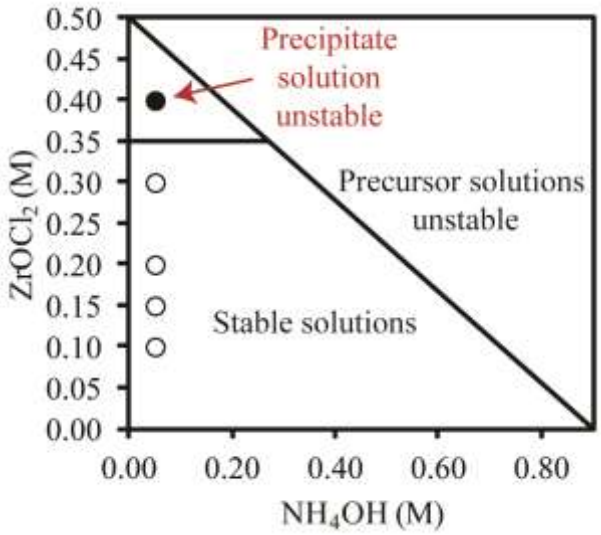

Figure 6 - 8. Stability diagram for obtaining stable solutions when mixing $ZrOCl_2$ and NH_4OH reverse micellar solutions with $\omega_o = 5$.

D. Conclusions

Changing the reverse micelle interior, such as ω_o or substituting other polar solvents for water, influences reverse micelle stability with salt additions and when precipitation reactions are initiated. Even with these changes, the reverse micelle size remains proportional to the electrical double layer thickness when salts are introduced into the modified systems. Even when no salt additions are made, the reverse micelle size changes when varying ω_o and was found to correlate well with the electrical double layer thickness formed by the surfactant counterions. Substituting methanol or acetone

for the polar solvent does not affect the counterion concentration, which may explain why initial substitution did not have a significant effect on the reverse micelle size. However, eventually a transition was observed such that increasing substitution of the solvent does cause a size decrease.

With the exception of the system with $\omega_o = 5$, the points of instability for the other systems can be demonstrated by turbidity measurements. However, the increased turbidity at the point of instability is relatively small and sometimes insignificant so that confidence in the measurements is low. Thus, turbidity measurements are best used as a supplemental technique when assessing the point of instability for a given system and not to be used to determine stability exclusively.

E. References

1. M.-F. Ruasse, I.B. Blagoeva, R. Ciri, L. Carcia-Rio, J.R. Leis, A. Marques, J. Mejuto, and E. Monnier, "Organic Reactions in Micro-organized Media: Why and How?" *Pure Appl. Chem.*, **69** [9] 1923-32 (1997).

2. N.E. Levinger and L.A. Swafford, "Ultrafast Dynamics in Reverse Micelles," *Annu. Rev. Phys. Chem.* **60**, 385-406 (2009).

3. L. Motte, C. Petit, L. Boulanger, P. Lixon, and M.P. Pileni, "Synthesis of Cadmium Sulfide in Situ in Cadmium Bis(ethyl-2-hexyl) Sulfosuccinate Reverse Micelle: Polydispersity and Photochemical Reaction," *Langmuir*, **8** [4] 1049-53 (1992).

4. M.P. Pileni, I. Lisiecki, L. Motte, C. Petit, J. Cizeron, N. Moumen, and P. Lixon, "Synthesis "In Situ" of Nanoparticles in Reverse Micelles," *Prog. Colloid Polym. Sci.*, **93**, 1-9 (1993).

5. J.H. Fendler, "Atomic and Molecular Clusters in Membrane Mimetic Chemistry," *Chem. Rev.*, **87** [5] 877-99 (1987).

6. R. Biswas, T. Chakraborti, B. Bagchi, and K.G. Ayappa, "Non-monotonic, Distance-dependent Relaxation of Water in Reverse Micelles: Propagation of Surface Induced Frustration along Hydorgen Bond Networks," *J. Chem. Phys.*, **137** [1] 014515 9pp. (2012).

7. B. Bagchi, “From Anomalies in Neat Liquid to Structure, Dynamics and Function in the Biological World,” *Chem. Phys. Lett.,* **529**, 1-9 (2012).

8. R. Pramanik, S. Sarkar, C. Ghatak, V.G. Rao, and N. Sarkar, “Solvent and Rotational Relaxation Study in Ionic Liquid Containing Reverse Micellar System: A Picosecond Fluorescence Spectroscopy Study,” *Chem. Phys. Lett.,* **512** [4] 217-22 (2011).

9. C.F. Sailer, R.B. Singh, J. Ammer, E. Riedle, and I. Pugliesi, “Encapsulation of Diphenylmethyl Phosphonium Salts in Reverse Micelles: Enhanced Bimolecular Reaction of the Photofragments,” *Chem. Phys. Lett.,* **512** [1-3] 60-5 (2011).

10. B.H. Robinson, “Colloid Chemistry: Applications of Microemulsions,” *Nature*, **320** [6060] 309 (1986).

11. R.D. Falcone, J.J. Silber, and N.M. Correa, “What are the Factors that Control Non-aqueous/AOT/n-heptane Reverse Micelle Sizes? A Dynamic Light Scattering Study,” *Phys. Chem. Chem. Phys.,* **11** [47] 11096-100 (2009).

12. H. Fathi, J.P. Kelly, V.R. Vasquez, and O.A. Graeve, “Ionic Concentration Effects on Reverse Micelle Size and Stability: Implications for the Synthesis of Nanoparticles,” *Langmuir,* **28** [25] 9267-74 (2012).

13. R. Alargova, J. Petkov, D. Petsev, I.B. Ivanov, G. Broze, and A. Mehreteab, “Light Scattering Study of Sodium Dodecyl Polyoxyethylene-2-sulfate Micelles in the Presence of Multivalent Counterions,” *Langmuir,* **11** [5] 1530-6 (1995).

14. J. Sjöblom, R. Lindberg, and S.E. Friberg, “Microemulsions – Phase Equilibria Characterization, Structures, Applications and Chemical Reactions,” *Adv. Colloid Interface Sci.,* **65**, 125-287 (1996).

15. J.C. Owrutsky, M.B. Promfret, D.J. Barton, and D.A. Kidwell, “Fourier Transform Infrared Spectroscopy of Azide and Cyanate Ion Pairs in AOT Reverse Micelles,” *J. Chem. Phys.,* **129** [2] 024513 10pp. (2008).

16. I. Lisiecki and M.P. Pileni, “Synthesis of Copper Metallic Clusters Using Reverse Micelles as Microreactors,” *J. Am. Chem. Soc.,* **115** [10] 3887-96 (1993).

17. A. Nanni and L. Dei, “$Ca(OH)_2$ Nanoparticles from W/O Microemulsions,” *Langmuir*, **19** [3] 933-8 (2003).

18. J. Eastoe, M.J. Hollamby, and L. Hudson, “Recent Advances in Nanoparticle Synthesis with Reversed Micelles,” *Adv. Colloid Interface Sci.,* **128-130**, 5-15 (2006).

19. O.A. Graeve, H. Fathi, J.P. Kelly, M.S. Saterlie, K. Sinha, G. Rojas-George, R. Kanakala, D.R. Brown, and E.A. Lopez, "Reverse Micelle Synthesis of Oxide Nanopowders: Mechanisms of Precipitate Formation and Agglomeration Effects," *J. Colloid Interface Sci.*, **407**, 302-9 (2013).

20. J. Tanori, N. Duxin, C. Petit, I. Lisiecki, P. Veillet, and M.P. Pileni, "Synthesis of Nanosize Metallic and Alloyed Particles in Ordered Phases," *Colloid Polym. Sci.*, **273** [9] 886-92 (1995).

21. M.P. Pileni, J. Tanori, and A. Filankembo, "Biomimetic Strategies for the Control of Size, Shape and Self-organization of Nanoparticles," *Colloids Surf., A*, **123-124**, 561-73 (1997).

22. P. Setua, R. Pramanik, S. Sarkar, C. Ghatak, V.G. Rao, N. Sarkar, and S.K. Das, "Synthesis of Silver Nanoparticle in Imidazolium and Pyrolidium Based Ionic Liquid Reverse Micelles: A Step Forward in Nanostructure Inorganic Material in Room Temperature Ionic Liquid Field," *J. Mol. Liq.*, **162** [1] 33-7 (2011).

23. P. Setua, A. Chakraborty, D. Seth, M.U. Bhatta, P.V. Satyam, and N. Sarkar, "Synthesis, Optical Properties, and Surface Enhanced Raman Scattering of Silver Nanoparticles in Nonaqueous Methanol Reverse Micelles," *J. Phys. Chem. C*, **111** [10] 3901-7 (2007).

24. S. Bas, U. Chatterjee, and M.D. Soucek, "Synthesis of Amphphilic Triblock Copolymers for the Formation of Magnesium Fluoride (MgF_2) Nanoparticles," *J. Appl. Polym. Sci.*, **126** [1] 998-1007 (2012).

25. F. Venditti, R. Angelico, G. Palazzo, G. Colafemmina, A. Ceglie, and F. Lopez, "Preparation of Nanosize Silica in Reverse Micelles: Ethanol Produced during TEOS Hydrolysis Affects the Microemulsion Structure," *Langmuir*, **23** [20] 10063-8 (2007).

26. T. Kinugasa, A. Konodo, S. Nishimura, Y. Miyauchi, Y. Nishii, K. Watanabe, and H. Takeuchi, "Estimation for Size of Reverse Micelles Formed by AOT and SDEHP Based on Viscosity Measurement," *Colloids Surf., A*, **204** [1-3] 193-9 (2002).

27. M.P. Pileni, "Reverse Micelles as Microreactors," *J. Phys. Chem.*, **97** [27] 6961-73 (1993).

28. X. Li, C.-K. Loong, P. Thiyagarajan, G.A. Lager, and R. Miranda, "Small-angle Neutron Scattering Study of Nanophase Zirconia in a Reverse Micelle Synthesis," *J. Appl. Cryst.*, **33** [1] 628-31 (2000).

29. A.P. Herrera, O. Resto, J.G. Briano, and C. Rinaldi, “Synthesis and Agglomeration of Gold Nanoparticles in Reverse Micelles,” *Nanotechnology*, **16** [7] S618-25 (2005).

30. A. Gardner, V.R. Vásquez, A. Clifton, and O.A. Graeve, “Molecular Dynamics Analysis of the AOT/Water/Isooctane System: Effect of Simulation Time, Initial Configuration, and Model Salts,” *Fluid Phase Equilib.*, **262** [1-2] 264-70 (2007).

31. M. Ghiaci, H. Aghaei, and A. Abbaspur, “Size-controlled Synthesis of ZrO_2-TiO_2 Nanoparticles Prepared via Reverse Micelle Method Investigation of Particle Size Effect on the Catalytic Performance in Vapor Phase Beckmann Rearrangment,” *Mater. Res. Bull.*, **43** [5] 1255-62 (2008).

32. P. He, X. Wang, Y. Liu, L. Yi, and X. Liu, “Reverse Micelle Synthesis of AuNi Alloy as Electrocatalyst of Borohydride Oxidation,” *Int. J. Hydrogen Energy*, **37** [2] 1254-62 (2012).

33. V.R. Vasquez, B.C. Williams, and O.A. Graeve, “Stability and Comparative Analysis of AOT/Water/Isooctane Reverse Micelle System Using Dynamic Light Scattering and Molecular Dynamics,” *J. Phys. Chem. B*, **115** [12] 2979-87 (2011).

34. A.M. Howe, C. toprakcioglu, J.C. Dore, and B.H. Robinson, “Small-angle Neutron Scattering Studies of Microemulsions Stabilized by Aerosol-OT. Part 3. – The Effect of Additives on Phase Stability and Droplet Structure,” *J. Chem. Soc., Faraday Trans.*, **82** [8] 2411-22 (1986).

35. E. Caponetti, A. Lizzio, R. Triolo, W.L. Griffith, and J.S. Johnson, Jr., “Alcohol Partition in a Water-in-oil Microemulsion from Small-angle Neutron Scattering,” *Langmuir*, **8** [6] 1554-62 (1992).

36. E. Bardez, R. Giordano, M.P. Jannelli, P. Migliardo, and U. Wanderlingh, “Hydrogen-bond Effects Induced by Alcohol on the Structure and Dynamics of Ionic Reverse Micelles,” *J. Mol. Struct.*, **383** [1-3] 183-90 (1996).

37. S. Perez-Casas, R. Castillo, and M. Costas, “Effect of Alcohols in AOT Reverse Micelles. A Heat Capacity and Light Scattering Study,” *J. Phys. Chem. B*, **101** [36] 7043-54 (1997).

CHAPTER 7: THE EFFECT OF COSURFACTANTS ON REVERSE MICELLE SIZE, REVERSE MICELLE STABILITY, AND PRECIPITATION OF ZIRCONIUM HYDROXIDE IN THE WATER-AOT-ISOOCTANE SYSTEM

A. Introduction

The stability of reverse micelles when adding electrolyte precursors and after a precipitation reaction is of great interest for encapsulating molecules and nanomaterials. The surfactant and any cosurfactants that are used can have important consequences on reverse micelle stability. Boutonnet *et al*, who provided the first known example of nanoparticles synthesis in reverse micelles, recognized that low water concentration and long-chain alcohol cosurfactants were most suitable for forming stable reverse micelle structures before any manipulations are performed.[1] The importance of low water concentration for forming stable reverse micelles during encapsulation of electrolyte precursors or precipitates was demonstrated in Chapter 6, but the effects of cosurfactants for encapsulation are not yet studied according to the concepts developed in this thesis.

The common use of AOT as a surfactant by other researchers is because a cosurfactant is not necessary to form stable reverse micelles, which is useful from a fundamental perspective.[2] However, it can be beneficial to add a cosurfactant even to reverse micelles formed by AOT, not because a cosurfactant is necessary for forming stable reverse micelle structures, but for the effect that cosurfactant can have on stability overall. For example, Darab *et al.* reported enhanced salt solubility in reverse micelles when sodium dodecyl sulfate was added as a cosurfactant with AOT.[3] Nonionic cosurfactants added to AOT increased the solubilization of NaCl in reverse micelles and the maximum solubilization occured for different salt concentrations depending on the type of cosurfactant that was added.[4,5] In another example, Lee *et al.* demonstrated that

nonionic cosurfactants influenced the percolation threshold of AOT reverse micelles.[6] Even mixtures of very similar surfactants, differing only in the structure of the hydrophobic tail, can have significant consequences on structure and stability of reverse micelles.[7]

Introducing cosurfactant adds complexity to the system. For example, nonionic surfactants have a tendency to partition between the water-oil interfaces to the oil, unlike ionic surfactants, and the composition of the droplets begins to depend on dilution of the reverse micelles in the bulk oil phase.[2] Partitioning between the water-oil interface and the polar phase was also observed for cosurfactants with short chain lengths.[8] Short chain alcohols prefer to partition to the polar phase, medium chain alcohols prefer the water-oil interface, and long chain alcohols have a tendency to partition to the bulk oil phase. Methanol and ethanol partition mainly to the water phase for AOT reverse micelles, but also associate increasingly with surfactant molecules at lower water-to-surfactant ratio (ω_o), while butanol and longer linear and branched alcohol molecules partition to the surfactant interface and oil phase.[9] Pentanol resides primarily at the water-oil interface when AOT is the primary surfactant.[10] It is also reasonable to assume that cationic-anionic surfactants can form complexes that partition between the reverse micelle interface and the oil phase. Multiple reverse micelle populations can also exist, having different surfactant chemistries that depend on ω_o.[11,12]

The type of surfactant and cosurfactants have been found to alter the exchange of material between reverse micelles and therefore particle nucleation and growth kinetics.[4,13-16] This can be understood from the perspective of changes to the interfacial rigidity, with cosurfactants decreasing rigidity and increasing the droplet exchange rate or

increasing rigidity and decreasing the exchange rate.[17,18] The nucleation and growth kinetics affect particle size, which may influence the stability of a reverse micelle containing a particle.

Surfactants or cosurfactants can bind to the surface of encapsulated molecules or particles and provide stabilization of the precipitate or arrest further particle growth, depending on the nature of the interaction.[19] The addition of a cosurfactant can provide stabilization of encapsulated molecules and particles or arrest particle growth when the primary surfactant fails.[20,21] Preferred absorption of surfactant or cosurfactant onto particle surfaces and changing relative quantities of each has also be used to influence the morphology of precipitates.[22,23] Sarda *et al.* found that the type of surfactant alters the chemistry of calcium phosphate formed in reverse micellar structures.[24] Amorophous tricalcium phosphate gel had to be crystallized into apatite when using a non-ionic surfactant, but crystalline precipitates were directly formed when using AOT as the surfactant. The interaction between surfactant molecules and a precipitate were thought to control crystallization and morphology due to the ordered array of the surfactant molecules and by preferential adsorption onto particle surfaces, respectively.

Here, the importance of cosurfactants was tested to determine the consequences that cosurfactants have on encapsulating electrolyte precursors and precipitates according to the concepts that were developed throughout this thesis. Various cationic and nonionic surfactants were substituted for AOT and the resulting reverse micelle sizes were characterized. $Mg(NO_3)_2$, $Al(NO_3)_3$, and $ZrOCl_2$ were added to the base system to study the effects of salt concentration on reverse micelle size, stability, the critical potential of overlapping electrical double layers at the point of instability, the polarity of the reverse

micelle interior, and the stability diagram for precipitation of zirconium hydroxide by mixing two reverse micellar solutions containing either NH_4OH or $ZrOCl_2$.

B. Experimental Methods

The preparation procedure for the reverse micellar solutions is similar to that presented in Chapter 2, Chapter 4, and Chapter 5. However, the difference is that solutions were prepared with partial substitution of cationic surfactant or nonionic surfactants for AOT. To study the base systems, without electrolyte additions, the amount of surfactant substituted was systematically varied. Cationic surfactant substitutions were made in amounts of 0.01, 0.05, 0.10, 0.50, 1.0 and 5.0 mole percent using either cetyltrimethylammonium bromide/CTAB (high purity grade, Amresco, Solon, OH), benzyltrimethylammonium/BTA, metacholine chloride/MCC, or choline chloride/CC. Nonionic surfactant substitutions were made in amounts of 1, 5, 10, and 20 mole percent using either undecanol/UD or isopropanol/IP. Besides surfactant substitutions, all other quantities were held constant according to the previous work, including the amounts of salts that were added.

The additions of salts were made to systems with 1% cationic surfactant substitution with CTAB or CC and to systems with 10% nonionic surfactant substitution of either UD or IP. Thus, to prepare one mole percent cationic surfactant substitutions, either 0.073 g of CTAB or 0.028 CC was added in addition to the reduced AOT amount of 8.802 g and to prepare ten mole percent nonionic surfactant substitutions, either 0.345 g of UD or 0.120 g of IP was added in addition the reduced AOT amount of 8.002 g.

Precipitation experiments were also performed. Previous precipitation reactions in the base system indicated that the stability of the reverse micelles is affected by the

amount of $ZrOCl_2$ used for the precipitation reaction (see Chapter 5). Amounts of 0.1 M $ZrOCl_2$ or more produced solutions that were not stable in the base system, as was noted by the turbid appearance of the solutions. The purpose of the precipitation reactions in this work was to determine if the surfactant substitutions can stabilize previously unstable reverse micellar solutions after the precipitation reaction is initiated. The precipitation reactions were done according to the procedure given in Chapter 5.

Dynamic light scattering measurements were performed on either a Nanotrac ULTRA instrument (Microtrac, Montgomeryville, PA) or a Nanotrac Wave DLS instrument (Microtrac, Montgomeryville, PA) according to procedures previously developed.[25] Where convenient, to make direct comparisons when using the two different devices, a correction factor for using the Nanotrac Wave DLS was used and pointed out in the appropriate plots by the addition of a correlation factor (CF) to the measured size. Turbidity measurements were made on a turbidity meter (Model 2020, LaMotte Chemical Products Company, Chestertown, MD) to compare to the points of instability of the solutions when electrolytes were added. The turbidity measurements consisted of an average of five readings and five of these measurements were made. All characterization was performed for two experiments.

C. Results and Discussion

1. Reverse Micelle Sizes with Cosurfactant Substitution

The average reverse micelle size when different cationic surfactants are substituted for AOT is given in Figure 7-1a. All of the cationic surfactants cause a decrease in the average reverse micelle size when substituted for AOT and there is not a significant difference in the extent of the decrease. The size decrease is most likely

caused by a decrease in the surface charge density as a result of electrostatic screening. Reduced surface charge density also reduces the potential of the electrical double layers. If the critical potential is assumed to be constant, as it is for all modifications made so far, then the electrical double layers inside of the reverse micelle would be allowed to move into closer proximity to achieve the extent of overlap necessary for the critical potential, which is depicted in Figure 7-1b. It is difficult to define the relationship between the average reverse micelle size and the amount of cationic surfactant substituted because the resulting surface charge density depends on both variables as well as the counterion concentration, which is also changing. However, the assumption that the critical potential is constant can be tested and was evaluated when electrolytes were added to these systems.

The average reverse micelle size when nonionic surfactant is substituted for AOT is demonstrated in Figure 7-2. A decrease in reverse micelle size with substitution of undecanol occurs for substitutions as high as 20%, which can be explained in the same way for the reduction in reverse micelle size when cationic surfactants are substituted for AOT, by the mechanism depicted in Figure 7-1b. A decrease in average reverse micelle size was also observed with an initial substitution of isopropanol for AOT. However, no further reduction in reverse micelle size was observed when more than 5% isopropanol was added. Isopropanol is an alcohol with a relatively short chain length so partitioning between the water-oil interface and the water core is possible.[8] Alternatively, nonionic surfactants are known to partition between the water-oil interfaces to the oil, unlike ionic surfactants.[2] However, free surfactant was not observed during the DLS measurements, so partitioning into the water phase is more likely. Thus, it is estimated that up to 5% of

isopropanol can be substituted for AOT and any additional isopropanol will cause some isopropanol to be displaced from the interface such that the average reverse micelles size no longer varies.

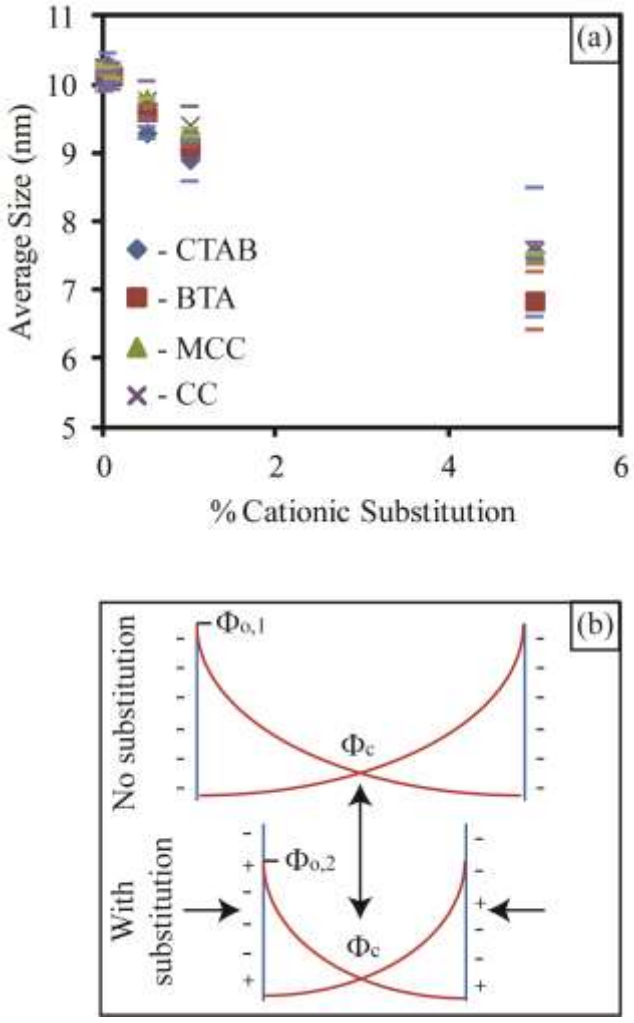

Figure 7 - 1. (a) Average reverse micelle size when AOT is partially replaced by cationic surfactants and (b) schematic demonstrating the mechanism for reverse micelle shrinkage.

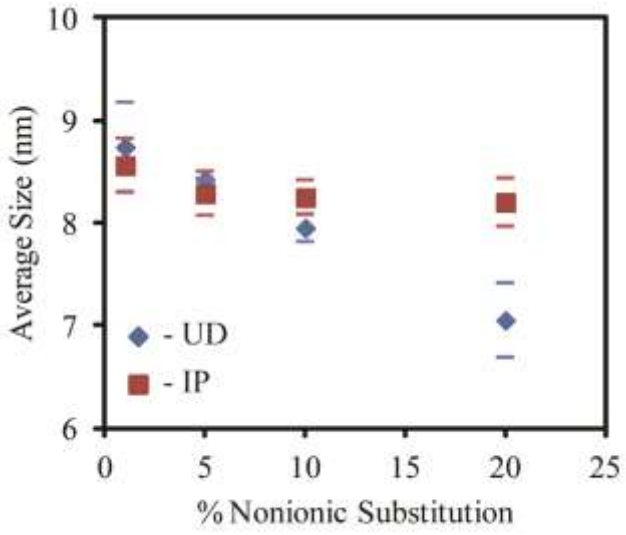

Figure 7 - 2. Average reverse micelle size measured with Nanotrac Wave DLS when AOT is partially replaced by anionic surfactants.

2. Effect of Electrolytes in Systems with Cosurfactant Substitutions

The average reverse micelle size remains proportional to the electrical double layer thickness when adding salts to the systems modified by substituting cationic surfactants for AOT. This is demonstrated by the linear trends in Figure 7-3a, Figure 7-3c, and Figure 7-3e, when adding $Mg(NO_3)_2$, $Al(NO_3)_3$, and $ZrOCl_2$, respectively. The slopes and intercept for the linear fits to the size data are slightly different when substituting CTAB versus CC for AOT. The slope when adding $Mg(NO_3)_2$ is greater in the CC system than it is in the CTAB system, but the opposite is observed when adding $Al(NO_3)_3$. The slope when adding $ZrOCl_2$ is greater for CC again, suggesting that the difference is within typical variability and most likely associated with measurement and experimental error. The same is true for the intercept of the linear fits to the data. The points of instability when adding these salts are also provided in Figure 7-3, along with turbidity measurements, which are 0.4, 0.3, and 0.2 M, respectively. Thus, the

substitution of cationic surfactants for AOT reduces the point of instability when compared to the base system. This is true of long-chained surfactants such as CTAB and short-chained surfactants such as CC. However, the destabilization when CC is substituted was more gradual than when CTAB is substituted and is more generally difficult to distinguish. As such, turbidity measurements do not capture the point of instability very well when $ZrOCl_2$ was added and is demonstrated in Figure 7-3f. The solutions do not appear turbid when 0.2 M $ZrOCl_2$ was added, but evidence of destabilization can clearly be established visually. The plot used to establish the critical potential is given in Figure 7-4 and the base system, without cationic surfactant substitution, is also provided. The identical slopes, within experimental error, indicate that the critical potential does not significantly change when 1% cationic surfactant is substituted for AOT and validates the assumption used to describe the decrease in average reverse micelle size when substituting cationic surfactant according to the mechanism described by Figure 7-1. The intercept of the linear fit used to determine the critical potential also did not vary significantly.

The average reverse micelle sizes and results from turbidity measurements when nonionic surfactant was substituted for AOT are demonstrated in Figure 7-5. Figure 7-5a, Figure 7-5c, and Figure 7-5d indicate that the average reverse micelle size remains proportional to the EDL thickness when adding electrolytes to the systems modified by substitution of anionic surfactants for AOT. The slope to the linear fits is lower when substituting UD instead of IP for AOT. The intercepts to the fit are similar, except when $Mg(NO)_2$ was added. In general, the systems with $Mg(NO_3)_2$ were anomalous. For example, the turbidity captured the points of instability for $Al(NO_3)_3$ and $ZrOCl_2$ salts

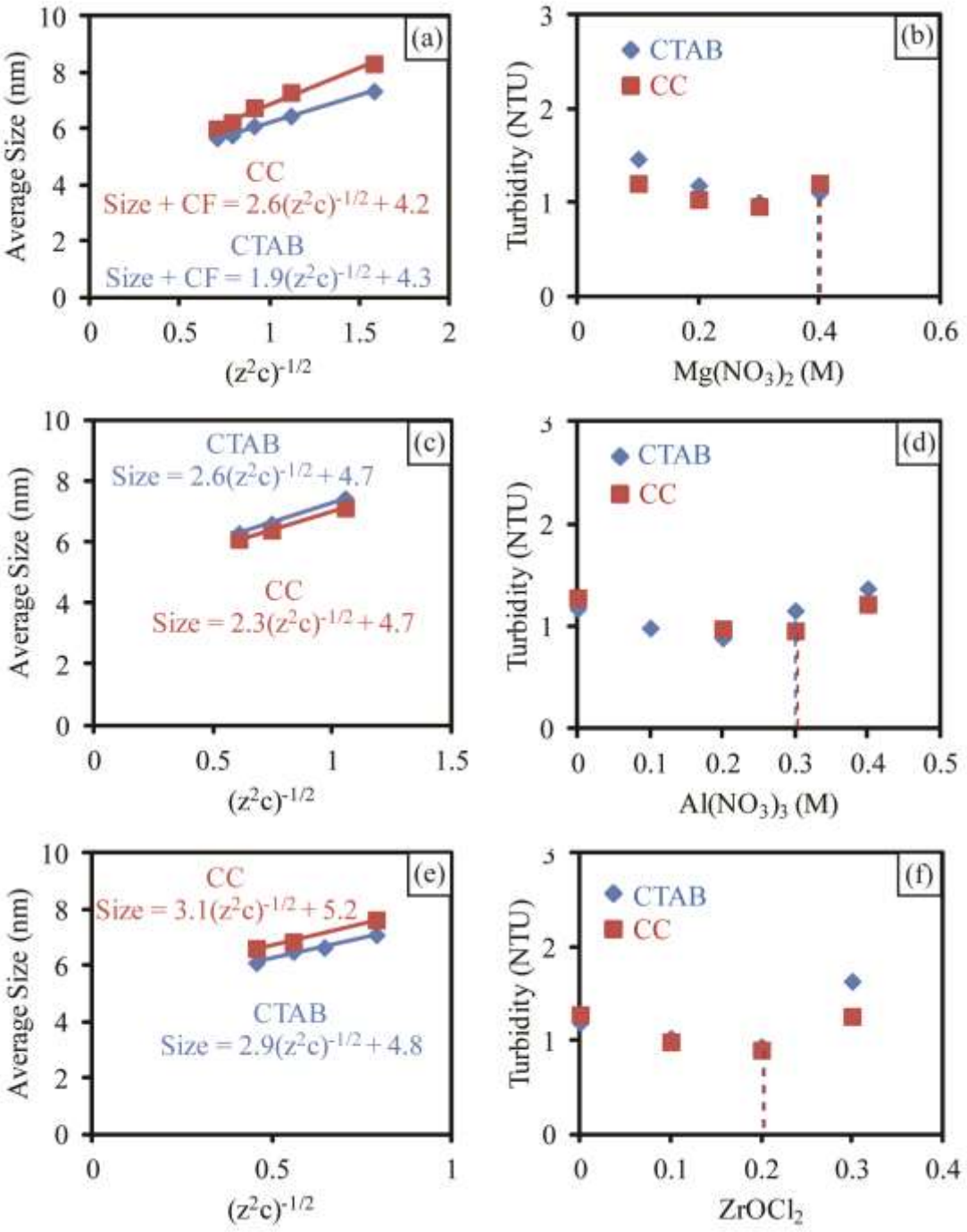

Figure 7 - 3. (a) Average reverse micelle size and (b) turbidity with addition of $Mg(NO_3)_2$, (c) average reverse micelle size and (d) turbidity with addition of $Al(NO_3)_3$, and (e) average reverse micelle size and (f) turbidity with $ZrOCl_2$ when cationic surfactants are partially substituted for AOT.

well, as demonstrated in Figure 7-5d and Figure 7-5f, but not very well for $Mg(NO_3)_2$, which is demonstrated in Figure 7-5b. The points of instability when susbstituting IP for AOT were 0.5, 0.4, and 0.3 M for $Mg(NO_3)_2$, $Al(NO_3)_3$, and $ZrOCl_2$, respectively, and were similar to the system without nonionic surfactant substitution. However, the points of instability were reduced when substituting UD for AOT. The destabilization is also more gradual when substituting IP than when substituting UD and can be demonstrated by the turbidity measurements in Figure 7-5d and Figure 7-5f, for example.

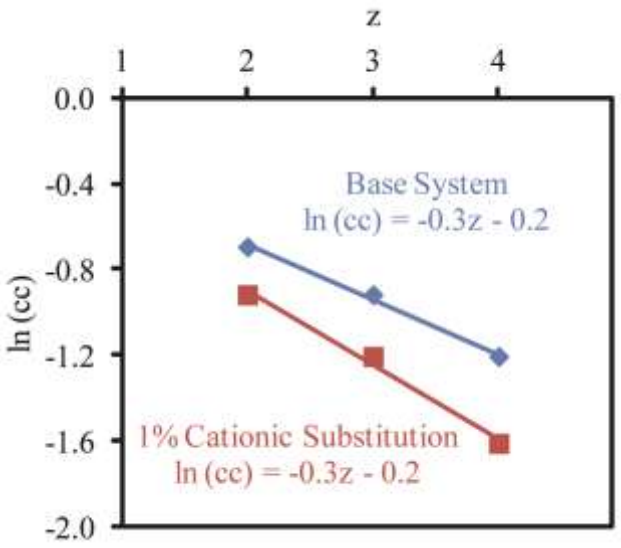

Figure 7 - 4. Plot used to determine critical potential from the counterion valence and critical concentration (point of instability, cc) with and without 1% cationic surfactant substituted for AOT.

The plot used to determine the critical potential when substituting nonionic surfactants for AOT is given in Figure 7-6. Since the points of instability are the same when substituting IP for AOT as they are for the base system, the slope of the fit demonstrated in Figure 7-6 is identical to that of the base system and is demonstrated by comparing to the fit given in Figure 7-4. The similar slope indicates that the critical

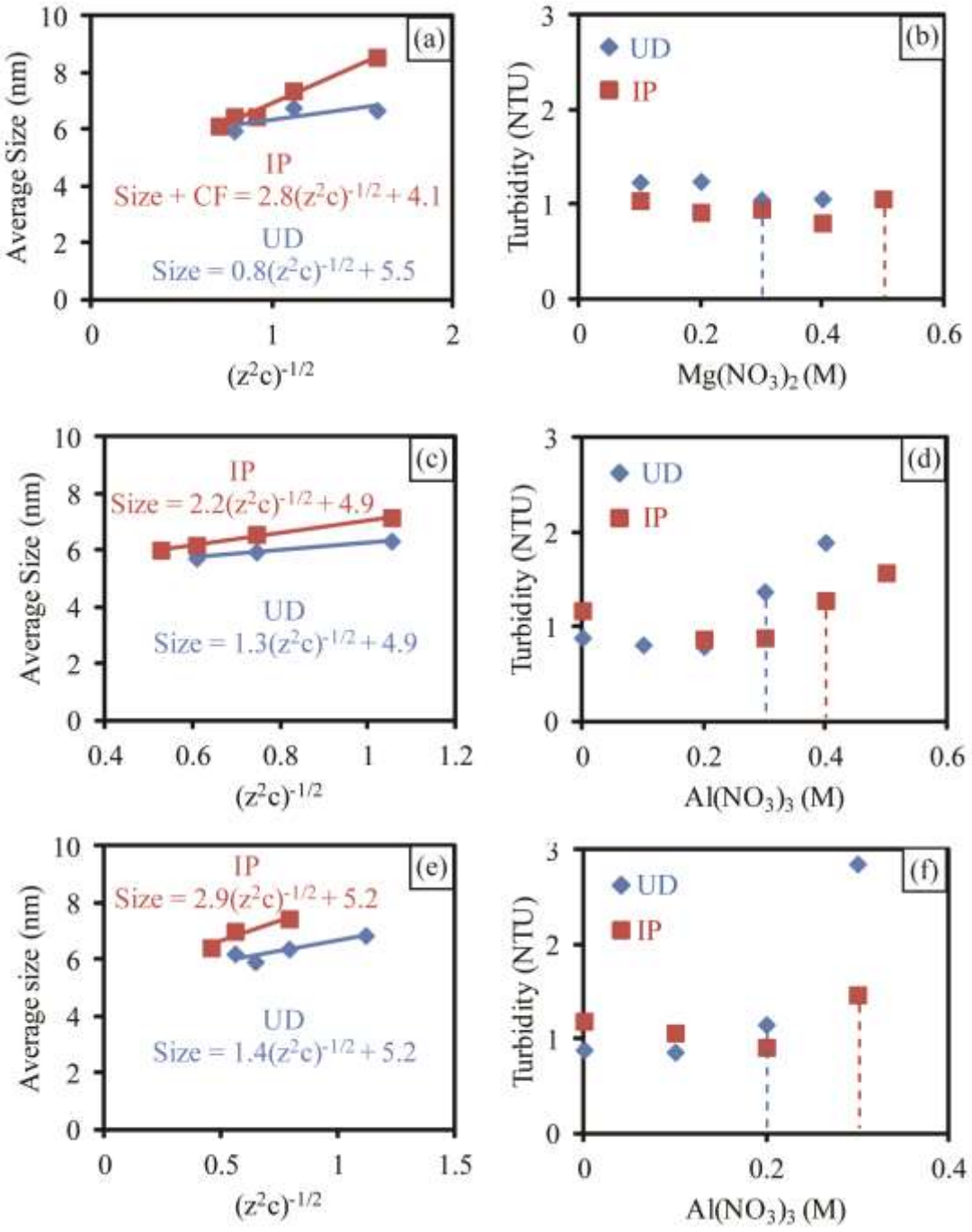

Figure 7 - 5. (a) Average reverse micelle size and (b) turbidity with addition of $Mg(NO_3)_2$, (c) average reverse micelle size and (d) turbidity with addition of $Al(NO_3)_3$, and (e) average reverse micelle size and (f) turbidity with $ZrOCl_2$ when nonionic surfactants are partially substituted for AOT.

potential does not change. When substituting UD for AOT, the slope also does not change signficantly. The appearance of a slight difference can be associated with too large of a step size, but is within experimental error. The intercept is also similar when substituting UD for AOT, but this can again be an artifact of the step size and associated error because the slope is expected to be lower if the slope and thus critical potential do not change.

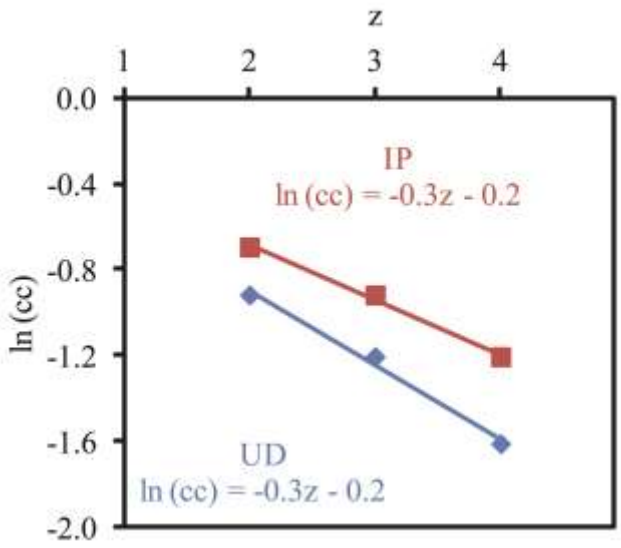

Figure 7 - 6. Plot used to determine critical potential from the counterion valence and critical concentration (point of instability, cc) with 10% nonionic surfactant substituted for AOT. The open symbols and black dotted line demonstrate potential error.

The slopes from the fitted data in Figure 7-3 and Figure 7-5 were used to estimate the dielectric constant of the electrolyte containing polar phase when either cationic or anionic surfactants was substituted for AOT and compared to the base system. The results of these calculations are given in Figure 7-7. Figure 7-7a demonstrates that substitution of 1% cationic surfactant for AOT did not have a significant effect on the estimated dielectric constant. The same is true when isopropanol was added as a

cosurfactant by susbstituting 10% for AOT. However, the addition of 10% UD significantly reduced the dielectric constant of the polar phase, by approximately one order of magnitude.

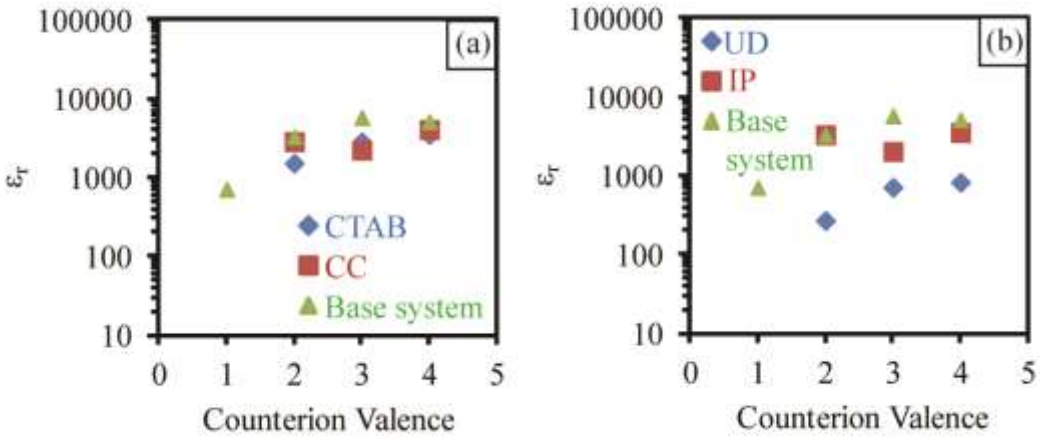

Figure 7 - 7. Estimated dielectric constant of the reverse micelle interior phase with partial substitution of (a) cationic surfactant or (b) nonionic surfactant for AOT.

3. Stability of Systems with Cosurfactant Substitutions for a Precipitation Reaction

Precipitation experiments were performed in the modified systems by mixing reverse micelle solutions containing either 0.10 M $ZrOCl_2$ or 0.05 M NH_4OH. The mixed solutions in all modified systems were unstable and indicate that the stability of the reverse micelles with precipitates is not improved when compared to the base system. Thus, precipitation experiments are not explored any further. This can be expected from the estimated dielectric constant of the reverse micelle interior, which was either similar to the base system or lower, if it is assumed to be a defining parameter for controlling reaction kinetics. The stability of reverse micelles once a precipitation reaction is

initiated was only improved by reducing the water to surfactant ratio, which resulted in an increase in the estimated dielectric constant (see Chapter 6).

D. Conclusions

The use of a cosurfactant in addition to AOT, either cationic or anionic, results in a decrease in the average reverse micelle size. A mechanism was proposed based on the concept of electrical double layers as they relate to reverse micelles containing electrolyte. More specifically, the cosurfactant screens electrostatic interactions and decreases the surface charge density of the surfactant containing interfacial layer and results in a reduced surface potential. The reduced surface potential also reduces the potential at any distance away from the interfacial film, in the electrical double layer, and allows the two overlapping electrical double layers to move into closer proximity to each other. The net result is a decrease in the average reverse micelle size. The reduction in size is limited when substituting IP for AOT and is believed to be because the IP partitions between the reverse micelle interface and interior.

When increasing salt concentration in the modified reverse micellar systems, the average reverse micelle size remains proportional to the electrical double layer. Besides IP, which has identical points of instability when compared to the base system, all other cosurfactants resulted in a decrease in the point of instability. Even with the reduced salt solubility, the points of instability with different electrolytes are such that the critical potential developed between the overlapping electrical double layers remains constant when making the cosurfactant substitutions, which further supports the proposed size change mechanism when making cosurfactant substitutions.

In addition to reducing stability with electrolyte additions, the cosurfactants also do not improve reverse micelle stability when initiating a precipitation reaction by mixing two reverse micellar solutions containing either $ZrOCl_2$ or NH_4OH. Including observations from Chapter 6, it is proposed that the estimated dielectric constant might control reaction kinetics in reverse micellar media and therefore reverse micelle stability during a precipitation reaction.

E. References

1. M. Boutonnet, J. Kizlin, P. Stenius, "The Preparation of Monodisperse Colloidal Metal Particles from Microemulsions," *Colloids Surf.,* **5** [3] 209-25 (1982).

2. P.D.I. Fletcher, A.M. Howe, and B.H. Robinson, "The Kinetics of Solubilisate Exchange between Water Droplets of a Water-in-oil Microemulsion," *J. Chem. Soc., Faraday Trans. 1,* **83** [4] 985-1006 (1987).

3. J.G. Darab, D.M. Pfund, J.L. Fulton, J.C. Linehan, M. Capel, and Y. Ma, "Characterization of a Water-in-oil Microemulsion Containing a Concentrated Ammonium Ferric Sulfate Aqueous Phase," *Langmuir,* **10** [1] 135-41 (1994).

4. D. Liu, J. Ma, H. Cheng, and Z. Zhao, "Solubilization Behavior of Mixed Reverse Micelles: Effect of Surfactant Component, Electrolyte Concentration, and Solvent," *Colloids Surf., A,* **143** [1] 59-68 (1998).

5. R.K. Mitra and B.K. Paul, "Effect of NaCl and Temperature on the Water Solubilization Behavior of AOT/Nonionics Mixed Reverse Micellar Systems Stabilized in IPM Oil," *Colloids Surf., A,* **255** [1-3] 165-80 (2005).

6. B.-K. Lee, D.-P. Hong, S.-S. Lee, and R. Kuboi, "Evaluation of Carboxylic Acid-induced Formation of Reverse Micelle Clusters: Comparison of the Effects of Alcohols on Reverse Micelles," *Biochem. Eng. J.,* **21** [1] 11-8 (2004).

7. A. Kljajić, M. Bešter-Rogač, S. Trošt, R. Zupet, and S. Pejovnik, "Characterization of Water/Sodium bis(2-ethylhexyl) Sulfosuccinate/Sodium Bis(Amyl) Sulfosuccinate/n-heptane Mixed Reverse Micelles and W/O Microemulsion Systems: The Influence of Water and Sodium Bis(Amyl) Sulfosuccinate Content," *Colloids Surf., A,* **385** [1-3] 249-55 (2011).

8. E. Bardez, R. Giordano, M.P. Jannelli, P. Migliardo, and U. Wanderlingh, "Hydrogen-bond Effects Induced by Alcohol on the Structure and Dynamics of Ionic Reverse Micelles," *J. Mol. Struct.*, **383** [1-3] 183-90 (1996).

9. S. Perez-Casas, R. Castillo, and M. Costas, "Effect of Alcohols in AOT Reverse Micelles. A Heat Capacity and Light Scattering Study," *J. Phys. Chem. B*, **101** [36] 7043-54 (1997).

10. V. Papadimitriou, C. Petit, G. Cassin, A. Xenakis, and M.P. Pileni, "Lipase Catalyzed Esterification in AOT Reverse Micelles: A Structural Study," *Adv. Colloid Interface Sci.*, **54**, 1-16 (1995).

11. I. Lisiecki, M. Björling, L. Motte, B. Ninham, and M.P. Pileni, "Synthesis of Copper Nanosize Particles in Anionic Reverse Micelles: Effect of the Addition of a Cationic Surfactant on the Size of the Cyrstallite," *Langmuir*, **11** [7] 2385-92 (1995).

12. M.P. Pileni, "Nanosized Particles Made in Colloidal Assemblies," *Langmuir*, **13** [13] 3266-76 (1997).

13. R.P. Bagwe and K.C. Khilar, "Effects of Intermicellar Exchange Rate on the Formation of Silver Nanoparticles in Reverse Microemulsions of AOT," *Langmuir*, **16** [3] 905-10 (2000).

14. Ch. Beck, W. Härtl, and R. Hempelmann, "Size-Controlled Synthesis of Nanocrystalline $BaTiO_3$ by a Sol-gel Type Hydrolysis in Microemulsion-provided Nanoreactors," *J. Mater. Res.*, **13** [11] 3174-80 (1998).

15. J.P. Cason, M.E. Miller, J.B. Thompson, and C.B. Roberts, "Solvent Effects on Copper Nanoparticle Growth Behavior in AOT Reverse Micelle Systems," *J. Phys. Chem. B*, **105** [12] 2297-302 (2001).

16. K.E. Marchand, M. Tarret, J.P. Lechaire, L. Normand, S. Kasztelan, and T. Cseri, "Investigation of AOT-based Microemulsions for the Controlled Synthesis of MoS_x Nanoparticles: An Electron Microscopy Study," *Colloids Surf., A*, **214** [1-3] 239-48 (2003).

17. S.P. Moulik and B.K. Paul, "Structure, Dynamics, and Transport Properties of Microemulsions," *Adv. Colloid Interface Sci.*, **78** [2] 99-195 (1998).

18. L.M.M. Nazário, J.P.S.G. Crespo, J.F. Holzwarth, and T.A. Hatton, "Dynamics of AOT and AOT/Nonionic Cosurfactant Microemulsions. An Iodine-laser Temperature Jump Study," *Langmuir*, **16** [14] 5892-9 (2000).

19. F. Pitré, C. Regnaut, and M.P. Pileni, "Structural Study of AOT Reverse Micelles Containing Native and Modified α-chymotrypsin," *Langmuir*, **9** [11] 2855-60 (1993).

20. M.L. Curri, A. Agostiano, L. Manna, M.D. Monica, M. Catalano, L. Chiavarone, V. Spagnolo, and M. Lugarà, "Synthesis and Characterization of CdS Nanoclusters in a Quaternary Microemulsion: The Role of the Cosurfactant," *J. Phys. Chem. B*, **104** [35] 8391-7 (2000).

21. A.M. Gonçalves, A.P. Serro, M.R. Aires-Barros, and J.M.S. Cabral, "Effects of Ionic Surfactants Used in Reversed Micelles on Cutinase Activity and Stability," *Biochim. Biophys. Acta*, **1480** [1-2] 92-106 (2000).

22. C.-L. Chiang, "Controlled Growth of Gold Nanoparticles in AOT/$C_{12}E_4$/Isooctane Mixed Reverse Micelles," *J. Colloid Interface Sci.*, **239** [2] 334-41 (2001).

23. B.H. Shi, L. Qi, J. Ma, and N. Wu, "Architectural Control of Hierarchical Nanobelt Superstructures in Catanionic Reverse Micelles," *Adv. Funct. Mater.*, **15** [3] 442-50 (2005).

24. S. Sarda, M. Heughebaert, and A. Lebugle, "Influence of the Type of Surfactant on the Formation of Calcium Phosphate in Organized Molecular Systems," *Chem. Mater.*, **11** [10] 2722-7 (1999).

25. H. Fathi, J.P. Kelly, V.R. Vasquez, and O.A. Graeve, "Ionic Concentration Effects on Reverse Micelle Size and Stability: Implications for the Synthesis of Nanoparticles," *Langmuir*, **28** [25] 9267-74 (2012).

CHAPTER 8: SUMMARY

A qualitative model was developed to explain the mechanisms of reverse micelle size and stability in the water/AOT/isooctane system by making systematic additions of salts and performing characterization with dynamic light scattering. The model is based on the development of a pair of electrical double layers within the reverse micelle structures that develop between the surfactant filled interface and the reverse micelle core that has mostly co-ions. Experimentally salt additions were observed to cause a decrease in the average reverse micelle size, which is believed to be a direct consequence of the electrical double layer thickness and the resulting potentials that develop in the interior of the reverse micelles when the salts are added. As salt concentration was increased, it decreases the electrical double layer thicknesses and allows the overlapping potentials to move into closer proximity to each other so that reverse micelle size is decreased. However, this phenomenon has a limit defined by the increasing concentration of co-ions in the reverse micelle cores with increasing salt additions. The optimum defines the point of instability and can be used to estimate the critical potential and local ion concentration at the critical potential by fitting a line to data that includes the critical concentration of salts having different counterion valences.

Mathematical analysis of the electrical double layer thickness and distance from the surface potential to the crticial potential according to the qualitative model provides support for the model. Specifically, the lengths of the two overlapping electrical double layers at the points of instability are short enough to support the formation of a central core that can accommodate co-ions. A core size of 3.4-6.9 nm was estimated for the

$ZrOCl_2$, $Al(NO_3)_3$, and NH_4OH systems, depending on the assumptions that were made. The core size is larger if sodium counterions, dissociated from the surfactant headgroups, are incorporated into the electrical double layer. However, the amount of sodium counterions in the electrical double layer cannot be determined from the methods used in this study. The core size is also increased by the incorporation of a Stern layer, which effectively results in a reduced potential that the electrical double layer extends from. However, the extent that the surface potential is reduced is unclear from numerical analysis alone. The study supports further development of the model to understand the precise location of the sodium counterions and extent of occupied states in the Stern layer.

Several specific ion effects on reverse micelle size and stability have been demonstrated in this work. Additions of $NaBH_4$ and $HAuCl_4$, having monovalent counterions relative to the AOT surfactant headgroup, demonstrated opposite average reverse micelle size dependence with increasing electrolyte concentration. The reverese micelle sizes with $NaBH_4$ decreased while those with $HAuCl_4$ increased. The effect of $NaBH_4$ is typical of salt additions to the reverse micelles, but the effect of $HAuCl_4$ is anomalous. One possible explanation is the large size of the co-ion complex of $HAuCl_4$. However, more complex interactions, such as the nature of the hydrogen bond network cannot be ruled out. The distribution, orientation, and dynamics of the water molecules in the reverse micelle interior form the hydrogen bond network, which is known to be semi-ordered and heterogeneous in reverse micelles, but not much is currently known about the hydrogen bond network when a salt is introduced into the reverse micelles.

Thus, there is a need to establish the exact distribution of all the components in the reverse micelle interior, including water.

A potential modification to the qualitative model was presented that incorporates the hydrogen bond network and can explain reverse micelle growth with addition of $HAuCl_4$. The modification is based on two water surfaces that form the overlapping electrical double layers instead of the surfactant interface and the hypothetical surface of the core. The orientation of the water molecules can produce a set of negative or positive potentials between the two water layers. Thus, the character of the water surfaces determines the nature of the counterion that interacts with the surfactant at the oil-water interface. If the counterions are oppositely charged, then reverse micelle shrinkage occurs and if the counterions are similarly charged, then the repulsive force creates reverse micelle growth with increasing salt concentration.

When adding different salts that introduce divalent counterions with respect to the surfactant headgroup, the slopes obtained by the linear fits established for the dependence of reverse micelle size on the electrical double layer thickness were similar. However, the size intercepts for the fits were different and can be directly correlated to the average ion hydration size for the added electrolyte. The size intercepts for the fits to data for salts introducing trivalent counterions were also correlated to the average ion hydration size for the added salt, but indirectly. The point of instability for the various salts with divalent or trivalent counterions can be described by two effects: (i) the traditional salting out mechanism by which surface tension increases with increasing interfacial area as the reverse micelle size is decreased to a critical value and (ii) a sufficiently large

hydrated ion size can also cause a lower point of instability. The salting out mechanism explains most of the points of instability.

An estimate of Stern layer occupation was provided by studying a slope transition for the reverse micelle size dependence on the electrical double layer thickness. It was estimated that 90-95% of the surfactant headgroups are dissociated, indicating 5-10% occupation of the Stern layer. This value is higher than counterion dissociation from the surfactant headgroup without an added salt, which can be because of the need to screen co-ions that are also introduced by the salt. A method for estimating the relative permittivity of the electrolyte solution in the confined space of the reverse micelle was also demonstrated when assuming that the slopes of the linear trends of reverse micelle size only depend on the electrical double layer thickness. Reasonable results are presented compared to other researchers in that the relative permittivity of the confined water, without electrolyte addition, is similar in magnitude to bulk water and that salts in the reverse micelle interior are found to increase the relative permittivity. The relative permittivity increased by up to two orders of magnitude with the salt additions, but the estimate is made cautiously because it assumes a constant relative permittivity for a given salt regardless of concentration and no other slope dependence.

The points of instability of various salts were characterized and demonstrate that stability depends on ion hydration sizes and the electrical double layer thickness. Thus, a foundation for understanding stability of reverse micelles containing precursors that are used for precipitation reactions within reverse micelles has been developed. However, precursor stability does not define the stability of the reverse micelles after a precipitation reaction is initiated. Up to 0.3 M $ZrOCl_2$ or 0.6 M NH_4OH can be incorporated into the

water/AOT/isooctane system with a water to surfactant ratio of ten, but concentrations of 0.1 M or higher are unstable when adding as little as 0.05 M NH_4OH to initiate a precipitation reaction. However, the stability of the reverse micelles is not affected at all by NH_4OH because concentrations within the precursor stability limits are stable when the $ZrOCl_2$ concentration was 0.05 M. Thus, in addition to considering precursor limits, precipitation limits must also be considered to ensure system stability. Transmission electron micrographs demonstrate that zirconium hydroxide precipitates that form in the stable reverse micellar solution are about 3-4 nm in size and slightly agglomerated, but changes to the system during sample preparation can cause agglomeration and make them uncomparable to the dispersed particles. Precipitates formed in unstable reverse micellar solutions are highly agglomerated into large structures and contain substructure that is larger than the precipitates formed under stable conditions.

Precursor salts added to microemulsions prepared with the cationic surfactant cetyltrimethylammonium bromide were found to cause growth of the reverse micelles and mostly produced unstable solutions. A notable exception is when $Mn(NO_3)_2$ was added to an unstable reverse micellar parent phase that resulted in stabilization, but eventually destabilized the reverse micellar structures at higher concentrations. These results support the importance of the hydrogen bond network and the corresponding changes to the qualitative model originally proposed in Chapter 2 and provided in Chapter 4. By using the anionic surfactant AOT, most salts reduce the size of the reverse micelles, indicating positively charged counterions in the negative potentials. If the specific ions introduced into the reverse micelles determine the configuration of the hydrogen bond network inside the reverse micelle, then growth of the reverse micelles

would be expected for the addition of most salts in systems with cationic surfactant because of the interaction between the positively charged surfactant headgroups and the positively charged counterions, according to the model presented in Chapter 4.

Changes to the reverse micelle interior, such as changing the water to surfactant ratio or substituting other polar solvents for water are expected to change the hydrogen bond network. The influence of reverse micelle stability with salt additions and when precipitation reactions are initiated after making such changes were also studied despite not knowing the exact effect that the changes have on the hydrogen bond network. The reverse micelle size remains proportional to the electrical double layer thickness when salts were introduced into the systems. Even when no salt addition were made, the reverse micelle size changes when varying the water to surfactant ratio were found to correlate well with the electrical double layer thickness formed by the surfactant counterions (lower water to surfactant ratio introduces more counterions, compresses the electrical double layers, and produces smaller reverse micelle sizes). Substituting methanol or acetone for the polar solvent has no effect on the counterion concentration, which may explain why initial substitution does not have a significant effect on the reverse micelle size. However, eventually a transition is observed such that increasing substitution of the solvent causes a size decrease.

With the exception of the system with water to surfactant ratio of five, the points of instability for the other systems can be demonstrated by turbidity measurements. However, the increased turbidity at the point of instability can be relatively small if significant at all so that confidence in the measurements is low. Thus, turbidity

measurements can be used as a supplemental technique when assessing the point of instability for a given system, but should not to be used exclusively to determine stability.

It can be beneficial to add cosurfactants for reverse micelle synthesis because the cosurfactant can interact favorably with precipitated particles, for example. The use of either a cationic or anionic cosurfactant in addition to AOT results in a decrease in the average reverse micelle size. A mechanism was proposed based on the concept of the electrical double layers that develop in the reverse micelles. More specifically, the cosurfactant screens electrostatic interactions at the oil-water interface and decreases the surface charge density at the interface. The reduced surface charge density weakens the influence of the interface on the hydrogen bond network of the confined water so that the potentials in the overlapping electrical double layers are also reduced at any distance away from the water surface and allows the two overlapping electrical double layers to move into closer proximity to each other to achieve the critical potential, similar to the size change mechanism originally developed in Chapter 2, and the net result is a decrease in the average reverse micelle size. The reduction in size is limited when substituting isopropanol for AOT and is believed to be because the isopropanol partitions between the reverse micelle interface and interior.

When increasing salt concentration in the reverse micelle systems modified by a cosurfactant, the average reverse micelle size remains proportional to the electrical double layer thickness. Besides the use of isopropanol as a cosurfactant, which has identical points of instability when compared to the base system, all other cosurfactants result in a decrease in the point of instability. Even with the reduced salt solubility, the points of instability with different salts are such that the critical potential developed from

the concept of overlapping electrical double layers remains constant when making the cosurfactant substitutions, which further supports the size change mechanism proposed when making cosurfactant substitutions. In addition to reducing stability with salt additions, the cosurfactants also do not improve reverse micelle stability when initiating a precipitation reaction by mixing two reverse micelle solutions containing either $ZrOCl_2$ or NH_4OH.

The critical potential remains constant for any modifications that were made in this study. Thus, the critical potential can be a system defined parameter in that the primary components may define the critical potential. If the critical potential controls reverse micelle sizes and reverse micelle sizes can be used as an indicator to determine stability, then it may be possible to establish the stability limits for any system if the critical potential is established, assuming that the critical potential changes when the primary components are changed and that a specific relationship can be established. While the critical potential does not change, estimates of the local ion concentration at the critical potential and the relative permittivity of the reverse micelle interior do change by modifying the base system and these parameters may prove to be useful for describing changes to reaction kinetics in reverse micellar media.